CHALMERS

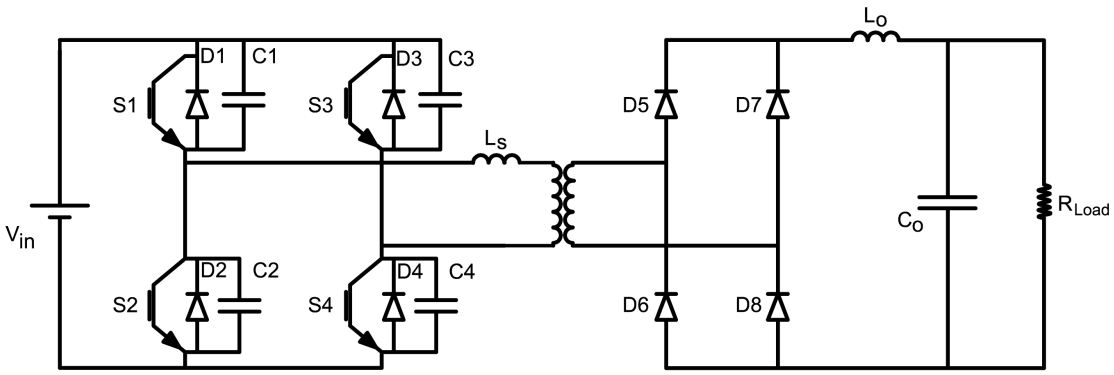

Design, simulation and evaluation of two different topologies for the 2.4 MW 4/6 kV DC-DC fullbridge converter

Master of Science Thesis

MAJID FAZLALI
MAZIAR MOBARREZ

Department of Energy and Environment
Division of Electric Power Engineering
CHALMERS UNIVERSITY OF TECHNOLOGY
Göteborg, Sweden 2012

Design, simulation and evaluation of two different topologies for the 2.4 MW 4/6 kV DC-DC fullbridge converter

MAJID FAZLALI
MAZIAR MOBARREZ

Department of Energy and Environment
Division of Electric Power Engineering
CHALMERS UNIVERSITY OF TECHNOLOGY
Göteborg, Sweden 2012

Design, simulation and evaluation of two different topologies for the 2.4 MW 4/6 kV DC-DC fullbridge converter

Department of Energy and Environment
Division of Electric Power Engineering
Chalmers University of Technology
SE–412 96 Göteborg
Sweden
Telephone +46 (0)31–772 1000

Chalmers Bibliotek, Reproservice
Göteborg, Sweden 2012

Design, simulation and evaluation of two different topologies for the 2.4 MW 4/6 kV DC-DC fullbridge converter

MAJID FAZLALI
MAZIAR MOBARREZ
Department of Energy and Environment
Division of Electric Power Engineering
Chalmers University of Technology

Abstract

In this thesis, a hard switched and zero-voltage switching fullbridge converter for high power applications are compared in terms of their losses. Important issues in designing these kind of converters are to achieve high efficiency with low cost and low weight. Managing the converter parasitics and calculating the losses for the switches as well as for the high frequency transformer with square wave input are important issues in designing such a high power density converter which are discussed in this thesis. The proposed fullbridge converters are designed to convert 4 kV input voltage to 6 kV with a rated power of 2.4 MW. The comparison is done for three different frequencies: 500 Hz, 1 kHz and 2 kHz. Also, the simulation result s and loss calculations are presented.

Based on the design and analysis of both hard and soft switching schemes of the high power density DC-DC full bridge converter, it has been concluded that since for the lower frequencies the efficiency is almost the same for the two topologies, hard switched is preferable due to the lower cost. However, for the higher frequencies where the total losses are dominated by the switching losses, the soft switched topology is superior. The core loss of the transformer which was exposed to the high frequency square wave excitation has been calculated by using FEM simulation and it shows that the transformer contribution of the total loss of the converter is about 30% at all three studied frequencies for the phase shift controlled converter.

The total efficiency of the hard switched converter is 97.3%, 96.3% and 94.5% for 500Hz, 1 kHz and 2 kHz switching frequencies respectively. For the zero voltage switching converter, the total efficiency changes like 97.8%, 97.1% and 96% for 500Hz, 1 kHz and 2 kHz respectively. As it is seen, for the low switching frequencies, the two topologies have almost the same efficiency. However, by increase in the switching frequency, the efficiency of the hard switched converter has higher reduction in comparison with the zero voltage switching converter. The less reduction of efficiency for the zero voltage switching topology is due to elimination of the switching losses in this topology.

Index Terms: DC-DC fullbridge converter, hard-switched converter, soft-switch converter, zero-voltage switching, phase shift control, switching losses, high power density transformer.

Acknowledgements

This work has been carried out at the Department of Energy and Environment at Chalmers University of Technology.
We would Like to express our sincere appreciation to our supervisor and examiner, Prof.Torbjörn Thiringer, for his time, patience and help during the thesis work. We enjoyed each of our meetings with him and learned new things.
A very special thank to Mohammadamin Bahmani for his help with the magnetics part of the thesis, availability and nice discussions.
Thank to all the employees and staff in the division for making our thesis work a pleasant stay.
Finally, we would like to thank our families continues supports and love.

Maziar Mobarrez
Majid Fazlali
Göteborg, Sweden
May, 2012

Contents

Chapter 1

Introduction

1.1 Problem Background

Today's world is moving toward replacing fossil fuels with renewable energy resources and undoubtedly, wind power is coming as an important energy source. Since the efficiency of the wind energy systems has been improved in recent decades, and its completely clean energy, wind power has become a suitable complement for the fossil fuels and non-renewable energy sources.

An attractive option to use wind energy, is to build large offshore wind farms instead of building small onshore units. There are several advantages with the offshore wind farms, usually the average wind speed is higher out in the sea so the cost of electricity production would be less, also lack of the space and environmental impacts of wind turbines is a problem for offshore installations. For all the offshore installations, cable transmission is the only solution [1]. In the case with long distances, it is not reasonable to use AC cable transmission and high voltage direct current(HVDC) cable transmission is usually considered [2].

If a HVDC system would be used instead of a AC transmission system in a wind farm, the traditional 50 Hz transformers could be replaced with DC-DC converters including medium or high frequency transformers. Also the AC cables should be replaced with DC cables. For wind farms, and especially for offshore locations, the weight of the components is an important issue; the weight of the medium frequency transformers in the DC-DC converters is significantly lower than the weight of an equivalent traditional 50 Hz transformers. Also, the DC cables have lower losses than the AC cables and there is no limitation for the transmission distance.

Today, the key component for the HVDC cable transmission is the DC-DC converters. It changes the ratio between the input and output voltages and currents by using power

electronics, and of course with the help of passive components. Today, low power DC-DC converters are common and make up for a major part of the turn-over in the power electronics market while high power and high voltage DC-DC converters in the MW range are not yet readily available on the market.

1.2 Previous Work

Most of the earlier studies on DC solutions for wind farms studied the possibility of using HVDC as transmission system. The losses and cost of a DC transmission has been compared to conventional AC transmission systems. The previous studies came to the conclusion that for the long distances DC transmission system has lower losses and lower cost in comparison with AC systems. As it was mentioned earlier, one of the key components in the HVDC transmission is the DC-DC converters which play the role of transformers in AC systems [3].

In previous studies, different topologies for the DC-DC converters has been studied, however a few studies has been done for high power DC-DC converters. This is due to lower demand for the high power converters. To reduce the weight and the size of the converters high switching frequency is required. Higher frequencies results in higher switching losses which leads lots of studies to be done in using soft switching technics [2]. Moreover, different switching patterns has been investigated for controlling the switches of the converter like PWM, phase shift.

1.3 Purpose

This thesis focuses on the high voltage and high power DC-DC converters, and two different DC-DC converter topologies in wind farm applications are discussed. The objective of this thesis is to compare two different DC-DC fullbridge converter topologies for a high voltage and high power application, like a wind park transmission system. Also, reduction of the losses in high power and high voltage DC-DC converters by using soft switching technic is a target to study.

The variations in the input and output voltage ratio makes the topology design a great challenge. An area of research itself is high frequency, high power and high voltage transformers, which are an essential component in DC-DC converters for the wind farms. In addition, the mechanisms for the losses, stray capacitances in the windings and the leakage inductance of the transformer have to be determined. It is obvious that simulations will be done only for the DC-DC converter topologies, not for the DC grid.

A part of the present work is to study previous materials; also make a model in power system block set in Simulink for the DC-DC-converter assuming an ideal magnetic material. Finally, make the design using available power electronic semiconductor components, and determine the losses for the two topologies.

Chapter 2

DC-DC Converter Topologies

One of the topologies that is used for converting DC voltage at a specific level to another level is the fullbridge converter.The topology of the fullbridge converter is shown in Fig. 2.1.

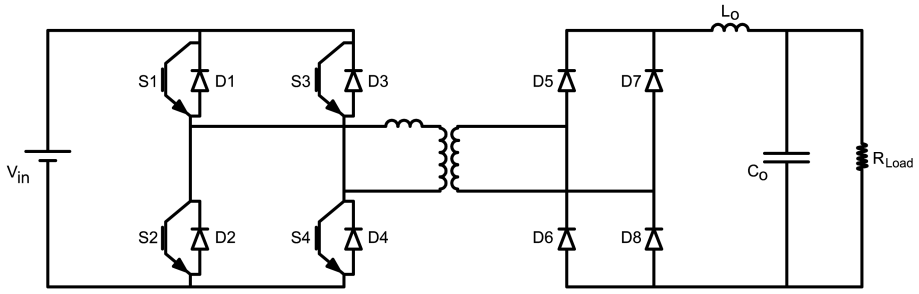

Fig. 2.1 Fullbridge converter topology

The four IGBT switches transform an DC input voltage to a square wave voltage, this square wave voltage is transformed to a higher voltage level in the transformer. After that, the square wave with the high voltage level will be rectified in the output diode rectifier at the secondary side. This converter is classified in the primary switch converter family since there is an isolation between input and output.

One of the most important things about the fullbridge converter is the control of its switches. The easiest method is using the duty cycle control; in this method, the output voltage is proportional to the duty cycle. This method causes high switching losses and affects the efficiency of the converter [4]. The second method is called phase-shift control, in this method each leg controlled individually. The operation of the fullbridge converter with these two methods will be discussed in the following.

2.1 Fullbridge DC-DC Converter

2.1.1 Duty Cycle Control

In the fullbridge converter with duty cycle control, the voltage across the transformer in on-state where the switches in the two legs are on is equal to the input voltage. And in off-state where all the switches are off, the load current freewheels in the output diodes, this gives zero voltage across the transformer. Based on this explanation, the mean voltage across the transformer in duty cycle control is equal to the output voltage divided by the transformer ratio [4].

The operation principle of the fullbridge converter with duty cycle control is shown in Fig. 2.1.1. For $t < t_1$, all the switches are off and the load current flows through the output diodes as it is shown in Fig. 2.2(a), this state is called passive state. The active state starts by switching on S_2 and S_3 at $t = t_1$, this has been shown in Fig. 2.2(b). It takes a while for the current to reach the load current, after that the output bridge is not short circuited anymore as in Fig. 2.2(c), and the current stays constant. At $t = t_3$ switches S_2 and S_3 are turned off and the current starts decreasing but due to leakage inductance of the transformer it takes some time for the current to reach zero, so the current is forced to flow through D_1 and D_4 until the current reaches zero Fig. 2.2(d). When the current reached zero at $t = t_4$, all the switches are off and the load current flow through the output bridge, as is shown in Fig. 2.2(e). The next half period starts at $t = t_5$ as the same way [4].

The idealized current and voltage waveforms for the switches and transformer in duty cycle control mode are shown in Fig. 2.3 and Fig. 2.4.

The relation between the input and output voltage is expressed as

$$\frac{V_o}{V_i} = 2\frac{n_1}{n_2}D \tag{2.1}$$

2.1.2 Phase Shift Control

Another way to control the switches in the fullbridge converter is to use the phase-shift control method. In this method, each leg of the converter is operated at 50 percent of the period, this means that the top switch is on for half of the period and the bottom switch is on for the other half of the period. The output of each leg is equal to the input voltage in half of the period and for rest of the period is equal to zero. By changing the phase between these two voltages, the voltage to the transformer can be controlled. The definition of the phase shift and the operation of the phase-shift control is shown in Fig. 2.5 and Fig.2.6.

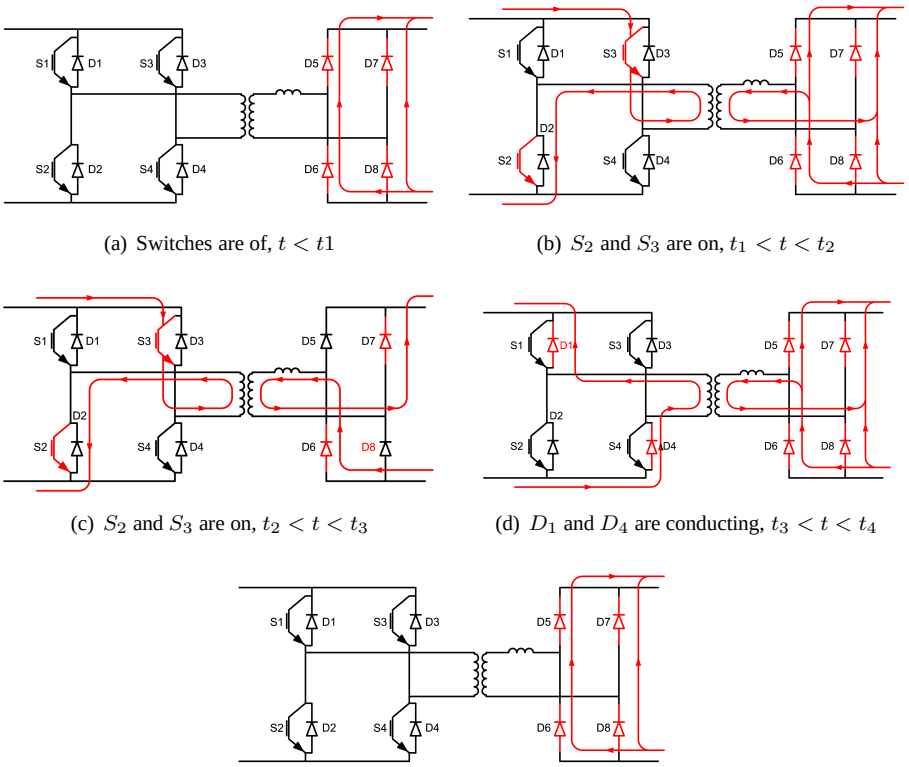

(a) Switches are of, $t < t1$

(b) S_2 and S_3 are on, $t_1 < t < t_2$

(c) S_2 and S_3 are on, $t_2 < t < t_3$

(d) D_1 and D_4 are conducting, $t_3 < t < t_4$

(e) Switches are of, $t_4 < t < t_5$

Fig. 2.2 The operation principle of a fullbridge converter with duty cycle control.

The phase shift variable ϕ is defined as [5]

$$\phi = \frac{(t_1 - t_0)}{(T_S/2)} \quad 0 \leq \phi \leq 1 \tag{2.2}$$

Also conversion ratio is defined as:

$$M(\phi) = \frac{V_{Load}}{V_d} = n\phi \tag{2.3}$$

2.2 Resonant DC-DC Converters

Switching frequencies in the range of kHz is used to reduce the size and the weight of transformer and filter components, in this way the size of the converter can be reduced.

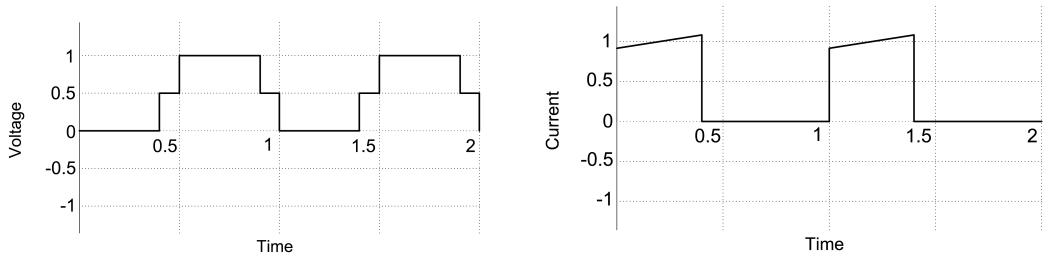

Figure 2.3: The voltage and current of the switches for duty cycle control$(D = 0.4)$

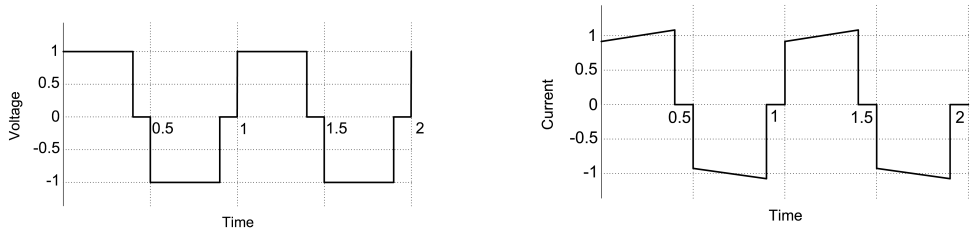

Figure 2.4: Voltage and current of the transformer for duty cycle control

To reduce the cost as well as the size, problems occur with an increase in switching frequency such as high switching losses, high switch stress and etc that should be solved. The topologies discussed in the previous section, are classified as hard switching DC-DC converters. Since the entire load current switches on and off during each period, there are high switching losses in these types of converters as well as switch stresses and the EMI(electromagnetic interface).

By using soft switching converters, the switches can change state in zero current and/or zero voltage condition. There are different topologies for achieving soft switching, most of them use an LC tank to achieve this, while snubber circuit in other topologies results in soft switching [5].

The two most important topologies of resonant converters are

- Load resonant converters
- Resonant switch converters

In load resonant converters, an LC tank is used to make the voltage and the current to oscillate, therefore the converter switches can be turned on and off at zero voltage and/or zero current. Resonant switch converters use resonant elements to shape the voltage across the switches and current through them.

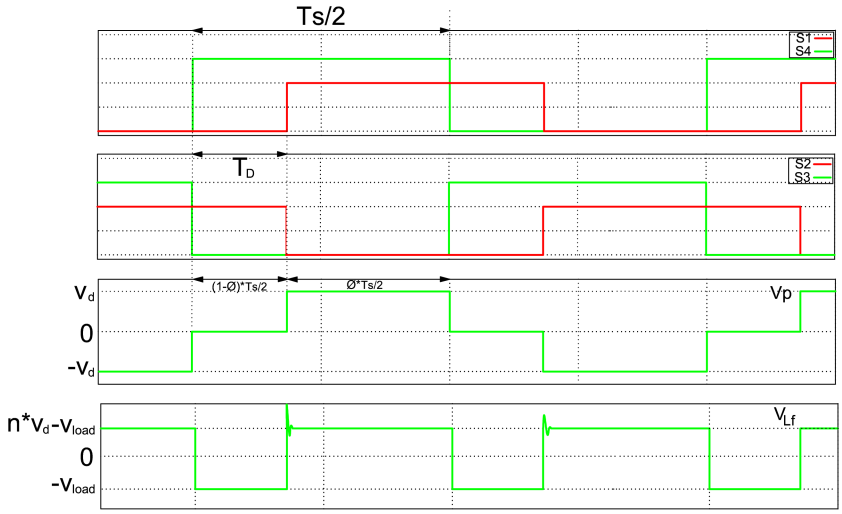

Fig. 2.5 Definition of the phase shift control concept

2.2.1 Load Resonant Converter

As it was mentioned above, load resonant converters use an LC tank which can be a series LC tank, a parallel LC tank or a combination of series and parallel. The LC tank shapes the switch voltage and current to provide zero voltage and/or zero current switching. The relation between switching frequency and resonant frequencies will result in three different operation modes [4].

$$Switching \;\; Frequency(W_s) \;\; = \;\; 2\pi f_{sw} \tag{2.4}$$

$$Resonant \;\; Frequency(W_r) \;\; = \;\; \frac{1}{\sqrt{LC}} \tag{2.5}$$

There are three different operation modes for load resonant converters which are

- Discontinuous-conduction mode $(DCM) : W_s < 1/2W_0$
- Continuous-conduction mode (CCM):$1/2W_0 < W_s < W_0$
- Continuous-conduction mode: $W_s > W_0$

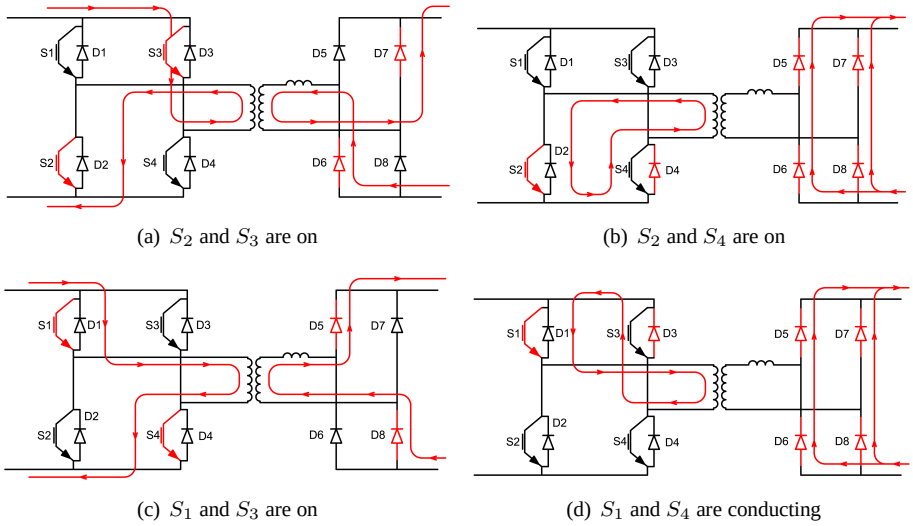

(a) S_2 and S_3 are on

(b) S_2 and S_4 are on

(c) S_1 and S_3 are on

(d) S_1 and S_4 are conducting

Fig. 2.6 Operation principle of a fullbridge converter with phase shift control.

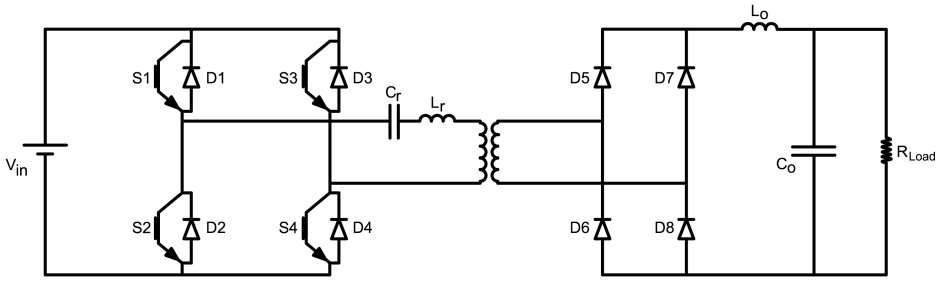

Fig. 2.7 Series-loaded resonant DC-DC converter topology

Series-loaded Resonant DC-DC Converters

In this topology, as shown in Fig. 2.7, the output load appears in series with the resonant tank. As a consequence, these converters appear as a current source to the load, i.e. they are not well-suited for multiple outputs. In return, this converters possess inherent short-circuit protection capability. Without transformer, this converters can only operate as a step-down converter [4].

For **Discontinuous-conduction mode (DCM):** $W_s < 1/2W_0$; current is forced to flow through the inductor and commutates to the diodes that are antiparallel to each switch,then no voltage appears over the switch during turn off. It means that the switches turn off at zero current and zero voltage. Because of the DCM operation, the turn on of switches occur in zero current, but not at zero voltage. Large peak current and high conducting losses are disadvantages of operation in this mode.

For **Continuous-conduction mode (CCM):** $1/2W_0 < W_s < W_0$; the switches turn on at a finite current and at a finite voltage, thus resulting in a turn on switching losses. The turn on occurs naturally at zero current and at zero voltage then there is not turn off losses.

For **Continuous-conduction mode (CCM):** $W_s > W_0$; the switches turn on at finite current, but they are turned on at zero current and zero voltage. The possible turn on losses in the switches can be eliminated by connecting a snubber consisting of a capacitor in parallel with each switch.

Parallel-loaded Resonant DC-DC Converters

The topology of this converter is shown in Fig. 2.7.

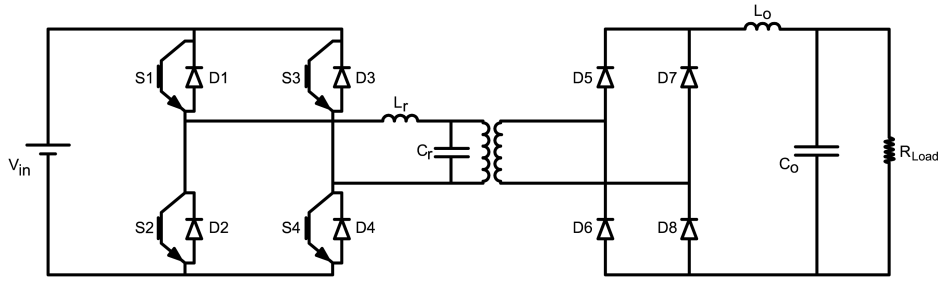

Fig. 2.8 Parallel-loaded resonant DC-DC Converter topology

This type of converter has the same operation as series-loaded resonant converters, but the output of this converter is connected in parallel with the resonant tank circuit. So, these converters appear as voltage source and will be more suitable for multiple outputs.

On the other hand, parallel-loaded resonant converters do not possess short circuit protection and peak inductor current, and peak capacitance voltage can be several times higher than the load current and input voltage [4].

For **Discontinuous-conduction mode (DCM):**$W_s < 1/2W_0$; the current of inductor and voltage of the capacitor cross zero when the switch is turned off and because of discontinuous operation turn on of switches will be done when current and voltage are zero. Consequently, there are no switching losses.

For **Continuous-conduction mode (CCM):** $1/2W_0 < W_s < W_0$; there is turn on losses in this operating mode, because both the voltage of the capacitor and the current of the inductor become continuous. However, there are no turn on losses in the switches since the reverse current of inductor commutates naturally to the antiparallel diodes, then the current and voltage of the switches cross zero.

For **Continuous-conduction mode (CCM):** $W_s > W_0$; there are no turn on losses because of natural commutation of the antiparallel diodes, the same as for the previous case.

But the switches are turned off at finite current and voltage then there are turn off losses, these losses can be eliminated by adding a snubber, such as a parallel capacitance for switches.

Hybrid-Resonant DC-DC Converters

This type of converter combines the characteristics of the series resonant and parallel resonant converters. There are different arrangements for the hybrid-resonant converters, but only the arrangement shown in Fig. 2.9 is considered [6].

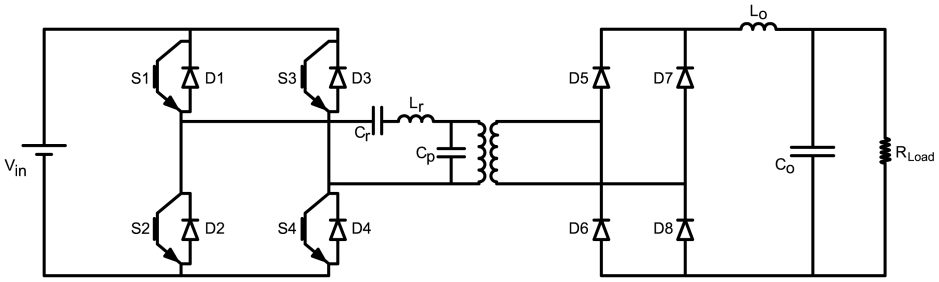

Fig. 2.9 Hybrid-resonant DC-DC converter topology

As it is shown in Fig. 2.9, the topology of this type of converter is like the series-loaded resonant converters with one capacitor C_P in parallel with the transformer. This converter behaves like a series resonant converter at low frequencies and like a parallel resonant converter at higher frequencies.

However there are some disadvantages in this converter; the need of a wide frequency range makes the dimensioning of passive components difficult, it means that large resonant inductance and capacitance are needed. Nevertheless, its easy controllability made this converter popular in high-frequency high voltage applications [6].

2.2.2 Resonant Switch Converter

Resonant switch converters use resonant elements to shape voltage across the switches and current through them. These elements are inductors, such as the transformer stray inductance and capacitors, like the output capacitance of a semiconductor switch. In the case, when parasitic elements of the converter devices that are not large enough, resonant components can be put in series or parallel with the devices for compensation. When the MOSFET is used as a switch, its output capacitor can be used to achieve soft switching, but when the IGBT is used, this capacitor is too low and a snubber capacitor should be used in parallel with the IGBT [7].

Single Active Bridge DC-DC Converters(SAB)

In this type of converters, a controllable fullbridge IGBT inverter on the primary side is connected via a high-frequency transformer to a fullbridge diode rectifier, this has been shown in Fig. 2.10. For this converter, soft switching is obtained by means of resonance between snubber capacitors, stray inductance and magnetizing inductance of the transformer. The snubber capacitors are used to achieve zero voltage turn off switching [4].

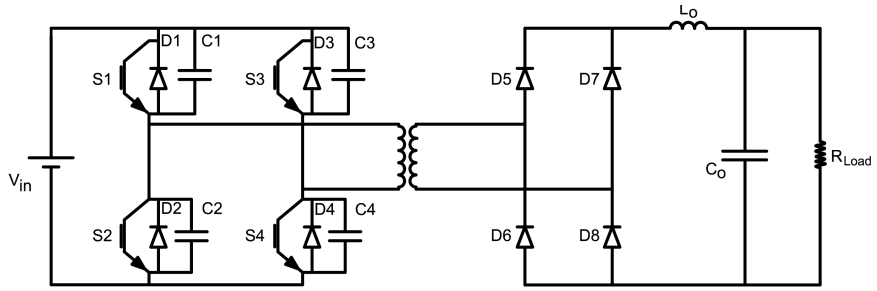

Fig. 2.10 Single active bridge DC-DC converter topology

The single active bridge converter can operate in two different modes, Discontinuous Conduction Mode (DCM) and Continuous Conduction Mode (CCM).

In the **discontinuous conduction mode**; because of snubber capacitors, switches turn off under zero voltage condition and turn on under zero current condition due to discontinuous current flow.

In the **Continuous conduction mode**; switches turn on and turn off under zero voltage condition. turn on of the switches are not at zero current condition since continuous current flows through the freewheeling diodes.

Dual Active Bridge DC-DC Converters (DAB)

This type of converter consists of two active bridges, unlike other cases with one active bridge and one diode rectifier, two active bridges are controllable, and one of them operates in the inversion mode and the other one operates in the rectification mode. More details are shown in Fig. 2.11.

Totally, in this topology, eight switches are needed, which makes the control more complex. A further drawback is the higher costs of switches compared to diodes, particularly for high power applications, where several parallel and/or series switches modules are necessary [6].

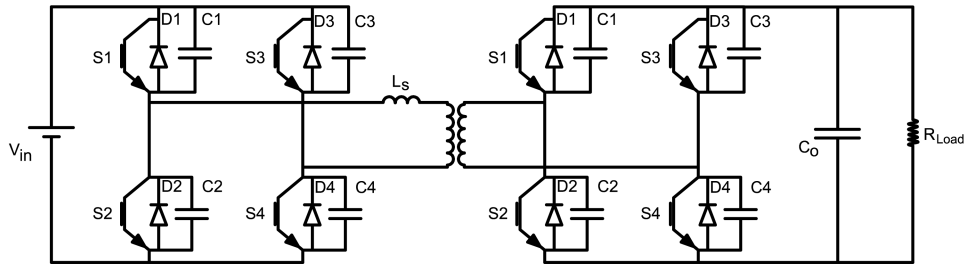

Fig. 2.11 Dual active bridge DC-DC converter topology

Full-Bridge DC-DC Converter with Phase-Shift controlled

The operation principle of the fullbridge converter with phase shift control is similar to the converter with traditional duty cycle control. The input voltage across the transformer is achieved by turning two switches on. The difference is the method of switching control.

In this control method, the switching losses can be lowered by the capacitors across the switches which are charged after turn off of a switch and they cause zero voltage during turn on switching.

In Fig. 2.12, the inductance L_s include both transformer leakage inductance and the the additional discrete inductance element. Also, for each switch, one lossless snubber is assumed and are shown as C_1, C_2, C_3 and C_4.

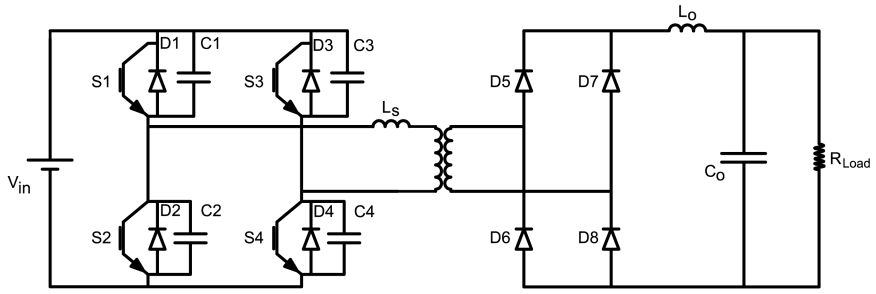

Fig. 2.12 Fullbridge DC-DC Converter with Phase-Shift controlled

In this topology, it can be seen that all the switching occur in soft switching conditions. At turn off, the snubber capacitors cause the voltage rise time of the switches to increase, which results in lower losses. This will be discussed in detail in Section 4.1.3. To achieve soft switching at turn on, the snubber capacitors that were charged during turn off, should be discharged before turning-on. Otherwise, huge amount of current goes through the switches and causes high turn on losses [5].

Actually, there are two different kinds of switching transitions in this type of converter; resonant transition and linear transition. The linear transition occurs under full load cur-

rent and the capacitor should be charged even under light load condition. In the linear transition, the leading leg capacitors are charged and discharged. However, the resonant transition depends on the stored energy in the stray inductance of the transformer and in the primary inductor. In the resonant transition, the lagging leg capacitors are charged and discharged. The primary inductor should be calculated carefully to make sure that the resonant transition is finished under desirable current level. In this kind of converters, larger snubber can be used for the leading lag and smaller ones for the lagging lag [8].

The conduction path of the fullbridge converter by phase shift control is shown in Fig.2.13. In this topology, the period that the energy is actively transmitted from the source V_d through the switches and the transformer is called "passive to active " and all the other subintervals are called "active to passive subinterval".

The conducting path can be divided into 10 subinterval that are explained respectively:

- Subinterval 1, Q_3 and Q_2 are conducting and the negative current in primary side of the transformer is nI, where n is the transformer ratio and I is the load current.
- Subinterval 2, Q_3 is turned off and the current charges the snubber capacitors on the leading leg C_3 and C_4. There should be sufficient energy in the output filter inductor to charge the C_3 to V_g while the voltage of C_4 becomes zero. It should be noticed that the parallel capacitor of Q_3, reduces the voltage rise time and causes lower turn off switching losses.
- Subinterval 3, the voltage of C_3 reaches to V_d then the diode D_4 clamps and Q_4 can be turned-on at zero voltage.
- Subinterval 4, Q_2 is turned off and the current charges the capacitors on the lagging leg C_1 and C_2. L_s ,C_1 and C_2 form a resonant network that rings with approximately sinusoid waveform. There should be sufficient energy in the primary inductance to charge C_2 to V_d while C_1 voltage becomes zero.
- Subinterval 5, the voltage of C_2 reaches V_d then D_1 clamps and Q_1 can be turned-on at zero voltage.
- Subinterval 6, Q_1 and Q_4 are conducting and the positive current in primary side of the transformer is nI.
- Subinterval 7, Q_4 is turned off and the current charges the snubber capacitors on the leading leg C_3 and C_4. It should be sufficient energy in the output filter inductor to charge C_4 to V_d while C_3 voltage becomes zero.
- Subinterval 8, the voltage of C_4 reaches V_d then D_3 clamps and Q_3 can be turned-on at zero voltage.

- Subinterval 9, Q_1 is turned off and the current charges the snubber capacitors on the lagging leg C_1 and C_2. L_s ,C_1 and C_2 form a resonant network that rings with approximately sinusoid waveform. There should be sufficient energy in the primary inductance to charge C_1 to V_d while C_2 voltage becomes zero.
- Subinterval 10, the voltage of C_1 reaches V_d then D_2 clamps and Q_2 can be turned-on at zero voltage.

The zero voltage switching allows operation with high reduction in switching losses and also in the stresses. So high switching frequencies can be used in this type of converter. These advantages make this converter well suited for high power, high frequency applications.

In addition, the diode turn off losses (reveres recovery losses) are also reduced since the voltage over the diode now slowly become negative so the diode with low losses can move into blocking status.

The driving signals for the switches $S1$ to $S4$ are explained in Section 2.1.1. Fig. 2.14 shows the formation of the primary side voltage V_p and current I_p of the transformer.

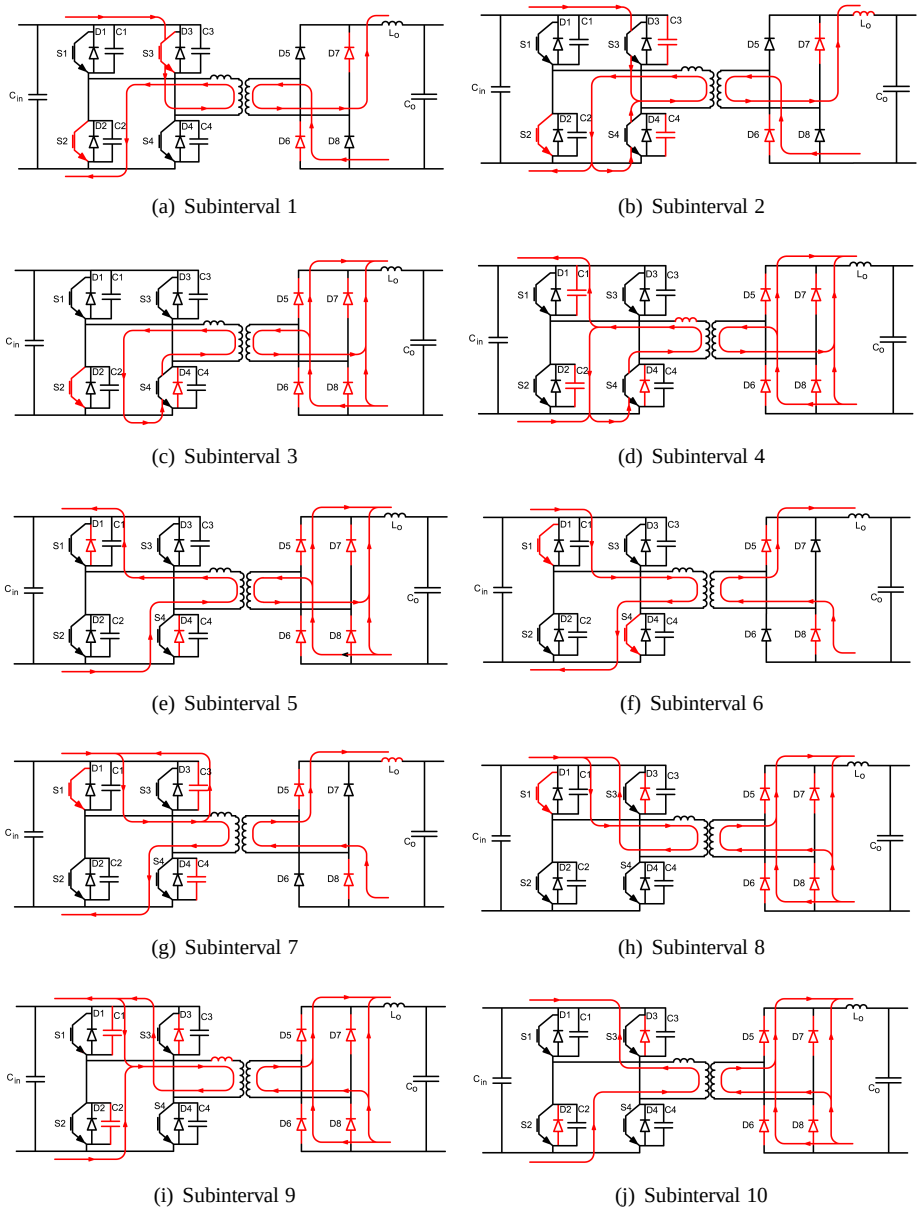

(a) Subinterval 1 (b) Subinterval 2

(c) Subinterval 3 (d) Subinterval 4

(e) Subinterval 5 (f) Subinterval 6

(g) Subinterval 7 (h) Subinterval 8

(i) Subinterval 9 (j) Subinterval 10

Fig. 2.13 The operation principle of a phase shift control converter.

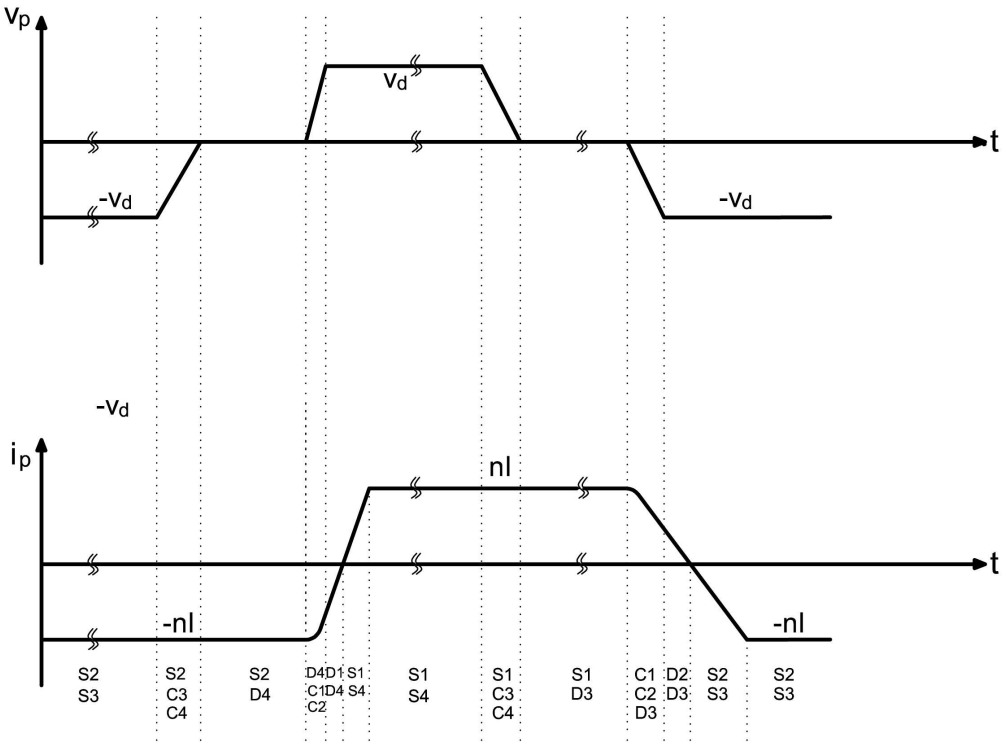

Fig. 2.14 Phase shift control-current and voltage waveforms, primary side of transformer

Chapter 3

Components of the DC-DC Fullbridge Converter

In this chapter the different components of the DC-DC fullbridge converter are explained. First of all the operation of the IGBT with its losses are studied. After that, the effect of the snubber circuits and the soft switching operation mode are discussed.

The diodes are some other components of the converter. There are two types of diodes in the converter, one type are called freewheeling diodes that are located in parallel with the IGBT and the second type are located in the secondary side of transformer and are used for rectifying. Further, the operation of diodes and their loss calculation is investigated.

The last part is about the output filter. The output filter consists of the inductor and the capacitor that are used to limit the ripple of output current and output voltage. The design of the inductor is mentioned at the end of this chapter.

3.1 IGBT

The idea of designing the Insulated Gate Bipolar Transistor (IGBT) cames from characteristics of MOSFETs and BJTs. BJTs have low voltage drop in the on state, but have longer switching times, especially at turn-off. MOSFETs can be turned on and off fast due to large gate impedance, but their on-state conduction losses are higher in comparison with the BJTs in the same ratings [4]. These characteristics led to the combining of BJTs and MOSFETs to achieve a new device with positive characteristics of both MOSFETs and BJTs (low conduction losses and fast switching). Regarding the physical setup IGBTs can be divided in to two groups [4]

- Non-punch-through IGBTs (NPT-IGBTs)

- Punch-through IGBTs (PT-IGBTs)

A circuit symbols for an n-channel IGBT are shown in the following Fig. 3.1:

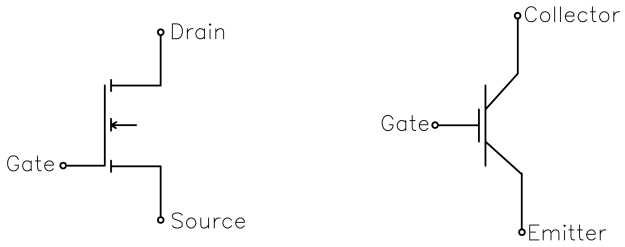

Fig. 3.1 Symbol of an IGBT

The i-v characteristic of the IGBT, Fig. 3.2, shows that the controlling parameter is an input voltage(the gate-source voltage) rather than an input current. So IGBTs are called voltage control devices.

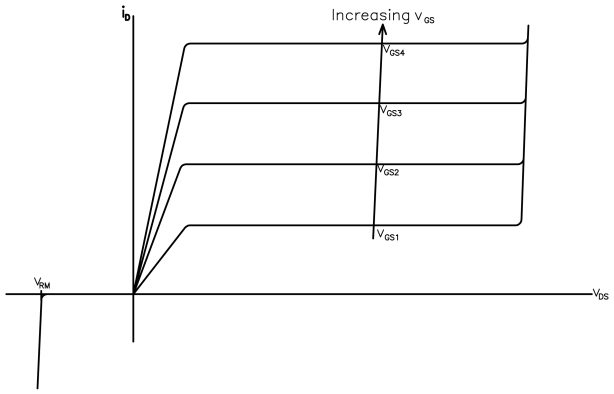

Fig. 3.2 IGBT characteristic

The transfer curve $i_D - V_{GS}$ is shown in Fig. 3.3, if V_{GS} is less than threshold voltage $V_{GS}(th)$, the IGBT is in the off state. The maximum voltage that should be applied to the gate-source terminal is usually limited by the maximum drain current that should be permitted to flow in the IGBT.

3.1.1 IGBT operation Characteristic

On-State Operation

In this part the voltage drop over the drain and source during conduction will be discussed. The equivalent circuit for IGBT during normal condition is shown in Fig. 3.4.

By using the equivalent circuit $V_{DS}(on)$ can be expressed as

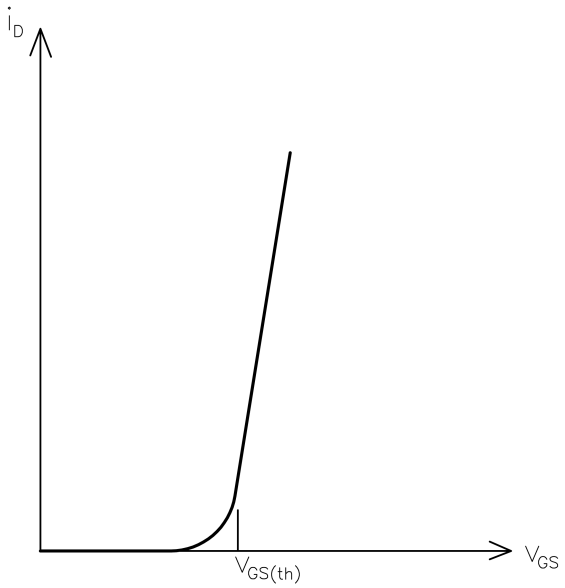

Fig. 3.3 i-v curve of an IGBT

$$V_{DS}(on) \quad = \quad V_{J1} + V_{drift} + I_D R_{on-stand} \tag{3.1}$$

The voltage drop across the injection junction $J1$ is like a voltage drop across a normal PN junction. This voltage can be considered to be 0.7-1 V. V_{drift} is much less in the IGBT than in the MOSFET, so the overall voltage drop across the IGBT for high current, is less than in the MOSFET.

Turn-on Transient

The voltage and current waveforms of an IGBT in the converter during turn-on is shown in the Fig. 3.5.

The turn-on switching period is $(t_{ri} + t_{fv1} + t_{fv2})$ and there is power dissipation during this period. The faster turn-on switching makes less power dissipation in the switch [4].

Turn-off Transient

The voltage and current waveforms of an IGBT in the converter during turn-off is shown in the Fig. 3.6

One of the differences between IGBTs and MOSFETs is in the drain current waveform. In the IGBT, the drain current has two distinct time intervals. There is a rapid current

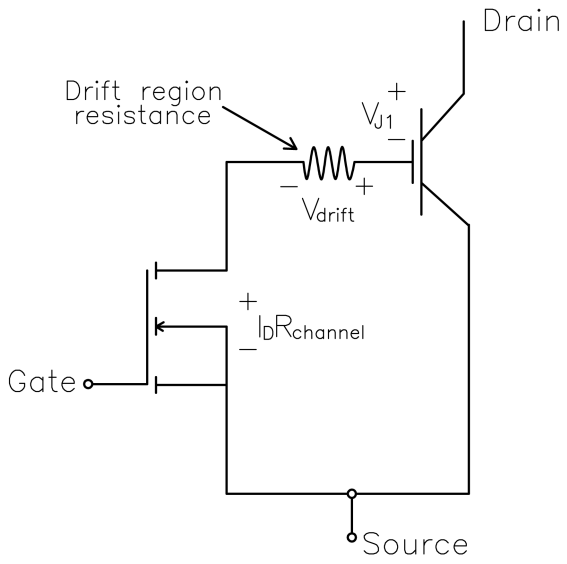

Fig. 3.4 Equivalent circuit of an IGBT

drop in t_{fi1} and the another voltage drop with slower speed is t_{fi2}. The current tail in the second time interval cause additional power loss during turn-off period, this phenomenon is called tailing [4].

3.1.2 IGBT Loss Calculation

There are two types of losses in a IGBT:

- Conduction losses due to voltage drop across the IGBT during the conduction state
- Switching losses, this type of loss is because of the turn-on and turn-off principle of IGBTs

$$P_{loss} = P_{sw} + P_c \tag{3.2}$$
$$P_{sw} = P_{on} + P_{off} \tag{3.3}$$

The calculation of these two types of losses is discussed in the following.

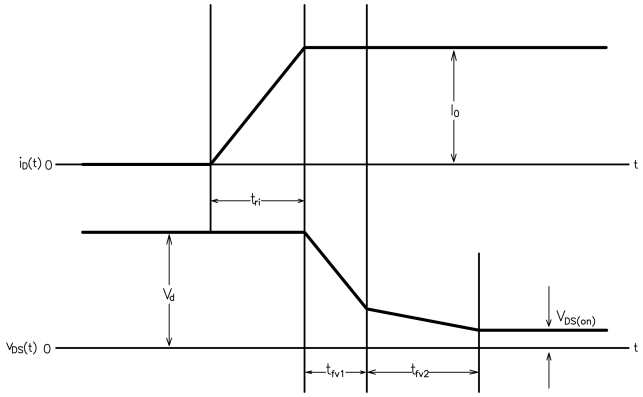

Fig. 3.5 IGBT i-v curve during turn-on

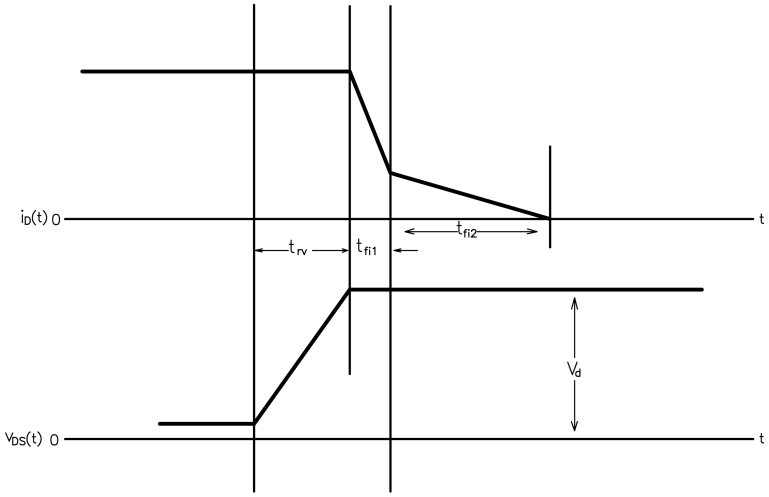

Fig. 3.6 IGBT i-v curve during turn-off

Conduction loss calculation

In conduction state there is a voltage drop across the IGBT $V_{ce}(on)$, this voltage drop adds a loss to our transistor losses that is called conduction loss. It can be calculated using

$$P_c = \frac{1}{T}\int_0^T V_{igbt} I_{igbt}; \tag{3.4}$$

Turn-on and Turn-off Loss Calculation

As it shown in Fig. 3.7 and Fig. 3.8 by having different times and the multiple of I_c and V_{ce} the switching losses can be calculated. Times that are mentioned here are on-time,

off-time, rise time and falling time of the IGBT that are defined as following [9]

- t_{don}: from 10% of V_{ge} to 10% of I_c
- t_r: from 10% of I_c to 90% of I_c
- t_{doff}: from 90% of V_ge to 90% of I_c
- t_f: from 90% of I_c to 10% of I_c

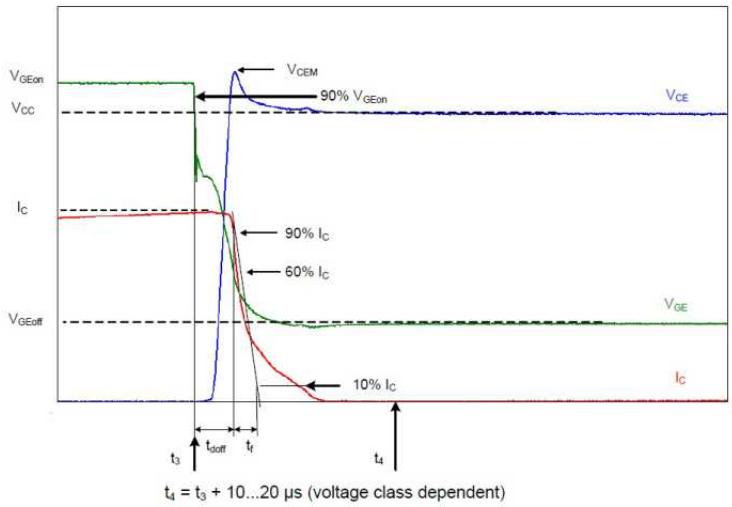

Fig. 3.7 Definitions of the turn off parameters for IGBTs

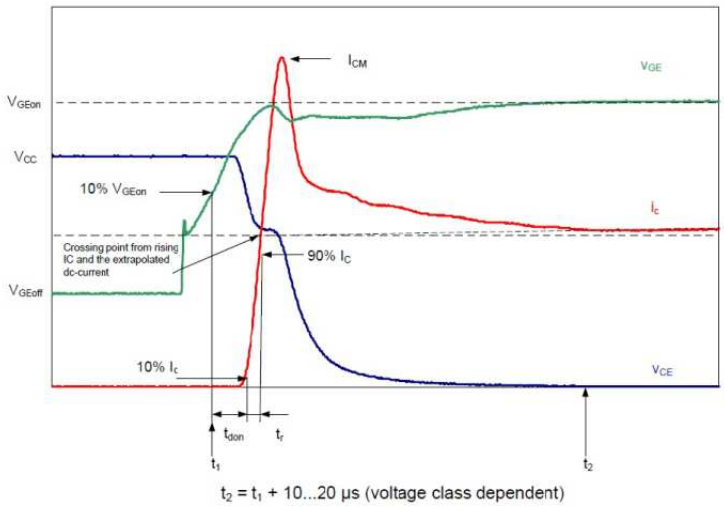

Fig. 3.8 Definitions of the turn on parameters for IGBTs

The needed times consist of off-time, rise time, on-time and fall time and those are mentioned in the data sheet but these quantities should be adjust based on the applied current.

For this reason, there is a Fig. 3.9 in one data sheet, where the sufficient value can be achieved as it shown.

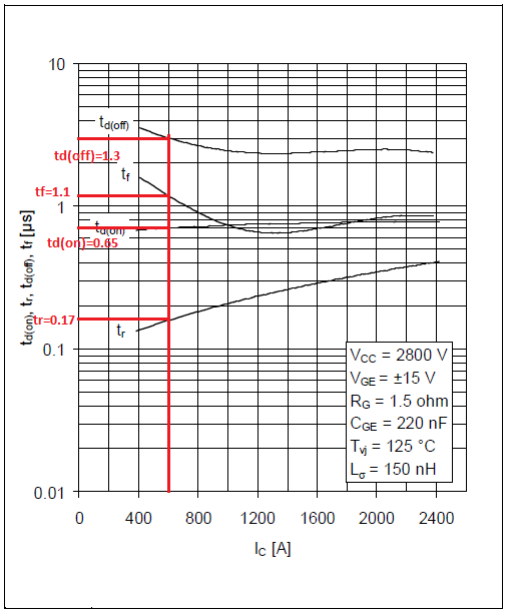

Fig. 3.9 Definition of switching time

In the IGBTs data sheet, the manufacturer provide information for the switching loss calculation. These information are the amount of the energy dissipating at each turn-on and turn-off, E_{on} and E_{off}, at a certain reference voltage V_{ref} and reference current I_{ref}.

Actually, the power dissipation of the IGBT switching is a function of the operation current, Voltage and temperature. Then, according to a SEMIKRON document [10]

$$
\begin{aligned}
P_{sw} &= f_{sw} E_{sw}(I; V_{cc}; T_j) \\
P_{sw-on} &= f_{sw} E_{sw-on} \left(\frac{\hat{I_{igbt}}}{\pi I_{ref}}\right)^{K_i igbt} \left(\frac{\hat{V_{igbt}}}{V_{ref}}\right)^{K_v igbt} \\
P_{sw-off} &= f_{sw} E_{sw-off} \left(\frac{\hat{I_{igbt}}}{\pi I_{ref}}\right)^{K_i igbt} \left(\frac{\hat{V_{igbt}}}{V_{ref}}\right)^{K_v igbt}
\end{aligned}
\tag{3.5}
$$

The constant $K_i igbt$ and $K_v igbt$ are 1 and 1.33 respectively, for the IGBT.

(3.5) Is used to calculate the switching loss in this project [10]. These procedures are valid for the hard switching method, and to reduce these losses, soft switching methods are used. The soft switching can be achieved by using a snubber in series or parallel of the IGBTs that are explained in next part.

3.1.3 Snubber Circuit

The snubber circuits are used to achieve soft switching in resonant switch converters such as a fullbridge and a single active bridge. By using the snubber capacitors in parallel with the IGBT modules, the turn-off switching losses will reduce significantly.

The turn-off snubber reduces turn-off losses by increasing voltage rise time of the IGBT, so high voltage and high current at the same time would be avoided. As it is seen in Fig.3.10 and Fig.3.11, there are two possible topologies for the turn-off snubber. In the first topology, a capacitor is put in parallel with the switch, this type of snubber is called the lossless snubber. This type of the snubber should discharge completely before the turn-off. If this is not done, the capacitor will be short circuited during turn-on and a huge current will flow in the switch. To reduce this huge current, a resistance can be connected in series with the capacitor, this has been shown in Fig. 3.11. The parallel diode with resistance provides the characteristics of a pure capacitance during charging. The negative point with this topology are the losses that are introduced with the resistance [2].

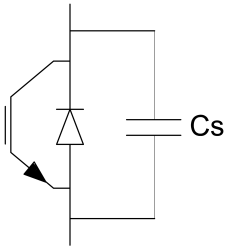

Figure 3.10: Without limited current at turn-on

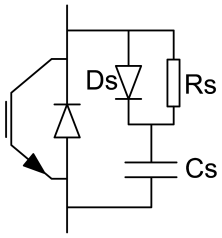

Figure 3.11: With limited current at turn-on

Hard Switching

A typical hard switching waveform for a switch in the input bridge shown in Fig. 3.12(a) can be seen in Fig. 3.12(b). For the case without snubber circuit (Hard switching) when the switch S_1 is on, the load current passes through this switch. To turn off S_1, the voltage across this switch must increase to lower the voltage across S_2 so D_2 can be forward biased. When D_2 is forward biased, the current in S_1 starts to decrease. This has been shown in Fig. 3.12(b). As it is seen, we have high voltage and high current at the same time which causes in high turn-off losses.

Soft Switching

As it was mentioned earlier, the switching losses at turn-off can be reduced by using a snubber circuit. A turn-off snubber can be connected in parallel with the switch. This type

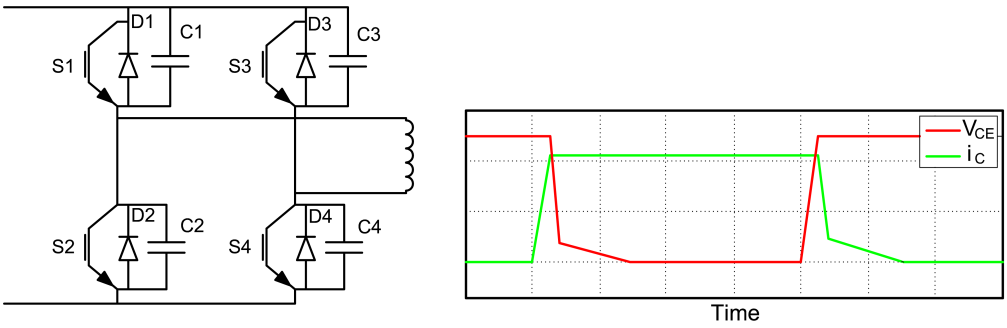

(a) Input bridge of fullbridge DC-DC converter (b) Typical voltage and current waveforms of an IGBT

Fig. 3.12 Hard switching of an IGBT of the input bridge of fullbridge DC-DC converter

of snubber is used to reduce turn-off losses of IGBTs in the fullbridge converter with phase shift control. The current and voltage waveforms of an IGBT during turn-off with and without snubber is shown in Fig. 3.13(a) and Fig. 3.13(b).

When a turn-off command is sent to the IGBT, the current in the IGBT, which is equal to the load current, starts to decrease immediately, because in this case the current can flow through capacitors C_1 and C_2. When the current flows through C_1, the capacitor will be charged so the voltage of the switch increases. This charging current is the difference between the load current and the current flowing through the switch. The capacitor keeps charging until the voltage of the switch reaches its maximum value and D_2 starts to conduct. As it is seen, the voltage and current in this case are not high at the same time so a high instantaneous power does not occur.

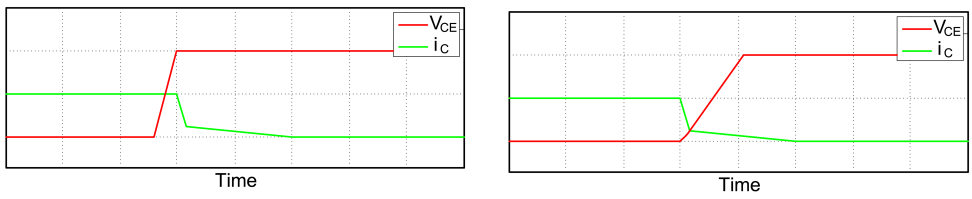

(a) S_2 and S_3 are on (b) S_2 and S_4 are on

Fig. 3.13 The Voltage and current waveform of an IGBT with snubber

3.2 Diode

3.2.1 Diode Characteristic

A diode is a semiconductor device that conducts electric current in only one direction. The symbol of the diode and its steady state i-v characteristic are shown in Fig. 3.14

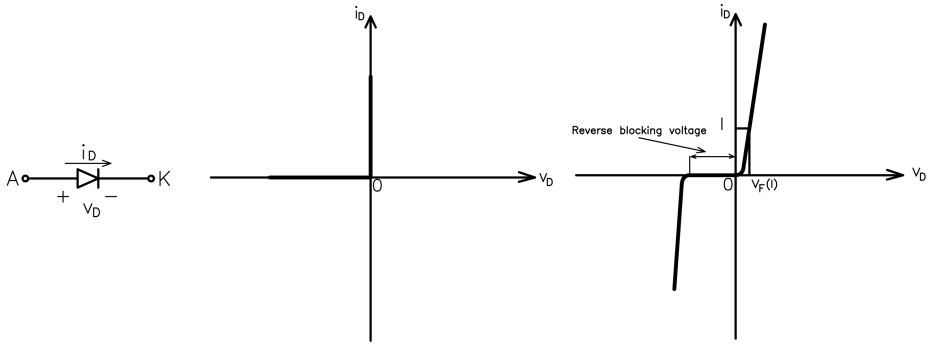

Fig. 3.14 Symbol of diode and characteristic

As it is seen, when the diode is forward biased, it begins to conduct with only a small forward voltage across it, which is in the order of 1 volt. When the diode is reversed bias it can be considered that zero current flows through the device. In normal operation condition, the reverse bias voltage should not reach the breakdown rating. In the ideal case, the forward voltage drop can be considered zero and the reverse breakdown voltage can be assumed infinite. The idealized characteristic can be used for analyzing the converter topology but should not be used for the actual design [4].

The diode turns on rapidly so the diode can be considered as an ideal switch at turn-on. However, for turning off the diode, a negative current should flow through the device for a short time, this time is called the reverse-recovery time, to sweep out the excess carriers in the diode and allow it to block a negative polarity voltage. This has been shown in Fig. 3.15.

The reverse recovery current I_{rr} and reverse recovery time $t_{rr}$of the diodes increase with increasing the carrier life time. On the other hand by increasing the carrier life time, the forward voltage drop will decrease.

Depending on the application requirements, various types of diodes are available:

- Schottky diode

  The structure of the schottky diode consists of a metal that is used as anode and the N-type semiconductor that is used as cathode. In this type of diode, electrons diffuse from the cathode to the anode because electrons have larger average energy in the semiconductor compared to the metal. Fig. 3.16 shows structure of schottky diode.

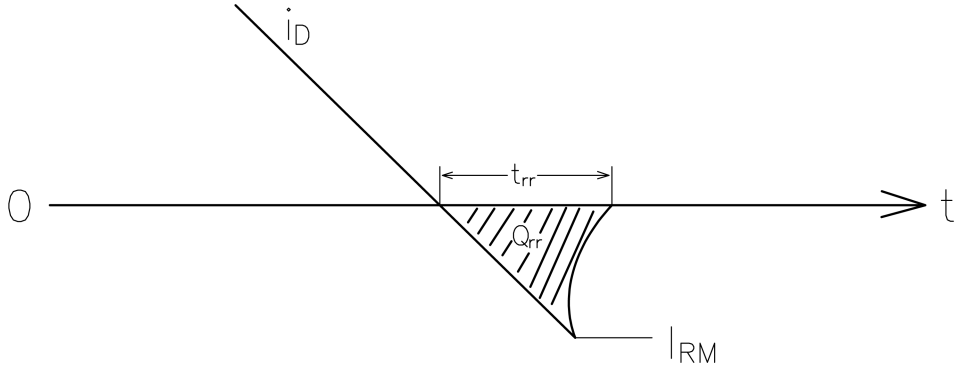

Fig. 3.15 Reverse recovery

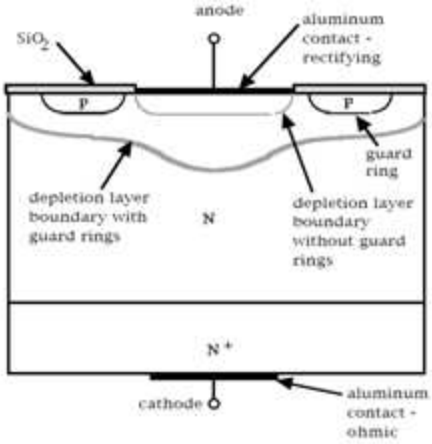

Fig. 3.16 schottkydiode

The type of schottky diodes are majority carrier device that do not have storage charge, as a result they have fast switching capability, the reverse recovery time t_{rr} and reverse recovery current I_{rr} in the schottky diodes are small in comparison to p-n junction diodes. If the required reverse blocking voltage is less $< 100V$ schottky diodes are preferred over fast recovery diodes. Also compared to p-n junction diodes schottky diodes have very little turn-off transient and almost no turn-on transient time. The scottky diodes have low forward voltage drop, it is between 0.3 to 0.5 volt, also they are limited to their blocking voltage to $50 - 100V$. [4]. They are suitable for low voltage very high frequency switching power supply applications. Power schottky diodes with forward current rating in excess of $100A$ are available [11].

- Fast-recovery diodes

  The structure of fast recovery diode is different compared to a schottky diode. One base region between P type and n-type silicon materials was added to make a P-I-N silicon. Because of the thin base region and the low reverse recovery charge,

the t_{rr} value is greatly reduced. Also, in this structure the transient forward voltage drop is reduced, the reverse working voltage is increased. Fig. 3.17 shows internal connection in fast recovery diodes.

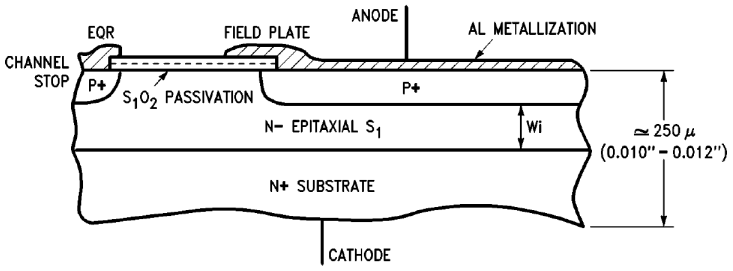

Fig. 3.17 fastrecoverydiode

The fast recovery diodes are used in high frequency systems when a small reverse recovery time is necessary. Fast recovery diodes offer reduction in both reverse recovery current and reverse recovery time. The reverse recovery time of a fast recovery diode is less than a few microseconds at a power level of several hundreds of volts and several hundreds of amperes [4]. This improvement in turn-off performance has a bad affect on the steady state performance, because the forward voltage drop in a diode is proportional to the drift region width and inversely proportional to the carrier life time. Then when the reverse recovery time and current decrease the forward voltage drop increase. In high voltage high frequency circuits, the overall power loss is dominated by switching loss and fast recovery diodes have faster switching times and less losses. The type of diodes need to be protected against voltage transients during turn-off by using an R-C snubber circuit. The schottky diodes offers non existence recovery time and their forward voltage is nearly half of fast recovery diodes but are not available in high voltage as those of fast recovery diodes.

- Line frequency diode

  The on-state voltage of these diodes is designed to be as low as possible and as a consequence, they have larger t_{rr}, which are acceptable for line-frequency applications.

3.2.2 Diode Loss Calculation

The diode losses are divided into conducting losses and switching losses, the same as for the other semiconductor devices. The conduction loss of power semiconductors is often calculating by considering a forward voltage drop V_{on} and on-state resistor r_{on}. The

formula for calculating loss can be written as

$$P_c = \frac{1}{T}\int_0^T V_{diode} I_{diode} \tag{3.6}$$

The diode switching losses depend on the reverse-recovery time t_{rr} of the diode and it occurs during the transition of the diode when the condition of diode is changed from a forward to reverse-biased. When the reverse voltage is applied to the diode, the electrical charges due to the forward current should exit, then a current spike in the opposite direction of the forward current occurs. As a result switching power loss occur, Fig. 3.18 present the changing of current and voltage of diode during switching.

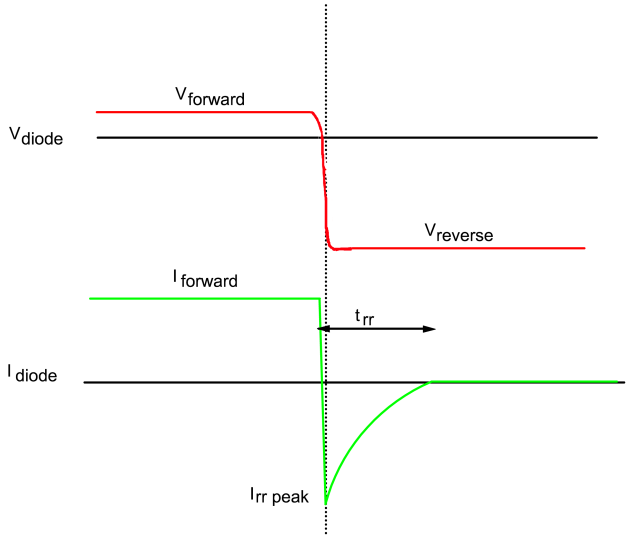

Fig. 3.18 Current and voltage of diode in switching

For calculation, the turn-off losses of diode, the relation found in [10] can be used.

$$P_{sw} = f_{sw} E_{rec} (\frac{\hat{I_{out}}}{\pi I_{ref}})^{K_i D} (\frac{\hat{V_{cc}}}{V_{ref}})^{K_v D} \tag{3.7}$$

$$\tag{3.8}$$

The constant $K_v D$ is 0.6 for diodes, and the constant $K_i D$ should be calculated according to typical diode reverse recovery characteristics, that is explained below.

For $K_i D$ calculation some approximation should be done but a linear approximation is not possible because the results would not be accurate enough. Therefore, the beginning and the ending points of the reverse recovery energy curve is selected: beginning Point: (X_1, Y_1), ending point: (X_2, Y_2), and based on (3.9) the constant $K_i D$ can be calculated.

$$(\frac{X_1}{X_2})^{K_i D} = \frac{Y_1}{Y_2} \tag{3.9}$$

3.3 Transformer

Transformers are usually used in the power electronic converters for the purpose of galvanic insulation and also for achieving a desirable voltage level. The transformers that are used for switch mode converters, operate in high frequencies with non-sinusoidal waveforms. Also the size of the transformer has a direct impact on the size of the converter. These characteristics lead to design a high-density power transformer for our full bridge converter [12].

3.3.1 Basic Magnetic Theories

Hysteresis Loop

The relationship between the magnetic flux density B, and the magnetizing force H is expressed by the hysteresis loop as it shown in Fig. 3.19.

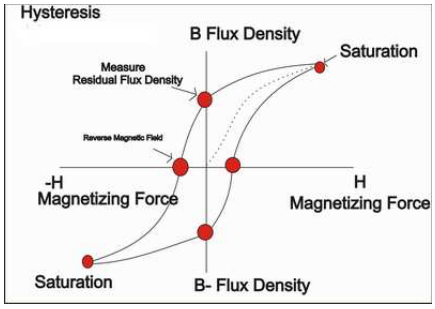

Fig. 3.19 Hysteresis Curve

To generate the hysteresis loop, the magnetizing force is changed then the magnetic flux is measured. If the ferromagnetic material has thoroughly demagnetized, by increasing the magnetizing force, it should follow the dashed line. This increasing continue until point ”a”. At point ”a” almost all of magnetics domains are aligned and by additional increase in the force, the flux will increase very little. This point is called magnetic saturated point. After that, when the magnetizing force reduce the curve move to point ”b”. In this point some magnetic flux remain but the magnetizing force is zero. Actually, in this condition some of the magnetic domains remain aligned but some have lost their alignment. This is referred to as the point of retentivity on the graph and indicates the level of residual magnetism in the material. When the magnetizing force is reversed, the curve moves to

point”c”. In this point the flux reaches zero. This point is the point of coercivity on the curve. This force that is required to remove the residual magnetism from the material is called the coercive force or coercivity of the material.

By increasing the magnetizing force in the negative direction, the material become saturated again in opposite direction, in point ”d”. By reducing the force to zero the curve will reach to point ”e”, and it will have a level of residual magnetism equal to that achieved in the other direction. To reach zero flux, the force should be increased. It should be notice that the curve did not return to the original of the graph because some force is required to remove the residual magnetism. And the curve will take a different path from point ”f” to the saturation point ”a” to complete the loop.

Magnetic Core Material

The loss that occurs in the magnetic materials has an important effect on the designing of transformers. So in this part some of the most important materials will be introduced. Iron alloys, this material is made with iron and small amount of other elements like chrome and silicon. Two types of losses exist in these alloys, hysteresis loss and eddy current loss. This type of material has large value of saturation flux density, 1.8 tesla (T). Iron alloy material usually used for low frequencies, around $2KHz$ or less for transformers, because of having eddy current loss. To reduce eddy current losses the core must be laminated [4].

Iron powdered and iron powdered alloys are another kind of material that are consist of small iron particles electrically isolated from each other. Because of that, they have a larger resistivity and less eddy current loss than iron alloys material. METGLAS is a group label for amorphous alloys of iron and other transition metals such as cobalt and nickel in combination with boron, silicon and other glass-forming elements. This alloy has a saturation induction of $0.75T$ at room temperature and $0.65T$ at 150 siliceous degrees. The electrical resistivity of METGLAS alloys is typically somewhat larger than the most magnetic steels. Amorphous alloys are good candidate core materials for high frequency applications [4].

Ferrites material are basically oxide mixtures of iron and other magnetic elements. They have quite large electrical resistivity but rather low flux density, around $0.3T$. Ferrites have only hysteresis loss, and no significant eddy current loss occurs due to high electrical resistivity. This material is used for transformer cores that operate at high frequencies because of low eddy currents [4].

3.3.2 Core Material Selection

Core material selection is an important issue in designing high-density power transformers. So in this chapter a short study of magnetic material characteristic is made.

A perfect magnetic material has low loss, high saturation density and high permeability. By using this kind of material as core of high frequency transformer, we will have a small size transformer with high efficiency. However, in reality there is no perfect material so a trade off should be done for selecting a material [12].

Magnetic materials are widely used in different applications. These materials are classified based on their magnetic behavior and their uses. Some materials are easily magnetized and demagnetized, these kind of materials are called soft magnetic materials. Some others are difficult to magnetize and demagnetize these are called hard magnetic materials. The soft materials are usually used as material of the transformer core.

For selecting a suitable material for a specific application, four characteristics of soft magnetic should study. These characteristics are [12]:

- Loss density of core W/cm3
- Saturation flux density (Tesla)
- Relative permeability
- Temperature characteristics

In Fig. 3.20 the development for different soft magnetic materials has been shown.

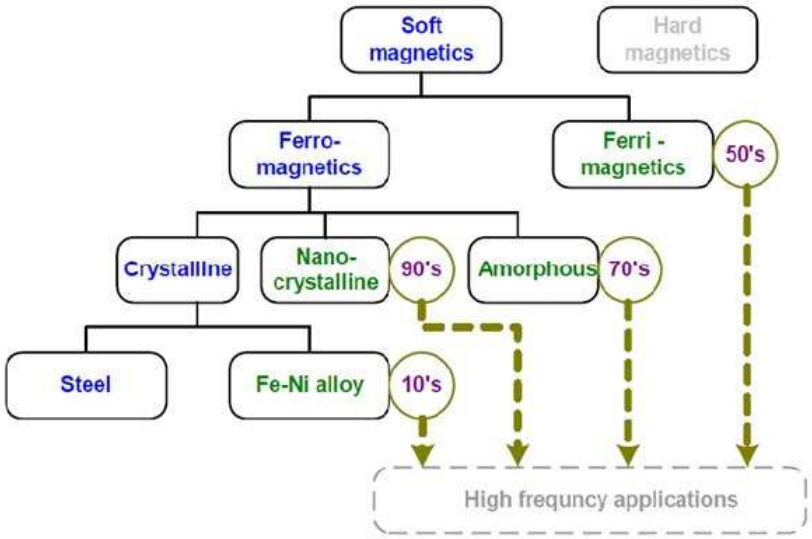

Fig. 3.20 The development for different soft magnetic materials [12]

As it was mentioned earlier, there are four characteristics that should be considered for selecting core material of transformer. The first one is loss density of the core; Fig. 3.21 shows the core loss density of different materials.

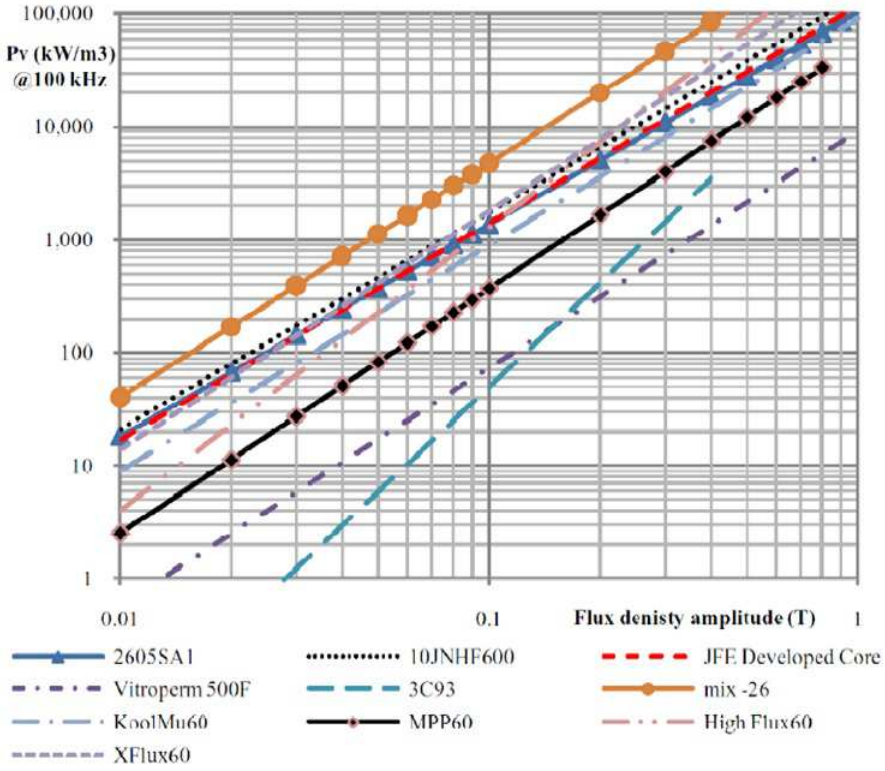

Fig. 3.21 Core loss density of different materials [12]

Finally among all the magnetic materials nanocrystalline and amorphous materials are the first choices for high power-density transformers due to:

- Low loss density
- High saturation flux density
- High relative permeability
- Good temperature characteristics

3.4 Output Filter

The diode full-bridge rectifier generates high ripples in the current and voltage. Therefore, in order to get a smooth output voltage and current, it is necessary to design an appropriate output filter, Fig. 3.23 shows the schematic of the used output filter [5].

Obviously, the value of the inductor and the capacitor should be calculated based on the rated current and voltage and their ripple limitations.

Fig. 3.22 LC filtter

The value of the inductor has to be high enough to keep the output current ripple within limits. It is usually acceptable with a current ripple between 5-10 percent of the average load current. Waveform of the inductor current, is shown in Fig. 3.23, the inductor current ripples around output current I_0.

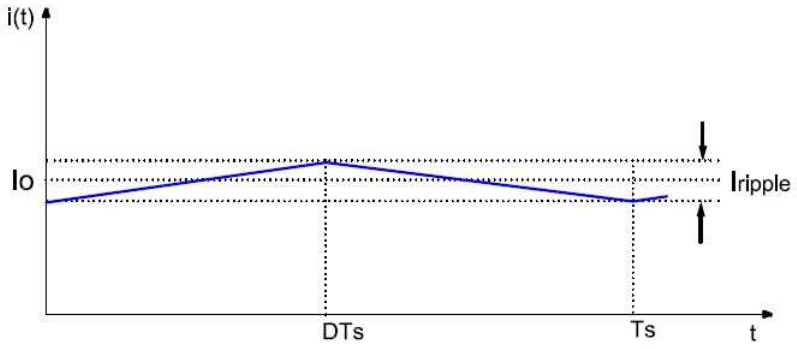

Fig. 3.23 LC filtter waveForm

For calculating the value of the inductor, the parameters are defined as following: L_o is output inductance, V_i is input voltage, V_o is output voltage, n is transformer ratio, D is duty cycle, F_{sw} is switching frequency, I_{ripple} is current ripple and, I_o is output current.

The lowest necessary value of the inductance in order to limit the current ripple is calculated as

$$L_o = (\frac{nV_i - V_o}{I_{ripple} I_o})(DT_{sw}) \tag{3.10}$$

The other component of the output filter is the capacitor. The value of the capacitor has to be high enough to keep the output voltage ripple within limits, as it shown in Fig 3.24 voltage across the capacitor can be expressed as

$$V_c(t) = V_c(t_0) + \frac{1}{c}\int i_c(t) \tag{3.11}$$

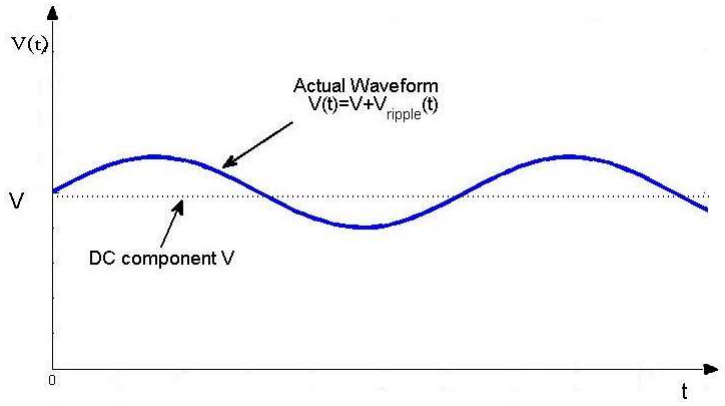

Fig. 3.24 Output voltage of the output filter

According to 3.11, the peak to peak ripple in the output voltage can be calculated

$$V_0 \quad = \quad V_c(t_0 + T_{sw/2}) - V_c = \frac{1}{c}\int I_c(t) = \frac{Q}{C} \tag{3.12}$$

The integration of the capacitor current is equal to the charge put into the capacitor. Fig. 3.25 shows the charge of capacitor, it is marked with grey.

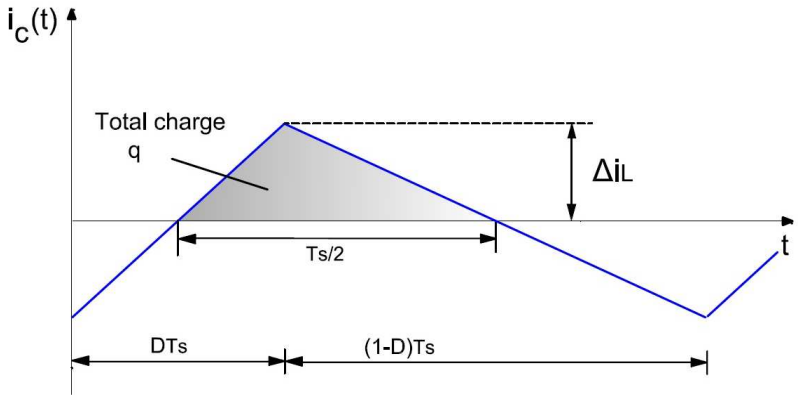

Fig. 3.25 Capacitor current

To calculate the value of capacitor, the parameters are defined as following: C_o is output capacitance, F_{sw} is switching frequency, I_{ripple} is current ripple, I_o is output current, V_{ripple} is voltage ripple and V_o is output voltage.

Finally, the capacitor size is calculated as

$$C_o \quad = \quad \frac{(\frac{1}{2F_{sw}})(I_{ripple}I_o)}{2V_{ripple}V_o} \tag{3.13}$$

Chapter 4

Design of the DC-DC Fullbridge Converter

In this chapter the design of one DC-DC fullbridge converter is discussed. First of all, IGBTs and diodes should be selected and according to their current and voltage the number of modules that are located in series or/and parallel, instead of each switch, is defined.

After that, the resonant components are calculated for three different frequencies. Then based on the maximum value of the leakage inductance, three different capacitor are calculated and the relationship between the minimum inductance and percentage of load is shown.

In the loss calculation part, the loss of IGBTs, diodes and transformer are calculated for two different topologies and the effect of soft switching is illustrated.

In this project the DC-DC fullbridge converter with these specifications will be considered:

- Input Voltage:$4000V$
- Output Voltage:$6000V$
- Output Power:$2.4MW$
- Transformer turn ratio:3

4.1 Component selection in this project

For this converter, the selection of IGBT, diode, transformer material and the resonant components are discussed. According to the characteristics of IGBT and diodes, that are selected from ABB HiPak, the conduction and switching losses should be calculated.

For this reason, a scrip is written in MATLAB and the losses are calculated for different frequencies.

4.1.1 IGBT Selection

Since the input voltage is $4000V$, the maximum applied voltage of each switch is $4000V$. And, due to the rating power $2.4MW$, the maximum current that goes through it is $600A$.

According to the voltage and current of the IGBT, different arrangement of the IGBTs can be defined . For this application, the IGBT module $5SNA0650J450300$ is selected. In this module when the current is $650A$ (half of this current value is allowed as maximum rms current) the collector emitter voltage can be $2800V$.

Based on the voltage and the current of this IGBT, the number of IGBTs that should be located in parallel or/and series, instead of each switch, is defined. By changing the number of IGBTs, the current and the voltage of them are changed and both losses, conducting losses and switching losses are recalculated. In this case, two parallel and two series of this IGBT module are used for each switch position.

After the selection of the IGBT module, the characteristics of it, should be specified to calculate the losses. Based on the typical on-state characteristic of the IGBT, the V_{ceon}, on-state voltage drop and R_{igbton}, resistive component are measured. As it shown in Fig. 4.1 the R_{igbton} is the slope of curve tangent line and V_{ceon} is the crossing point of tangent line in the V_{ce} axis.

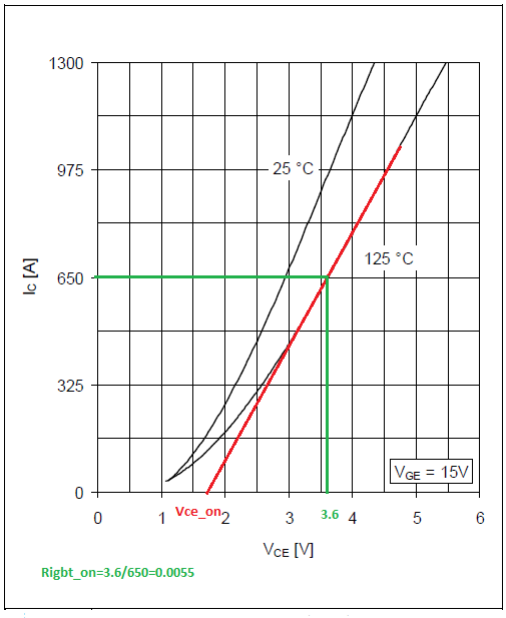

Fig. 4.1 IGBT on stat characteristics

The switching loss is an other subject that can be calculated based on the typical switching energies per pule. In Fig. 4.2 the relationship between the IGBT switching current and the energy that is wasted during each turn-on and turn-off is depicted.

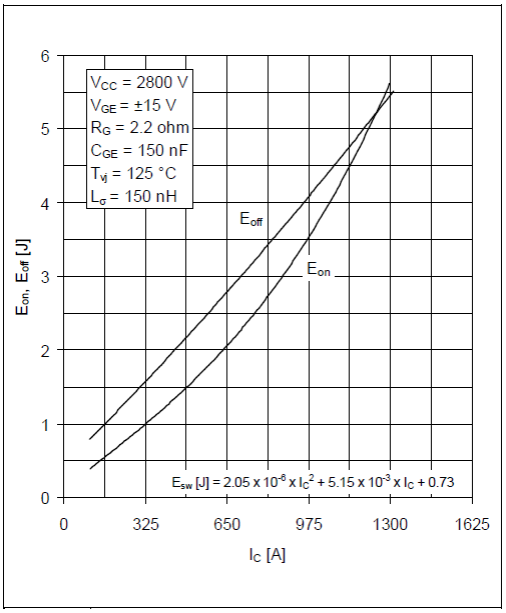

Fig. 4.2 Typical switching energies per pulse

In Table 4.1 the selected IGBT with its on-stand voltage drop, on-stand resistance and its switching energies are mentioned.

Table 4.1: IGBT module characteristics

ABB HiPak	V_{CE}(V)	I_C(A)	Vce_{on}(V)	$Rigbt_{on}$	E_{on}(J)	E_{off}(J)
5SNA 0650J450300	2800	650	1.25	0.011	2.4	2.9

4.1.2 Diode Selection

In this converter, the output voltage is $6000V$, then the maximum applied voltage to each diode is $3000V$. For the rated power $2.4MW$, the maximum current that goes through the each diode is $400A$. Then, the diode $5SLD0600J650100$ is selected from ABB HiPak. This diode module can stand $3600V$ reverse voltage and $600A$ forward current, but only half of this current is allowed current.

Based on the voltage and the current of each diode, the number of diodes that should be located in parallel or/and series, is defined. By changing the number of diodes, the current and the voltage of them are changed and both losses, conduction losses and switching

losses are modified, reasonably. In this case, two parallel diode module is used instead of each diode block.

After selecting the diode module, the forward voltage V_F and the on-state resistance R_F of it should be measured by using the typical diode forward characteristics. The typical diode forward characteristic is shown in Fig. 4.3.

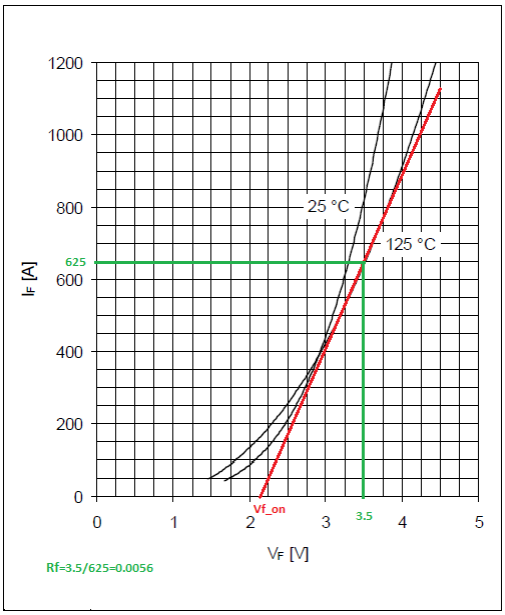

Fig. 4.3 Diode on stat characteristics

The switching losses of a diode are approximately the same as the turn-off losses since the turn-on losses are negligible in comparison with the turn-off losses. The power losses at turn-off is depending on reverse recovery characteristic. Fig. 4.4, shows the reverse recovery characteristic of the diode.

For the diode $5SLD0600J650100$, the constant K_iD is found to be 0.838. The calculation is mentioned below. The beginning Point of typical reverse recovery characteristics: (200, 0.650), The ending point of typical reverse recovery characteristics: (1200, 2.92).

$$\begin{aligned} (\frac{x_1}{x_2})^{K_iD} &= \frac{y_1}{y_2} \\ (\frac{1200}{200})^{K_iD} &= \frac{2.92}{0.650} \\ 6^{K_iD} &= 4.492 \\ K_iD &= 0.838 \end{aligned} \tag{4.1}$$

In Table 4.2, the selected output diode with its forward voltage, on-state resistance and its reverse recovery energy are presented.

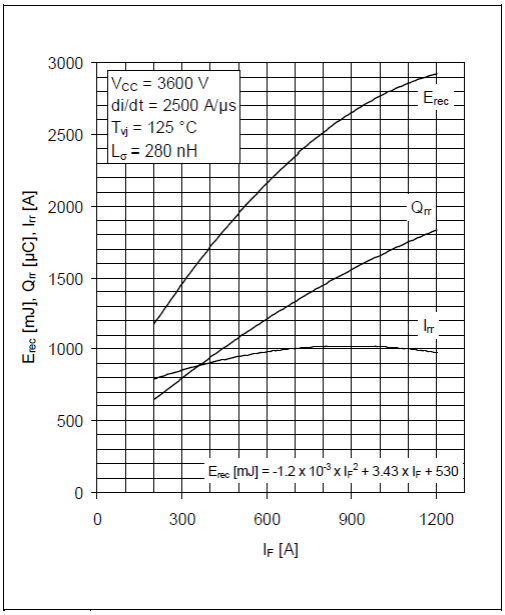

Fig. 4.4 Diode typical reverse recovery characteristics

Table 4.2: Diode module characteristics

ABB HiPak	V_R(V)	I_F(A)	V_F(V)	R_F	E_{rec}(J)	K_iD
5SLD 0600J650100	3600	600	1.2	0.0075	1.61	0.838

For the freewheeling diodes, $5SLD0600J650100$ diode from ABB HiPak is selected. The maximum voltage that is applies to these diodes is $4000V$ and the maximum current that goes through it is $600A$. Then two series and two parallel diode should be used together. Other explanations for these diodes are same as the output diodes.

4.2 Resonant Components for Soft Switching

4.2.1 Design of the Snubber Circuit

In Chapter 2, the operation of the fullbridge DC-DC converter was discussed and it was mentioned that there are two different transitions in this type of converter, the linear transition and resonant transition. The leading leg snubber capacitors charge through the energy stored in the output filter inductance. And the lagging leg snubber capacitors use energy stored in the leakage inductance of transformer to be charged. It should be taken into account that in some cases additional inductance is needed to put in series with the leakage inductance of transformer to have enough energy stored for achieving soft switching [8].

Design Criteria

There are some design matters that should be considered when designing of the snubber circuit [8] and [2].

- The first subject that need to be considered is the minimum value of the snubber capacitor that can be used. The time for charging the snubber capacitor should be at least 5 times higher than the fall time of the IGBT current.
- The second subject that is very important to take into account is finding a maximum value for the leakage inductance of the transformer. Very large inductances should be avoided due to high duty cycle loss.
- The third subject is the maximum value of snubber capacitors. The maximum value for the snubber capacitors of the lagging leg should be calculated based on the maximum leakage inductance. In this thesis, three values for the lagging leg snubber capacitors have been considered. It is obvious that the values for these capacitors should be placed between the calculated maximum and minimum values.
- In the forth step, the minimum inductances required to charge capacitors in the pervious item is calculated.
- In the last step, the leading lag snubber capacitors will be calculated based on their charging time.

To design soft switching components, some basic parameters such as: transformer ratio, duty cycle (in our case phase shift) and input current should be known. These parameters can be calculated by using (4.2) and (4.3). In our calculation, it is assumed that the current remains constant during on-state.

$$D = \frac{V_{load}}{V_d n} \tag{4.2}$$

$$i_{in} = \frac{P_{in}}{V_d D} \tag{4.3}$$

In this thesis, since the input voltage and current are too high, the switches should be consist of several IGBT modules connected in series or parallel. If the voltage, current and the snubber capacitor of the switch are V_{sw}, I_{sw} and C_{sw} respectively, then the voltage, current and the capacitor of the single IGBT module by considering n_s modules in series and n_p modules in parallel would be according to

$$V_{mod} = \frac{V_{total}}{n_s}, \quad I_{mod} = \frac{I_{total}}{n_p} \quad and \quad C_{mod} = C_{total}\frac{n_s}{n_p} \tag{4.4}$$

Then the total energy stored in the snubber capacitor can be calculated as

$$W_{cap} = n_s n_p \frac{1}{2} C_{mod} V_{mod}^2 = n_s n_p \frac{1}{2} C_{total} \frac{n_s}{n_p} \frac{V_{tot}^2}{n_s^2} = \frac{1}{2} C_{tot} V_{tot}^2 \tag{4.5}$$

As it was mentioned earlier, the principle of the turn-off snubber capacitor is to increase the rise time of the voltage during turn-off. The snubber capacitor causes a decrease in the switch current and an increase in the switch voltage to start simultaneously. However, to have a very low turn-off losses, the rise time of the voltage should be much more than the fall time of the current. In this thesis, the rise time of the voltage is considered 5 times higher than fall time of the current. This assumption is used for calculating the minimum capacitor that can be used as snubber capacitor. In the Fig. 4.5 t_{rv} is considered equal to $5t_{fi}$.

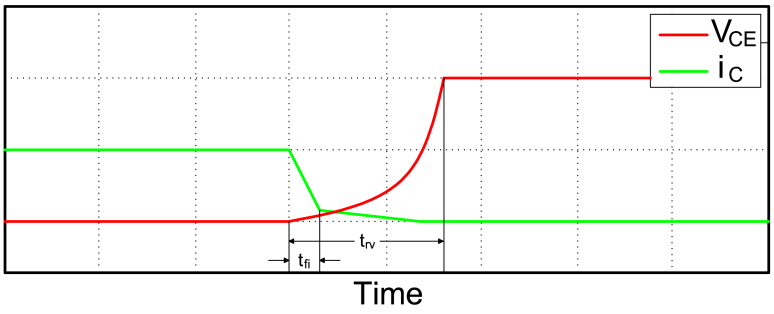

Fig. 4.5 Rise time of the voltage and fall time of the current

The minimum snubber capacitor can be calculated by using (4.6) where V_d is input voltage and Δt is equal to $5 * t_{fi}$. Also t_{fi} can be obtained from data sheet of the selected IGBT.

$$C_{min} = \frac{i_{in}\Delta t}{V_d} \tag{4.6}$$

The next step in the design of the soft switching components, is to find a maximum value for the leakage inductance of the transformer. It is not reasonable to have a very large leakage inductance to achieve soft switching. Because, the time reversal of the current will be too large in comparison with one period and cause in a high duty cycle loss. To make it clear, let us consider an operation frequency of $1kHz$, so the period would be $1000\mu s$. Since there are two current reversal in each period, Δt should not exceed from

$100\mu s$. So, the duty cycle loss would be limited to 20%. In this thesis, the maximum allowed time for current reversal is considered to be 10% of the whole period. However, the current reversal time should be much lower in reality. So a large leakage inductance will cause the duty cycle loss when the current in the transformer changes direction. The maximum leakage inductance, when the required time for the current to change from i_{in} to $-i_{in}$ is equal to 10% of the whole period, can be calculated by using

$$L_{Smax} = \frac{V_d \Delta t}{2 i_{in}} \tag{4.7}$$

Based on L_{Smax} calculated in (4.7), a maximum value for lagging leg snubber capacitors can be obtained by putting the energy stored in the maximum leakage inductance equal to the energy stored in the capacitors.

$$C_{Smax} = \frac{1}{2} \frac{L_{Smax} i_{in}^2}{V_d^2} \tag{4.8}$$

It is seen that two limits are obtained for lagging leg snubber capacitors. Three capacitors was selected between these two limits for each frequency. Table shows the values of selected capacitors in different frequencies.

Table 4.3: Lagging leg snubber capacitors for different frequencies

Frequencies	500 Hz	1 kHz	2 kHz
C_1	$6.8\ \mu f$	$3.3\ \mu f$	$1.5\ \mu f$
C_2	$4.7\ \mu f$	$2.2\ \mu f$	$1\ \mu f$
C_3	$3.3\ \mu f$	$1.5\ \mu f$	$0.9\ \mu f$

Since the leakage inductance should be able to charge the lagging leg snubber capacitors, the minimum leakage inductances will be calculated based on the lagging lag snubber capacitors. For this purpose the energy stored in the capacitors should be put equal to the energy stored in the leakage inductance. So the minimum inductance is obtained from

$$L_{Smin} = 2 \frac{C V_d^2}{i_{in}^2} \tag{4.9}$$

As it is seen in (4.9), the energy stored in the leakage inductance should be twice the energy required for charging one snubber capacitor, since two snubber capacitors are connected in series and while one of them is charging, the other one is discharging.

The results of the minimum inductances required to achieve soft switching for different frequencies and different snubber capacitors are shown in Fig.4.6.

Another design consideration for the snubber capacitors is the time for charging the capacitors of the leading leg. In this thesis, an assumption has been made that the maximum

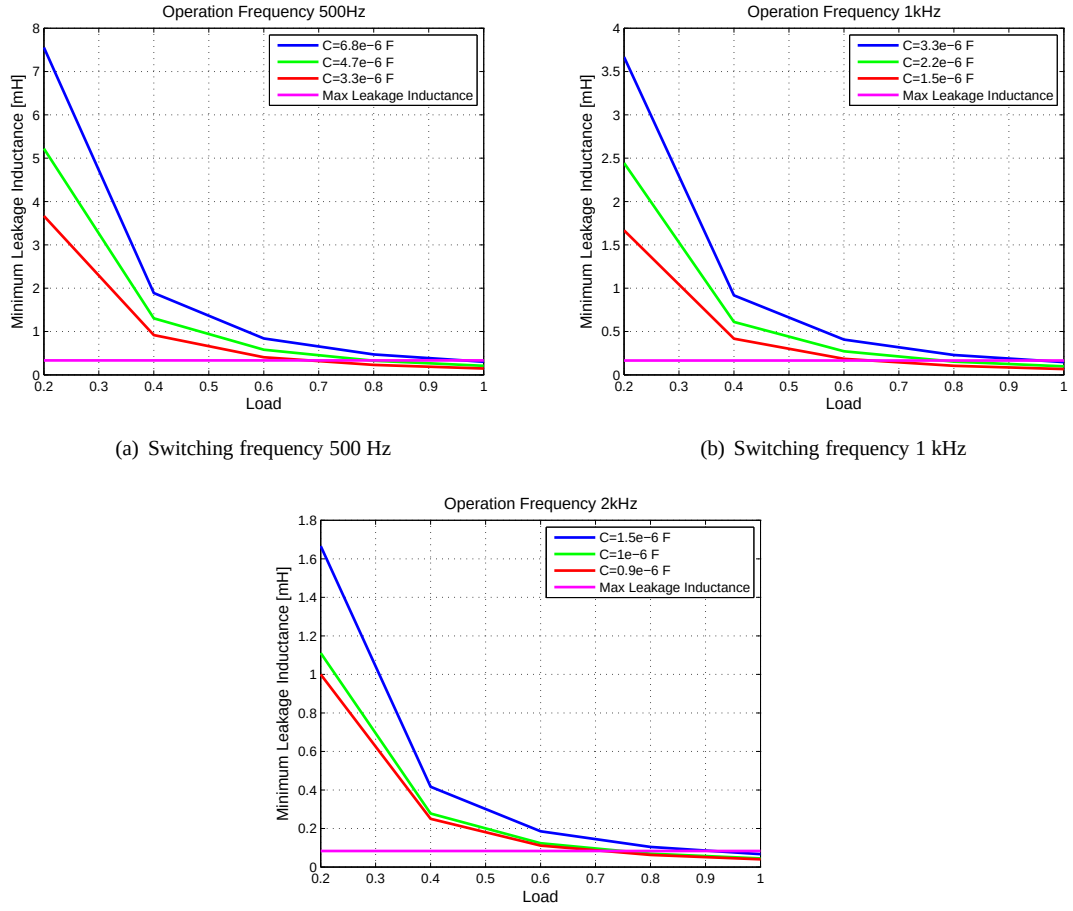

(a) Switching frequency 500 Hz

(b) Switching frequency 1 kHz

(c) Switching frequency 2 kHz

Fig. 4.6 Minimum leakage inductance versus load, for different frequencies and different lagging leg snubber capacitors

allowed time for charging the capacitors should be 2% of the whole period. The snubber capacitors of the leading leg can be calculated by using

$$C_{slead} = \frac{\Delta t i_{in}}{V_d} \tag{4.10}$$

Where δt is equal to 2% of the whole period.

4.2.2 Evaluation of the Converter for Different Load Conditions

The designed converter should be able to achieve the soft switching for different load conditions. It can be seen in Fig. 4.2.1 that for the best case the converter can achieve soft switching in 60 % of the full load current. It is obvious that the converter does not always work in 60 % of the full load and higher. Therefore some modification should be done in order to make the converter work in at least 20 % of the full load current. Two methods that can be used for this purpose are

- Reducing the switching time of the IGBT by decreasing the current fall time. In this method the current fall time of the IGBT during turn-off is decreased by changing the gate resistors. So it is possible to use smaller snubber capacitors in parallel with the switches, the smaller the capacitors can be charged with lower currents. Therefore the performance of the converter is improved in the low load conditions. Fig. 4.7 shows that the change in the current fall time by changing the gate resistance of the IGBT is small so this method is not able to make the converter to work in very low load conditions.

- Using a semi-soft fullbridge converter topology. In this topology, the lagging leg of the converter is hard-switched and the leading leg is soft-switched. As it was mentioned earlier, the energy stored in the leakage inductance (in some cases plus some additional inductance). Since this inductance should be kept small to prevent high duty cycle losses, the charging current (proportional to load current) of this inductance should be high and this high current means that it is not possible for the converter to work in the low load. Therefore semi-soft topology is used. The topology of this type of converter is shown in Fig. 4.8.

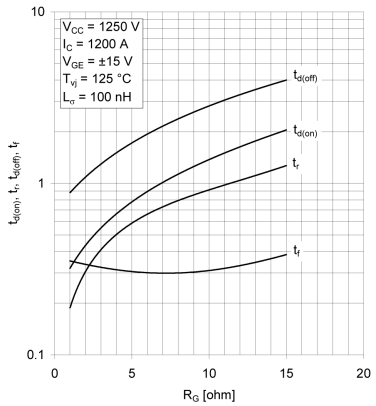

Fig. 4.7 Switching time of the IGBT vs its gate resistor

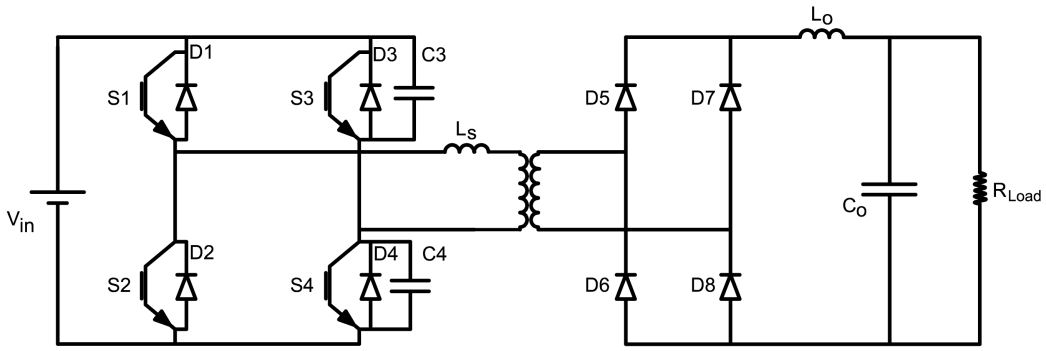

Fig. 4.8 Topology of the semi-soft fullbridge converter

4.3 The Output Filter Inductor Design

In this section, the principle of inductor design will be discussed. Also, the output filter inductor will be designed based on the converter ratings. Core material selection, core size and geometry calculation, windings number of turn and the cross section calculation will be discussed in the following.

To design the inductor, it should be modeled as an electrical circuit. The electrical circuit for a C-shape inductor core is shown in Fig. 4.9.

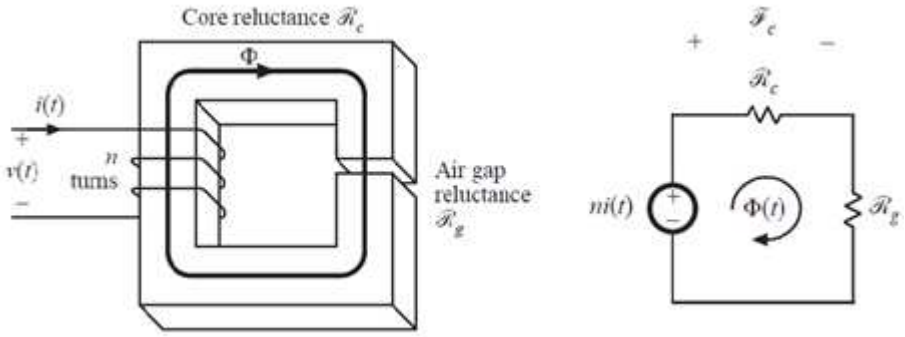

Fig. 4.9 Inductor geometry and the equivalent circuit

The equivalent circuit consists of two reluctances, the core reluctance and the air gap reluctance. The core reluctance is much lower than the air gap reluctance and it is negligible. Then the emf can be expressed as

$$ni = \Phi \Re_g \tag{4.11}$$

Some quantities should be specified in order to design the inductor. These quantities can be obtained by using calculations and simulations. For our case, the required quantities are shown in the following

- $L = 9.4mH, 18.7mH, 37.5mH$, L is the required inductance of the output filter to keep the ripples in the desired range. The values are for $2kHz$, $1kHz$ and $500Hz$ operation frequencies respectively.
- $I_{dc} = 413A$, I_{dc} is the average current that passes through the inductor.
- $I_{peak} = 467A$, I_{peak} is the peak current that passes through the inductor.
- $I_{rms} = 415A$, I_{rms} is the rms current that passes through the inductor.

These values has been calculated based on the simulations in Simulink and MATLAB.

A C-shaped core has been selected for the inductor core. The inductor geometry and the equivalent magnetic circuit is shown in Fig 4.9. There are some constraints for the inductor design and the selected core and winding should satisfy these constraints. These constraints are discussed in the following

By giving a peak winding current, it is expected to the core flux density operate at a peak value B_{max}. The saturation flux density B_{sat} of the core material should be higher than the B_{max}.

$$nI_{max} = (B_{max}A_c)\Re_g = B_{max}\frac{l_g}{\mu_o} \tag{4.12}$$

(4.12) is the first constraint. The turns ratio n and air gap length l_g are unknown.

The inductance of the inductor can be calculated as

$$L = \frac{n^2}{\Re_g} = \frac{\mu_o A_c n^2}{l_g} \tag{4.13}$$

(4.13) is the second constraint. The turns ratio n, core area A_c,and air gap length l_g are unknown.

Another design constraint is that the total area of the copper in the window nA_w, should be less than the available area for the winding conductors, the following inequality should be satisfied in designing the output inductor

$$K_u W_A => nA_w \tag{4.14}$$

where K_u is the fraction of the core window area that is filled by copper or fill factor, W_A is core window area, n is the turns ratio of the winding, A_w is wire bare area.

K_u or fill factor is a constant with a value less than 1. Insulation of the wire and the fact that round wire does not pack perfectly, will reduce K_u. The typical value of K_u for a C-shaped core in design of the inductor is 0.35 [13].

The resistance of the winding can be calculated as

$$R = \rho \frac{l_b}{A_W} \tag{4.15}$$

where ρ is the resistivity of the conductor material, l_b is the length of the wire and can be calculated as

$$l_b = n(MLT) \tag{4.16}$$

where MLT is the mean length per turn of the winding . By combining (4.15) and (4.16) the forth constraint can be shown as

$$R = \rho \frac{n(MLT)}{A_W} \tag{4.17}$$

Combining these four constraints, (4.12) (4.13) (4.14) (4.17), and eliminating n,l_g andA_w will results in

$$\frac{A_c^2 W_A}{MLT} >= \frac{\rho L^2 I_{max}^2}{B_{max}^2 R K_u} \tag{4.18}$$

The specifications and other known quantities are in the right-hand side of (4.18) and the function of the core geometry is in the left-hand side. So in our design, we should choose a core geometry that can satisfy (4.18). For this purpose, the core geometrical constant K_g is defined as

$$K_g = \frac{A_c^2 W_A}{(MLT)} \tag{4.19}$$

The number of turns, n, of the inductor can be calculated as

$$n = \frac{LI_{max}}{B_{max}A_c} \tag{4.20}$$

To make (4.18) simple, it can be combined with (4.17) and (4.20),so the following inequality will be obtained. And the selected core must satisfy this inequality.

$$\frac{LI_{max}A_W}{B_{max}K_u} =< A_cW_A \tag{4.21}$$

As it can be seen in (4.18), the size of the core can be reduced by choosing a core material having higher B_{sat} and also by allowing more copper loss. However, if there is no control on the core material and the copper loss, then the larger K_g is needed. Larger K_g can be achieved by increasing A_c and W_A which means choosing bigger core.

Metglas magnetic alloy 2605SA1 is used as the core material for this inductor. High saturation flux density (1.56 T), low core loss and high permeability make Metglas a suitable core material for the high frequency inductors [14].

Some other values that should be specified for designing the inductor are presented in the following

- Wire resistivity $\rho = 1.67e^{-}6\ \Omega - cm$, windings wire is copper.
- Peak winding current $I_{max} = 467A$.
- Inductance $L = 0.0094H, 0.0187H, 0.0375H$, the values are for $2kHz$, $1kHz$ and $500Hz$ respectively.
- Wire bare area$A_W = 210mm^2$, A_W is calculated by dividing rms current that passes through the inductor by maximum allowed current density. The maximum allowed current density is 2 $[A/mm^2]$ [4].
- Winding fill factor $K_u = 0.35$, [13].
- Core maximum flux density $B_{max} = 1.1T$, is considered around 0.75 of the saturation flux density [13].

The selected cores have almost the same size as the transformer core and they have been checked to satisfy the constraints. Table 4.4 shows the core dimensions for three different frequencies.

As it was mentioned earlier, one of the important issues in designing the converter is its weight, and weight of the inductor has a direct impact on the total weight of the converter. Weight of the inductor in three different frequencies with Metglas magnetic alloy 2605SA1 as the core material is shown in the following

Table 4.4: The output filter inductor core dimensions for 500Hz, 1kHz and 2kHz operation frequencies

Operating frequency	$500Hz$	$1KHz$	$2KHz$
Core cross section[m^2]	0.16	0.09	0.04
Core window height[m]	0.15	0.15	0.2
Core window width[m]	0.4	0.35	0.35
Number of turns[m]	100	88	100
Air gap length[m]	0.053	0.047	0.053
Core losses[kW]	8.89	11.58	12.58
Winding losses[kW]	2.19	1.43	1.09

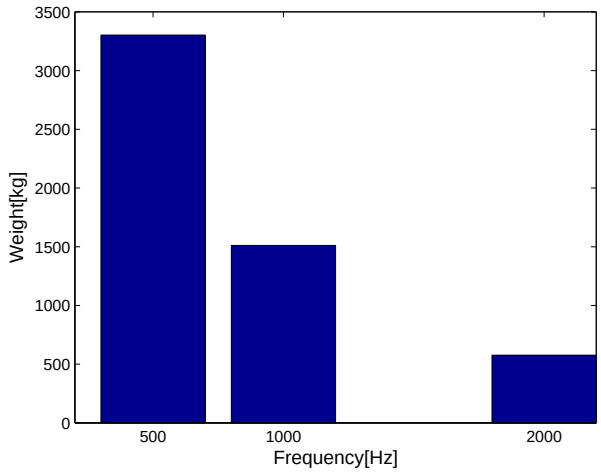

Fig. 4.10 Weight of the output filter inductor in 500Hz, 1kHz and 2kHz operating frequencies with Metglas magnetic alloy 2605SA1 as the core material

Since the shape and dimension of the core is known, the core volume can be calculated. By knowing the volume and the density of the core material, core weight can be calculated based on the following equation

$$W = V\rho \tag{4.22}$$

where W is the core weight, V is the volume of the core and ρ is the density of the core material.

As it can be seen in Fig.4.10, the weight of the inductor decreases by increase in the operating frequency. So it can be concluded that increase in frequency will reduce the size of the inductor as well as the costs of it.

4.4 Loss Calculation

4.4.1 IGBT and Diode Loss Calculation

In this section, the conduction and the switching losses for the selected IGBTs, freewheeling diodes and output diodes are calculated. The loss calculation is done for two different topologies and the results are shown in figures for comparison.

The losses for two different topologies will be calculated, the first case is in hard switching mode and the second case is in soft switching mode. For the hard switching mode, the IGBT losses consist of the conduction loss and the switching loss but for soft switching, only conduction loss is considered.

In the hard switching mode, the current and voltage waveforms of the IGBTs, and output diode are shown in Fig. 4.11 and Fig. 4.12. In these figures $\Delta t1$ is the current reversal time of the leakage inductance and t_b is the blanking time and Φ is the phase shift angle. The blanking time is defined to prevent the switches that are located in the same leg to be on simultaneously. According to these figures the value of the rms, average and peak of the currents and voltages are measured and the losses are calculated.

For the soft switching mode the switching loss for IGBT is neglected and conduction loss is calculated by considering the current wave form and IGBT characteristics. The waveforms of current and voltage of IGTBs and the output diodes in soft switching mode are shown in the Fig. 4.13 and Fig. 4.14.

The calculations are done in three different frequencies and the results for hard switching mode, are shown in Fig.4.11, Fig.4.12 and Fig.4.13. Actually, the switching loss increases by increasing the switching frequencies and in higher frequencies the total loss is dominated by the switching loss.

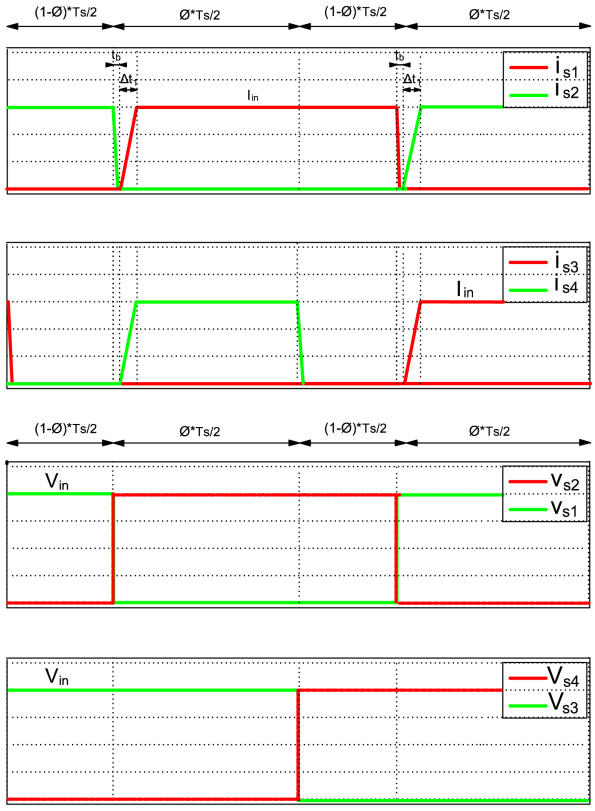

Fig. 4.11 Currents and voltages of IGBTs in hard switching mode

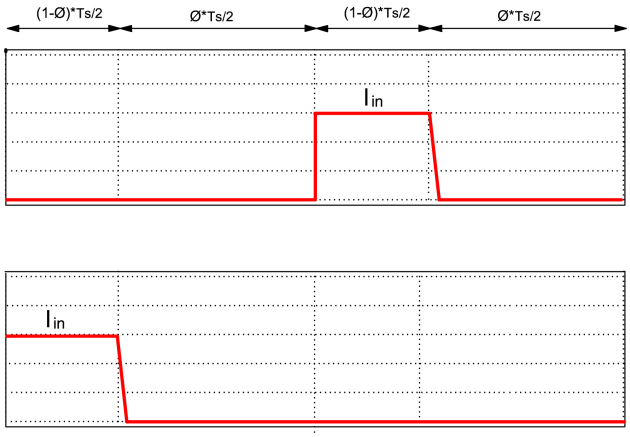

Fig. 4.12 Current and voltage of freewheeling diodes in hard switching mode

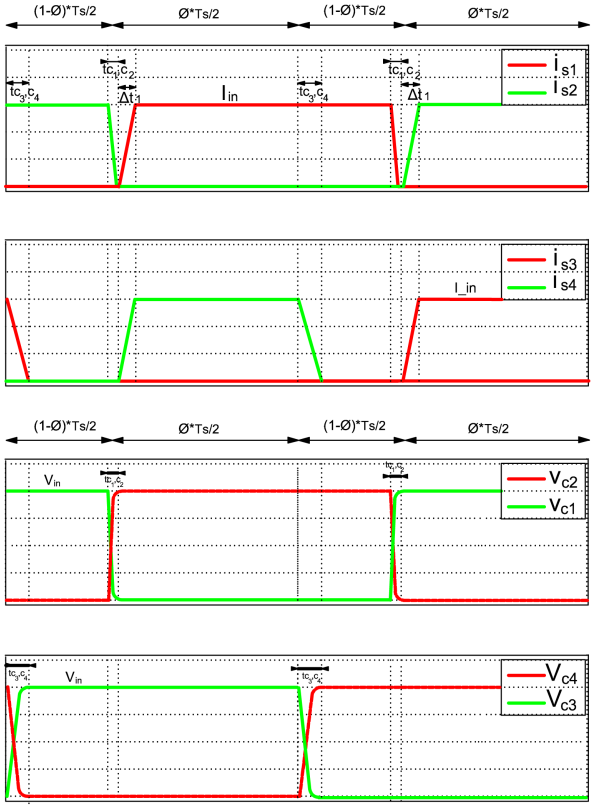

Fig. 4.13 Currents and voltages of IGBTs in soft switching mode

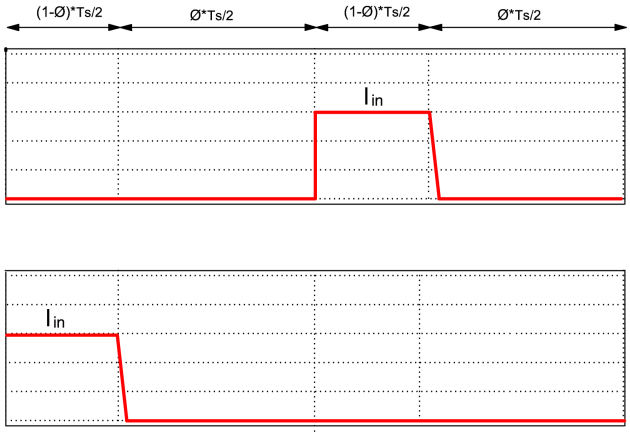

Fig. 4.14 Current and voltage of freewheeling diodes in soft switching mode

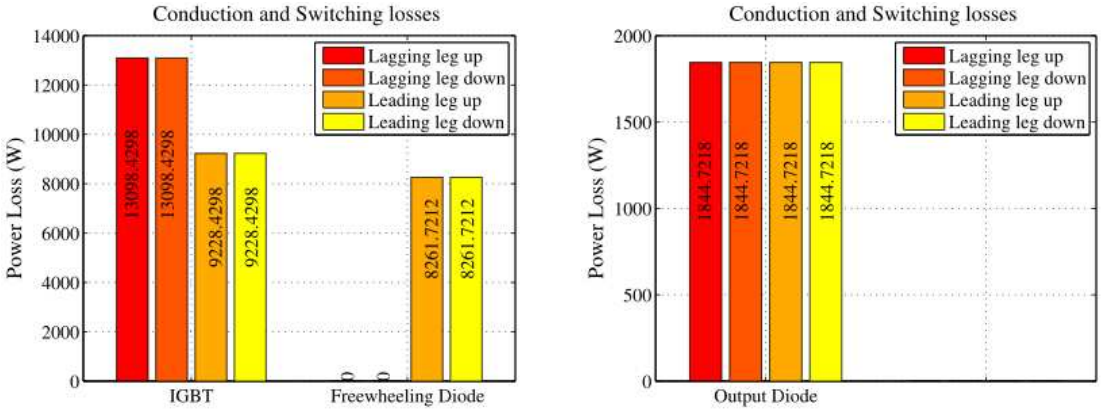

(a) IGBTs and freewheeling diodes losses (b) Output diodes losses

Fig. 4.15 IGBTs and diodes losses with 500 Hz switching frequency

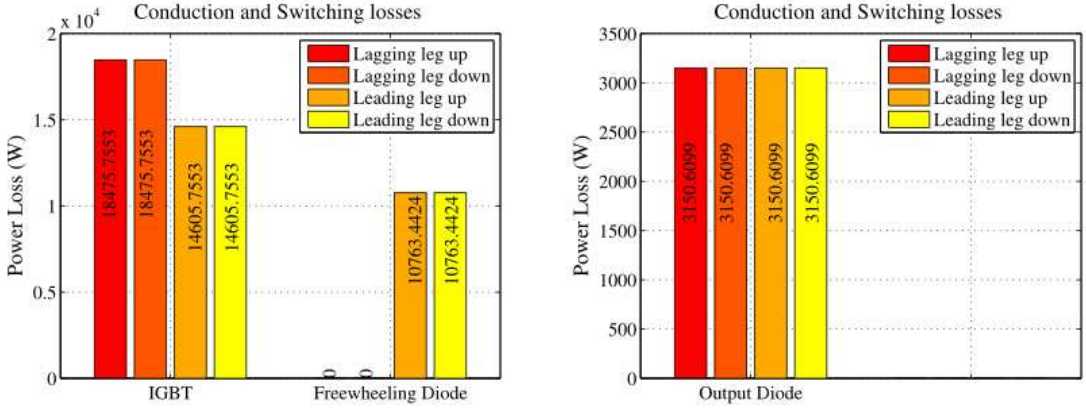

(a) IGBTs and freewheeling diodes losses (b) Output diodes losses

Fig. 4.16 IGBTs and diodes losses with 1000 Hz switching frequency

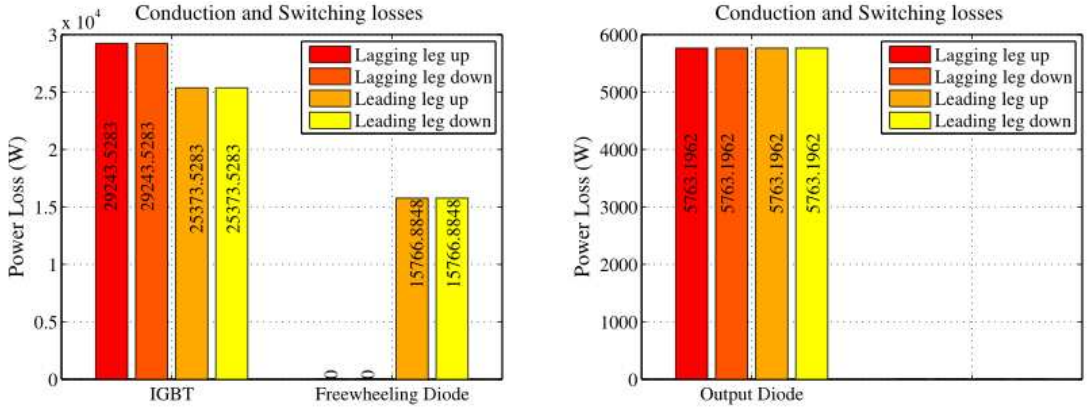

(a) IGBTs and freewheeling diodes losses

(b) Output diodes losses

Fig. 4.17 IGBTs and diodes losses with 2000 Hz switching frequency

The result of the soft switching loss calculations are shown in Fig.4.14, Fig.4.15, Fig.4.16.

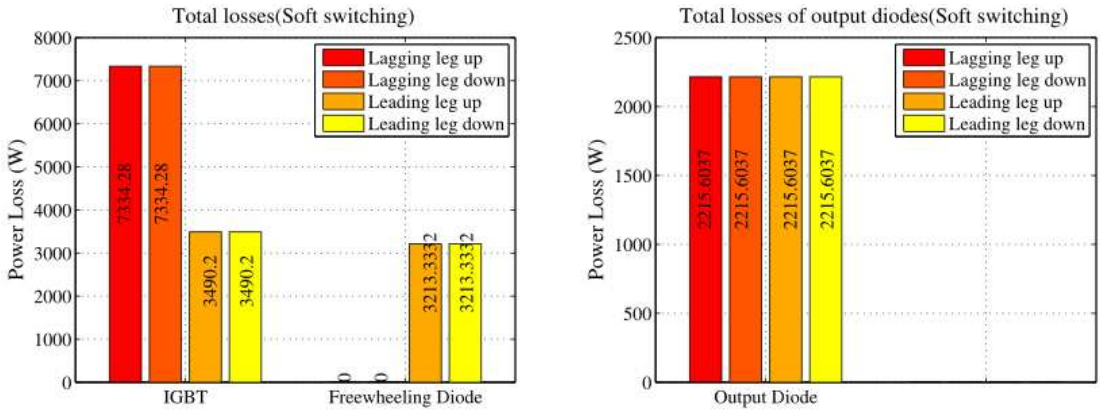

(a) IGBTs and freewheeling diodes losses (b) Output diodes losses

Fig. 4.18 IGBTs and diodes losses with 500 Hz switching frequency

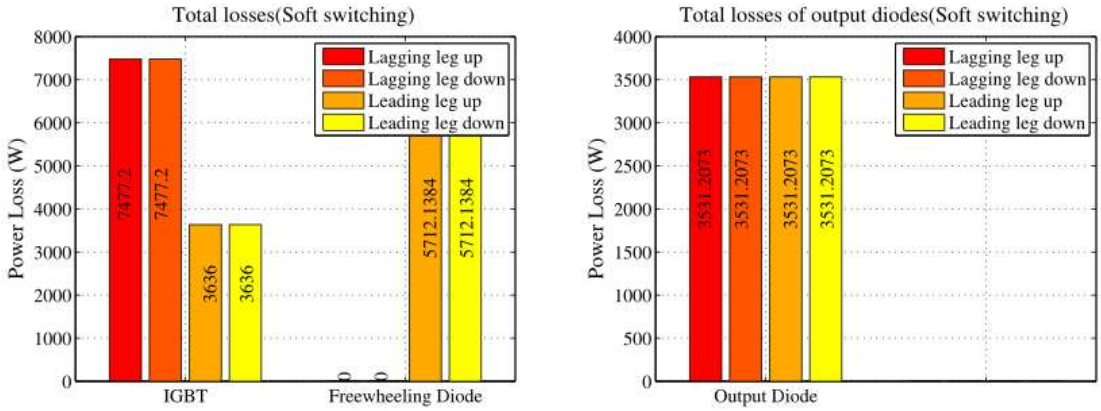

(a) IGBTs and freewheeling diodes losses (b) Output diodes losses

Fig. 4.19 IGBTs and diodes losses with 1000 Hz switching frequency

4.4.2 Transformer

The transformer design and its loss calculation is not the purpose of this thesis. However, losses and accordingly design of the transformer should be known in order to calculate the efficiency of the converter and make our two topologies comparable. In this section,

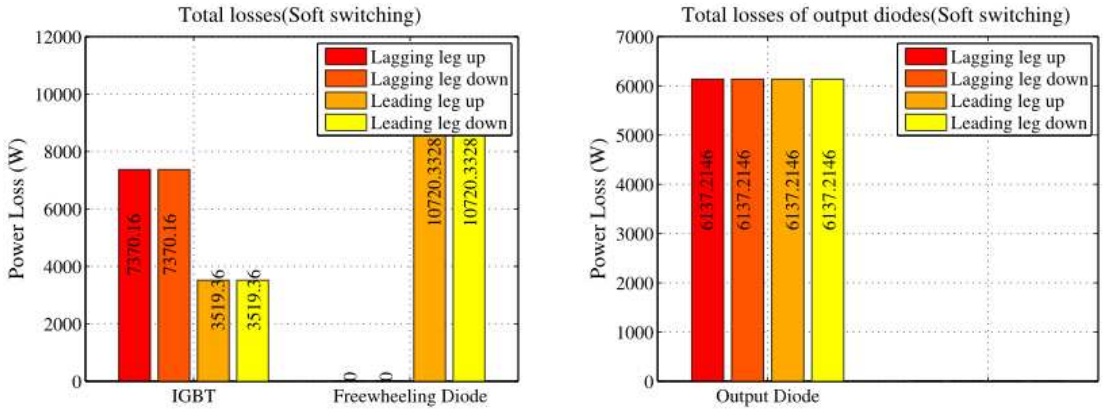

(a) IGBTs and freewheeling diodes losses

(b) Output diodes losses

Fig. 4.20 IGBTs and diodes losses with 2000 Hz switching frequency-

a short summery for different methods of loss calculation is mentioned and the results of the transformer design and transformer loss calculations are shown.

There are two kinds of losses in a core material, hysteresis losses and eddy current losses. Energy is required to make a change in the magnetization of a core material. Not all of this energy is recoverable in electrical form; a fraction is lost as heat. This power loss can be observed electrically as hysteresis of the B-H loop. A current will be induced in the core materials with electric conductivity, which is called eddy current. This current dissipates power in the core, so there is another core loss that is called eddy current losses.

Core Loss Calculation Methods

There are several empirical and macroscopic loss calculation methods that can be found in literatures. Some of these methods are:

- Loss separation method: This method calculates the total core losses by calculating the static hysteresis loss and the dynamic eddy current loss which includes classic eddy current loss and excess eddy current loss separately.
- Equivalent Elliptical Loop Approach: Is one kind of loss separation methods than can be used in finite element Ansys Maxwell 3D for core loss calculation.
- Empirical Steinmetz Equations: This method is the most convenient method to use by designers, because it needs a limited number of measurements and it does not need much knowledge about magnetism.

The model and simulation procedure in order to calculate the core dimensions and core loss is the same procedure as [15]. In this procedure, three kind of parameters in the model: system specifications, free parameters and design parameters are defined. First of all, the required parameters from system point of view including primary and secondary voltages, rated power, operating frequency should be specified. The second group of parameters, free parameters, can be selected and varied. Maximum flux density and number of turns in the primary winding are the examples of these group of parameters. At the end, the design parameters include the geometrical values like core and windings dimensions can be calculated from the other two groups parameters. A C-shaped core is selected for the transformer in our converter, Fig. 4.21 shows the geometry of the transformer and its core. Core loss is calculated by using the loss separation method as [15]. Specifications of the transformer and its core loss and winding loss are shown in table 4.21 for three different frequencies. It should be noticed that the ratio of the transformer was considered to be 3.

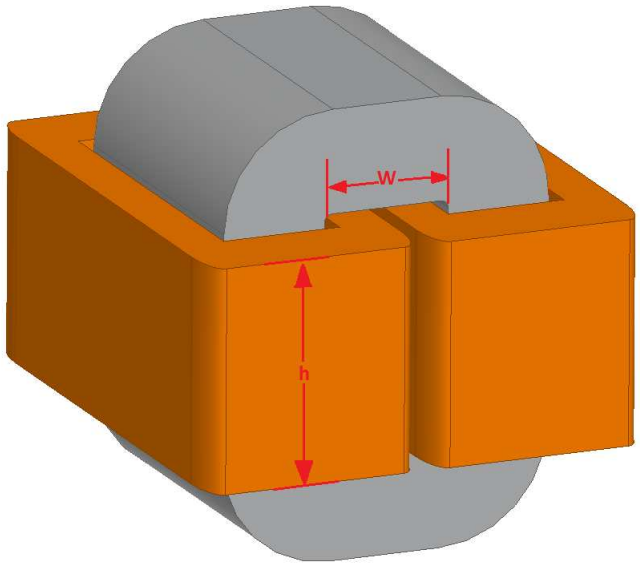

Fig. 4.21 Transformer geometry

To achieve the highest efficiency, the winding losses have been assumed to be equal to core loss, (4.23) shows that core losses should be equal to winding losses in order to have the highest efficiency [13].

$$\eta = \frac{P_{out}}{P_{out} + P_{core} + P_{winding}} \quad , \quad P_{winding} = kP_{out}^2 \tag{4.23}$$

$$\frac{d\eta}{dP_{out}} = 0 \quad gives \quad P_{winding} = P_{core} \tag{4.24}$$

Table 4.5: Specifications of designed transformer for different frequencies

Frequency	500 Hz	1 kHz	2 kHz
Phase Shift	0.5	0.5	0.5
Input Voltage $[V]$	4000	4000	4000
Cross Section $[m^2]$	0.15	0.07	0.03
Window Height $[mm]$	98.99	148.49	197.98
Window Width $[mm]$	386.88	311.52	311.52
Core Losses $[kW]$	7.42	10.31	15.42
Core Weight $[kg]$	2429.02	991.5	452.13
Leakage Inductance $[\mu H]$	20.91	14.43	8.94

Fig. 4.22 shows the distribution of the flux density in transformer core.

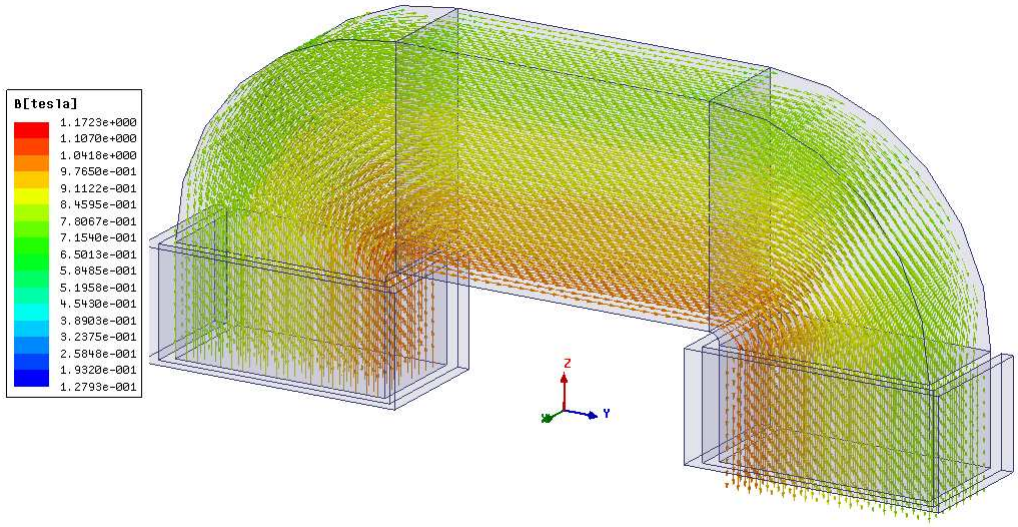

Fig. 4.22 Flux density distribution in transformer core

4.4.3 The Output Filter Inductor

There are two kinds of losses in the magnetic components like the inductors and the transformers. One of them is core losses and another on is the winding losses. In section 4.2.1, the core losses types and their origin was discussed. In this section, the principle of core loss and winding loss calculations will be explained and the total losses for the inductors designed in the previous section will be calculated.

$$P_{total} = P_{cu} + P_{core} \tag{4.25}$$

where P_{cu} is the copper losses and P_{core} is the core losses. Copper losses can be calculated using the following equation

$$P_{cu} = RI_{rms}^2 \tag{4.26}$$

where I_{rms} is the rms current that passes through the inductor and R is the resistivity of the winding wire that can be calculated like following

$$R = \frac{\rho n(MLT)}{A_W} \tag{4.27}$$

where $\rho = 1.68e-8\ \Omega.m$, n is the number of turns, MLT is the mean length turn and A_W is the wire cross section.

Some manufacturers like Metglas has provided their own formula for core loss calculations. From [16] the core losses can be calculated as

$$P_{core} = 6.5 f^{1.51} B^{1.74} W \tag{4.28}$$

where f is the frequency in kHz, B is the flux density and W is the weight of the core. Based on the above explanation, values of the core losses and the winding losses of the output filter inductor would be like the following

Table 4.6: The output filter inductor core losses for 500Hz, 1kHz and 2kHz operation frequencies

Operating frequency	$500Hz$	$1KHz$	$2KHz$
Core losses[kW]	8.89	11.58	12.58
Winding losses[kW]	2.19	1.43	1.09
Total losses[kW]	11.08	13.01	13.67

4.5 Comparison and total results

4.5.1 Comparison between semiconductor losses

In this section, the semiconductor losses of two mentioned converters are compared. As it was shown before, the losses are calculated in three different switching frequencies. Fig. 4.24 and fig. 4.25 show the total losses of the semiconductor devices in the converter in hard-switched and soft-switched mode, respectively.

In the hard-switched mode, by increasing the switching frequency the semiconductor losses are dominated by switching losses. But in the soft-switched mode the switching losses of the IGBT are almost zero in three different frequencies. Consequently, the total loss variation between hard-switched mode and soft-switched mode is increased by increasing the switching frequency as is shown in fig. 4.26.

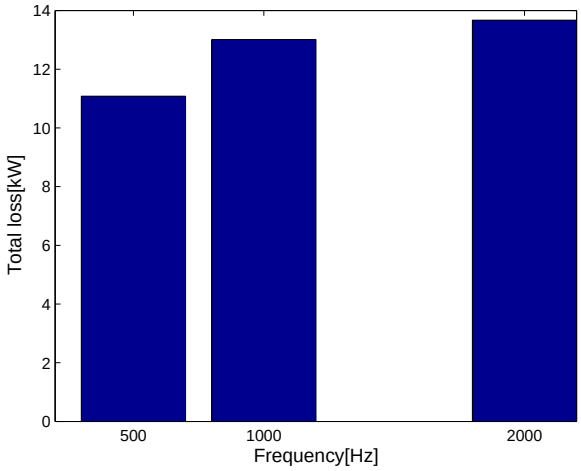

Fig. 4.23 Total losses of the output filter inductor in 500Hz, 1kHz and 2kHz operating frequencies

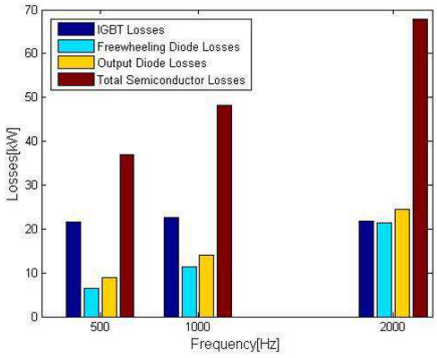

Fig. 4.24 The semiconductor losses in hard-switched mode for three different frequencies

4.5.2 Comparison Between Converter Magnetic Components

In this section, losses and weight of the converter magnetic components(transformer and the output filter inductor) will be compared in the three operation frequencies. It is expected that the size of the components reduce by the increase in the frequency but at the same time, the losses of them should be increased. The following figures show this fact

4.5.3 Total Efficiency of the Converter

In this part, the total efficiency of the converter in three different frequencies for both mentioned topologies are calculated. From the previous sections, the losses of the IGBTs, freewheeling diodes and output diodes have been calculated and the losses were shown in Section 4.2. Also the losses of the transformer were shown in table4.5. So, the total

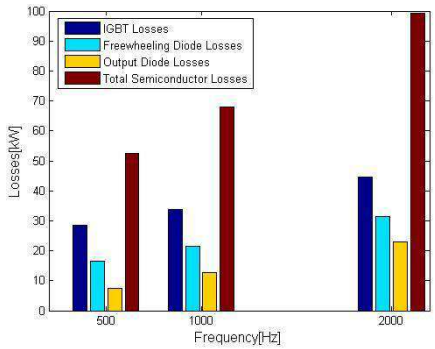

Fig. 4.25 The semiconductor losses in soft-switched mode for three different frequencies

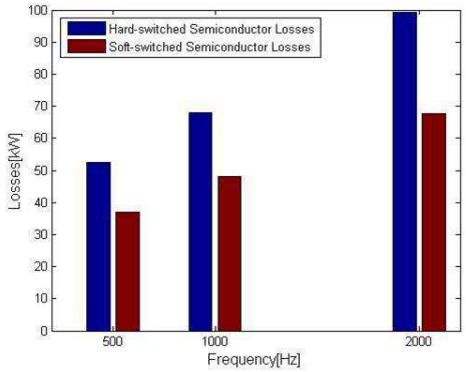

Fig. 4.26 Caparison between the semiconductor losses in hard-switched and soft-switched mode

efficiency of the converter for the hard switched topology and the zero-voltage switching topology would be as it is shown in Table 6.1 and Table 6.2 respectively.

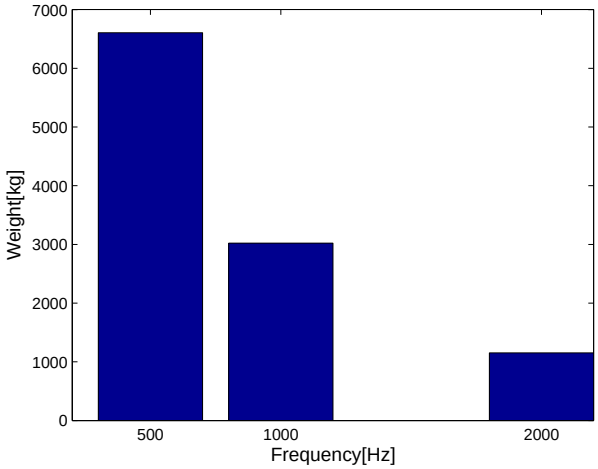

Fig. 4.27 Total weight of the converter magnetic components in 500Hz, 1kHz and 2kHz operating frequencies

Table 4.7: Total losses and efficiency of the converter, hard-switching mode

switching frequency	$500Hz$	$1KHz$	$2KHz$
IGBTs losses[W]	$28.48e3$	$33.83e3$	$44.56e3$
Freewheeling diodes[W]	$16.52e3$	$21.52e3$	$31.53e3$
Output diodes[W]	$7.37e3$	$12.6e3$	$23.05e3$
Transformer losses[W]	$14.8e3$	$20.6e3$	$30.8e3$
Inductor losses[W]	$11.08e3$	$13.01e3$	$13.67e3$
Total losses[W]	$75.25e3$	$101.56e3$	$143.61e3$
Efficiency[$\%$]	96.8	95.7	94.01

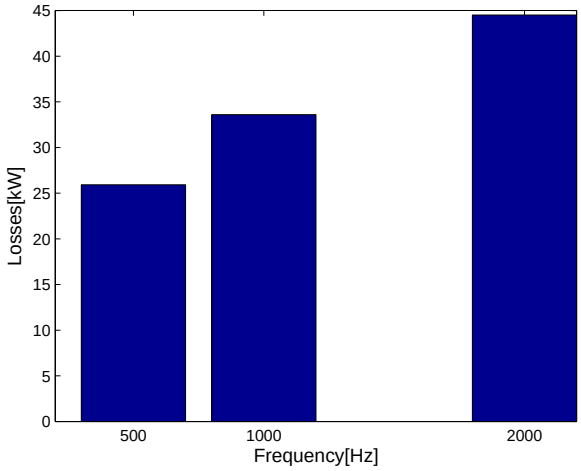

Fig. 4.28 Total loss of the converter magnetic components in 500Hz, 1kHz and 2kHz operating frequencies

Table 4.8: Total losses and efficiency of the converter, soft-switching mode

switching frequency	$500Hz$	$1KHz$	$2KHz$
IGBTs losses[W]	$21.64e3$	$22.7e3$	$21.77e3$
Freewheeling diodes[W]	$6.42e3$	$11.42e3$	$21.44e3$
Output diodes[W]	$8.86e3$	$14.12e3$	$24.54e3$
Transformer losses[W]	$14.8e3$	$20.6e3$	$30.8e3$
Inductor losses[W]	$11.08e3$	$13.01e3$	$13.67e3$
Total losses[W]	$62.8e3$	$81.85e3$	$98.55e3$
Efficiency[$\%$]	97.3	96.58	95.32

Chapter 5

Simulation Setup

In this chapter, two topologies of the DC-DC converter are simulated, the fullbridge converter in hard switch mode and the fullbridge converter with phase shifted control. Also the results of simulation are presented in this chapter. The simulations are done in MATLAB.

5.1 Fullbridge Converter

In the simulation of the fullbridge converter, it is assumed that all the devices operate ideally and no losses are considered. The internal resistance of the IGBTs and the diodes are set very low. For the transformer, the magnetizing resistance and magnetizing inductance are set very large, and the resistance and inductance of the transformer winding is considered to be negligible. The switching method of IGBTs is phase shift control that was explained in Chapter 2. Fig. 5.1 shows the simulation setup for the fullbridge converter:

In these topologies, the inductance and capacitor of the output filter are calculated based on the allowed ripples of the output current and the output voltage. For this purpose, the formulas for calculation of the inductor and capacitor are written in an M-file and the results are used in simulation file. In the simulation the ripple values are limited to

$$\begin{aligned} I_{ripple} &= 0.1 Iload \\ V_{ripple} &= 0.01 Vout \end{aligned} \tag{5.1}$$

For load calculation, the power and the output voltage of the converter should be considered, then the output resistance R is calculated as

$$R = \frac{Vo^2}{Po}. \tag{5.2}$$

To investigate the operation of the fullbridge converter, the present characteristics are applied in the simulation

- $V_i = 4000$ (Input voltage)
- $V_o = 6000$ (Output voltage)
- $P_o = 2.4e6$ (Output power)
- $I_{oripple} = 0.1$ (Maximum allowed current ripple)
- $V_{oripple} = 0.01$ (Maximum allowed voltage ripple)
- $F_{sw} = 1000$ (Switching frequency)
- $n = 3$ (Transformer ratio)

According to the input and output voltage and the ratio of the transformer, the phase shift angle would be 0.5. However, because of blanking time and voltage drop over the leakage inductance it should be slightly larger. The defined pulse generated that are used for turning on and turning off the IGBTs are shown in Fig.5.2.

The wave form of the input current, the input voltage, the output current and the output voltage of the converter are shown in Fig.5.3

The voltage wave formes of the primary and secondary side of the transformer are square wave form and are changed with transformer ration, these voltages are shown in Fig.5.4.

The current in the primary side and secondary side of the transformer is shown in Fig.5.4. It is seen that the waveforms are not absolutely square-wave, which is due to the leakage inductance of the transformer.

By using the pulse generators, the IGBTs are turned on and turned off. In some intervals the current goes through two IGBTs and in some other intervals current goes through one IGBT and one diode. In this topology, two diodes that are in parallel with the IGBTs 1 and 2 are never used, but the other diodes that are in parallel with IGBT 3,4 conduct when one switch is turned off. The currents and the voltages of the IGBTs in two periods, are shown in Fig.5.5.

The output current and the output voltage are DC with some ripples. Fig.5.6 shows the waveforms of the output current and the output voltage. Ripples of the current and the voltage should be limited to 0.1 and 0.01 respectively. By calculation the needed inductor and capacitor the ripples are in the allowed margins as it is shown in Fig.5.6.

The second configuration is the phase shift control converter. As it is shown in Fig. 5.7, the turn-off snubber circuit is placed in parallel with the IGBTs, L_s is the leakage inductance of the transformer plus additional inductance which has been calculated in REF to achieve soft switching.

Waveforms of the voltage and current in both side of the transformer, in the phase shift topology, are shown in Fig.5.8.

In this topology, by using snubber capacitors the switching losses are eliminated. The current waveforms of the IGBTs and the voltage waveform of the the capacitors are shown in Fig.5.9. In this topology, when the IGBTs are turned on, the voltage of their parallel capacitance reaches zero and then there are no turn-on switching losses, and when they are turned off their voltage increase based on charging of the parallel capacitors. As a result, the switching losses in this case are neglected.

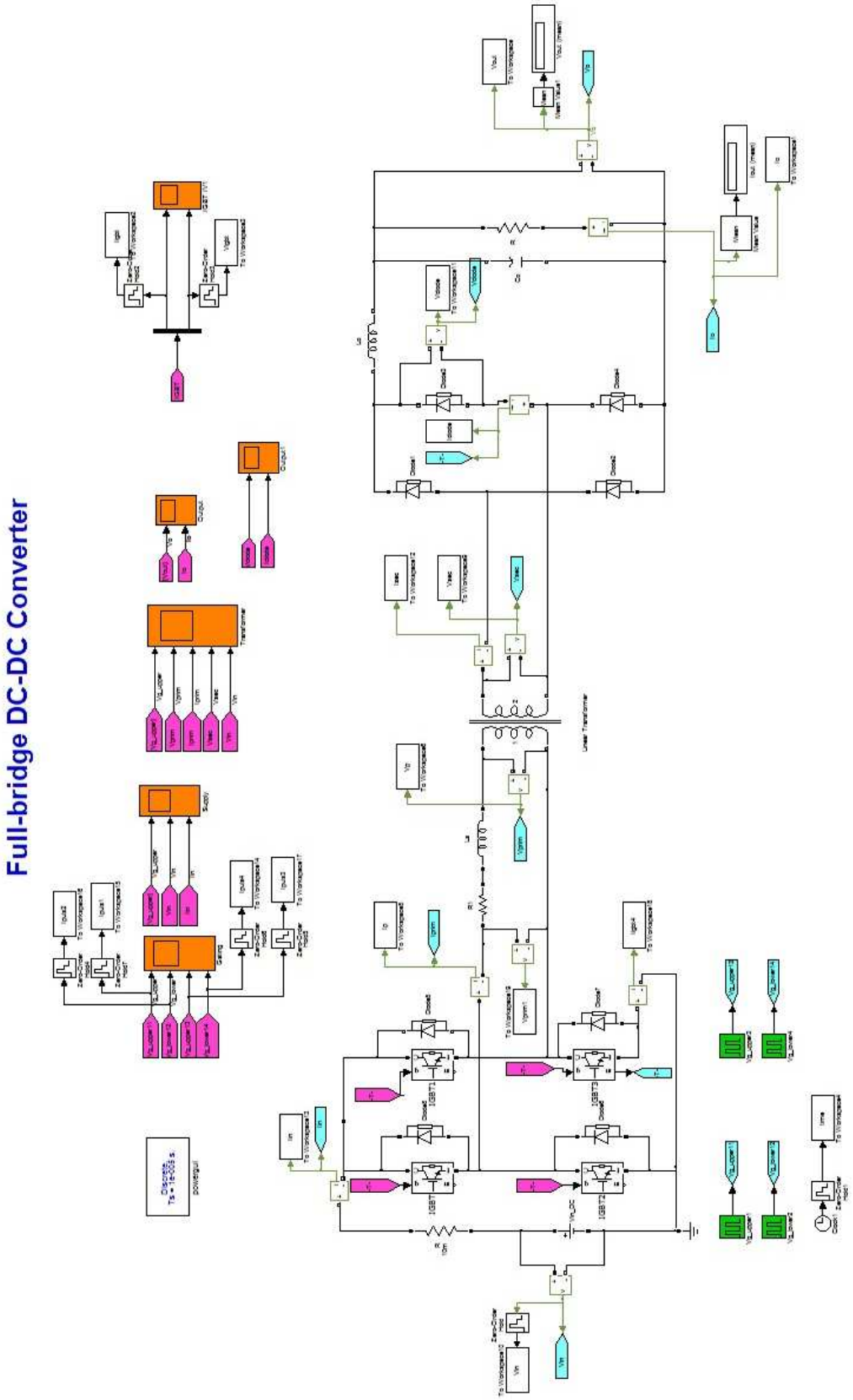

Fig. 5.1 Fullbridge converter conFiguration in MATLAB

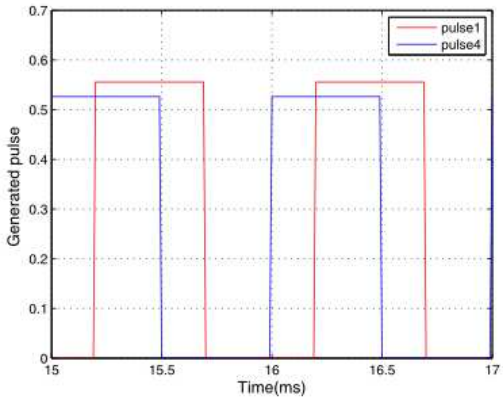

(a) Generated pulses for IGBT 1 and IGBT 2

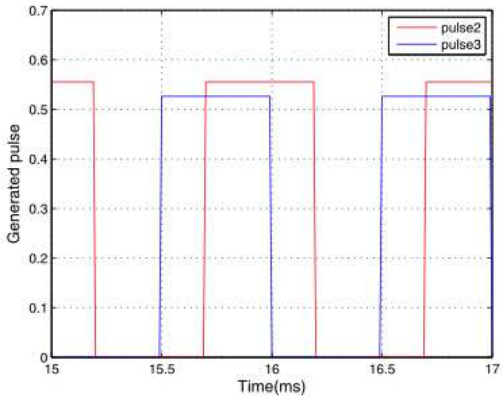

(b) Generated pulses for IGBT 3 and IGBT 4

Fig. 5.2 Generated pulses for the IGBTs

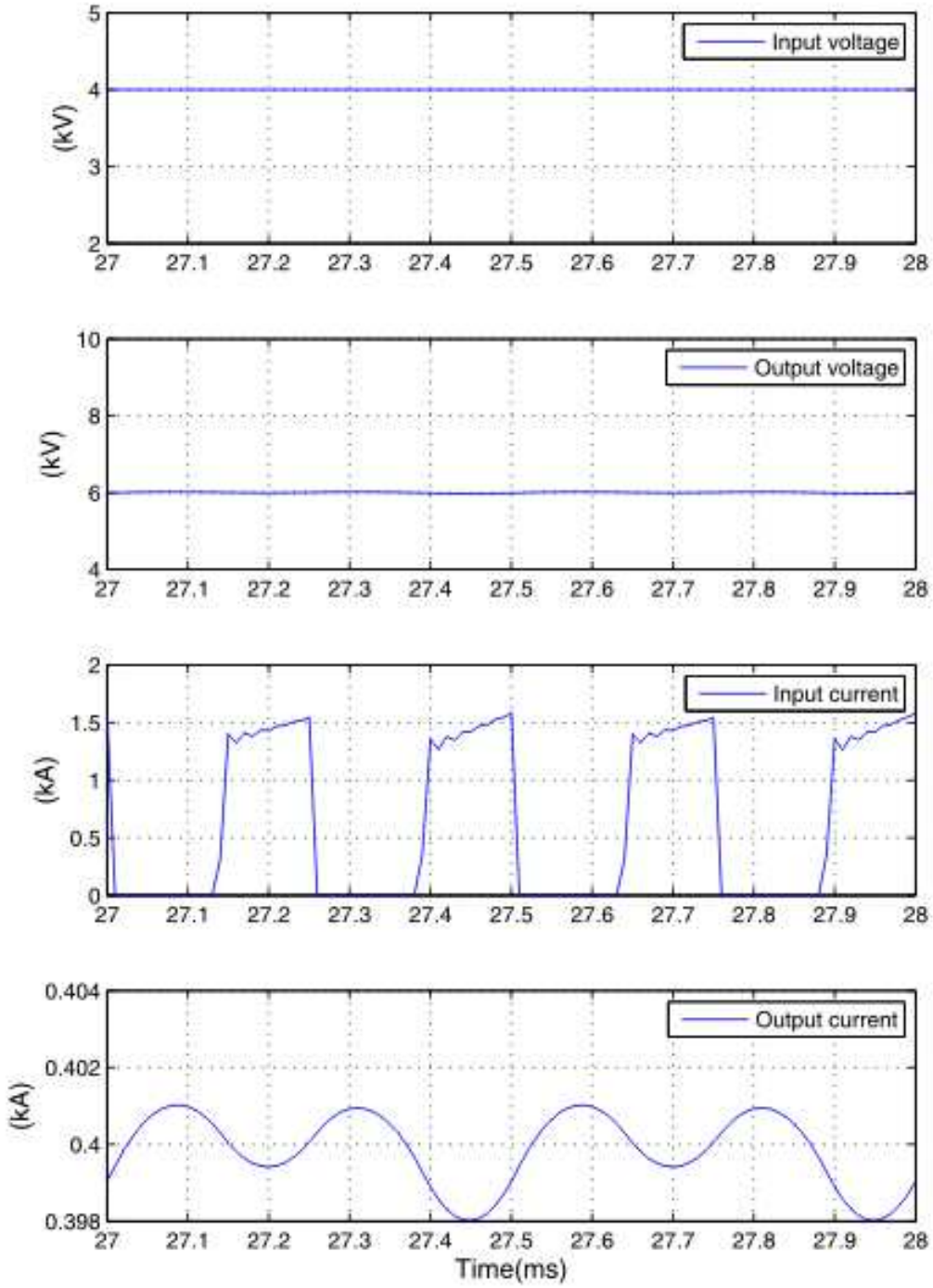

Fig. 5.3 Input and output waveforms of the converter

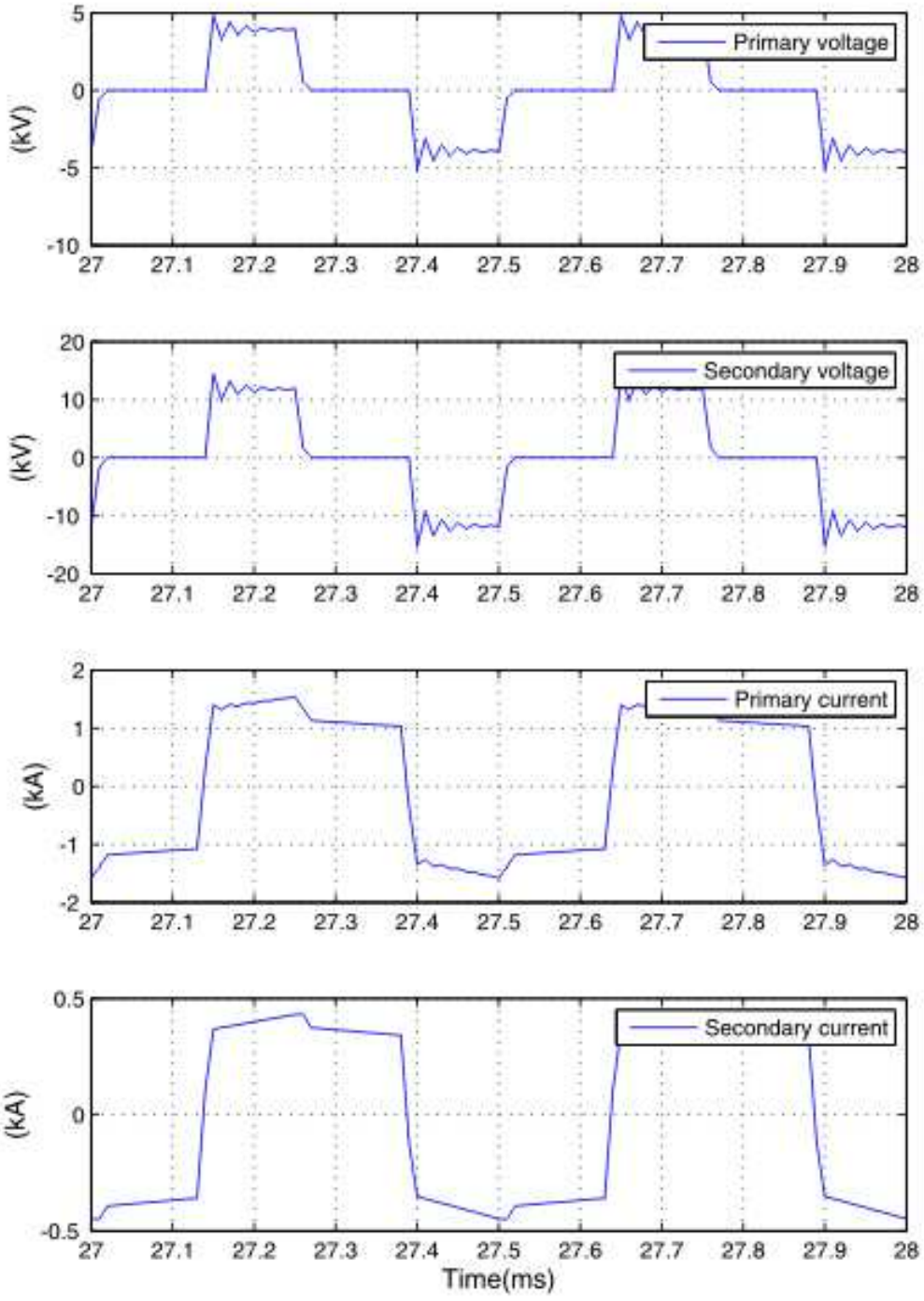

Fig. 5.4 Voltage and current of the transformer

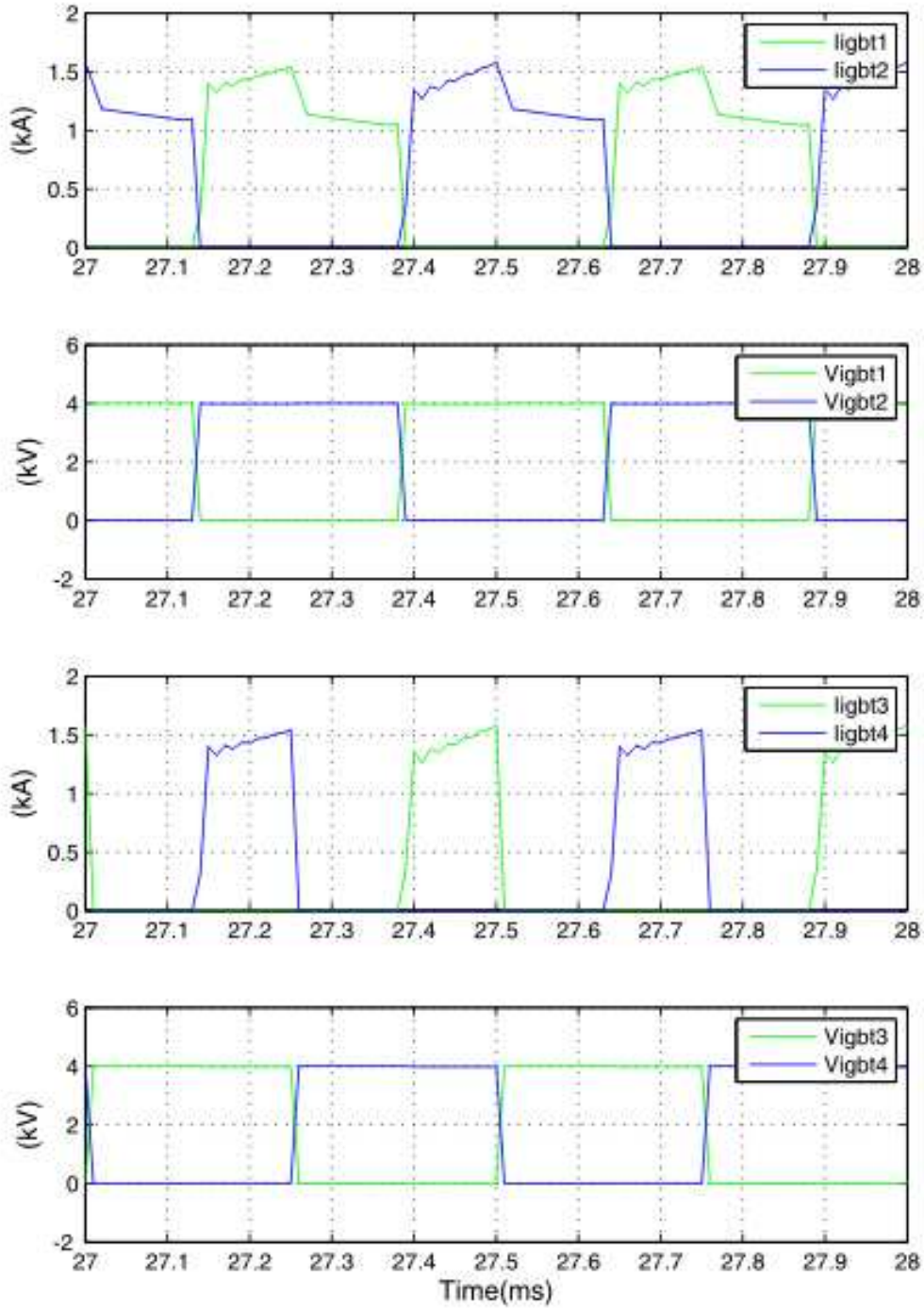

Fig. 5.5 IGBTs current and voltage waveforms

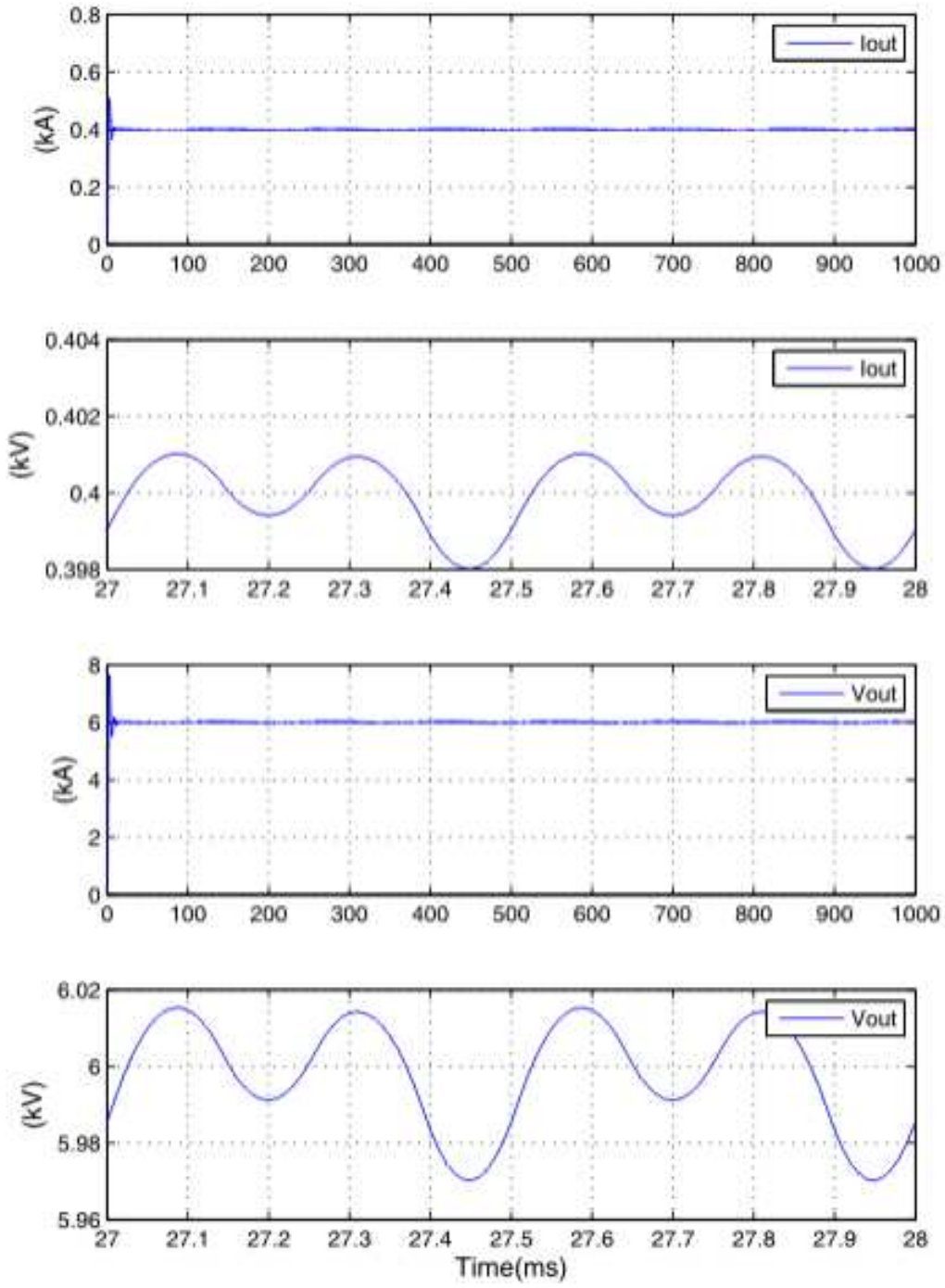

Fig. 5.6 The output current and voltage and their ripples

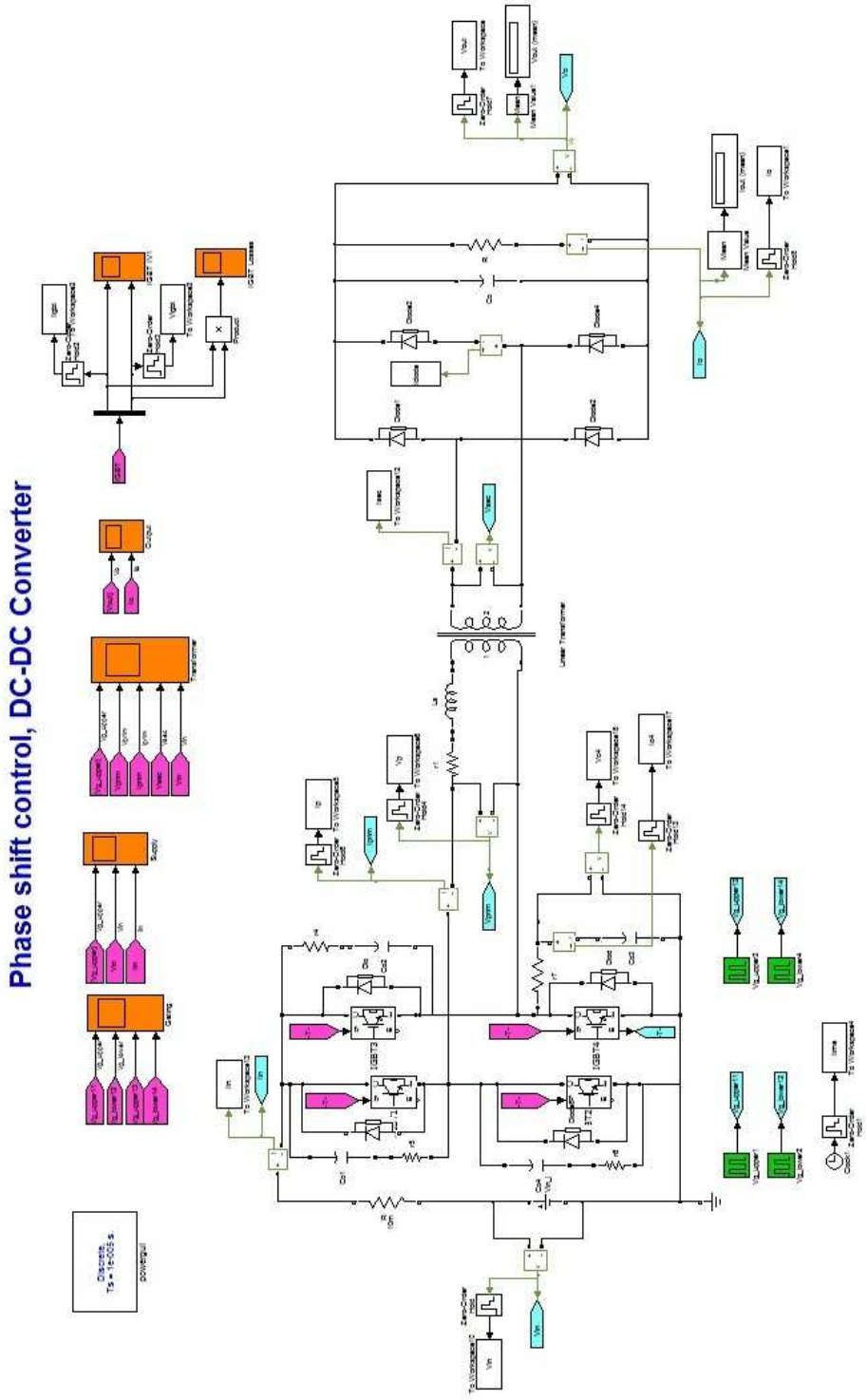

Fig. 5.7 Phase shift control DC-DC converter

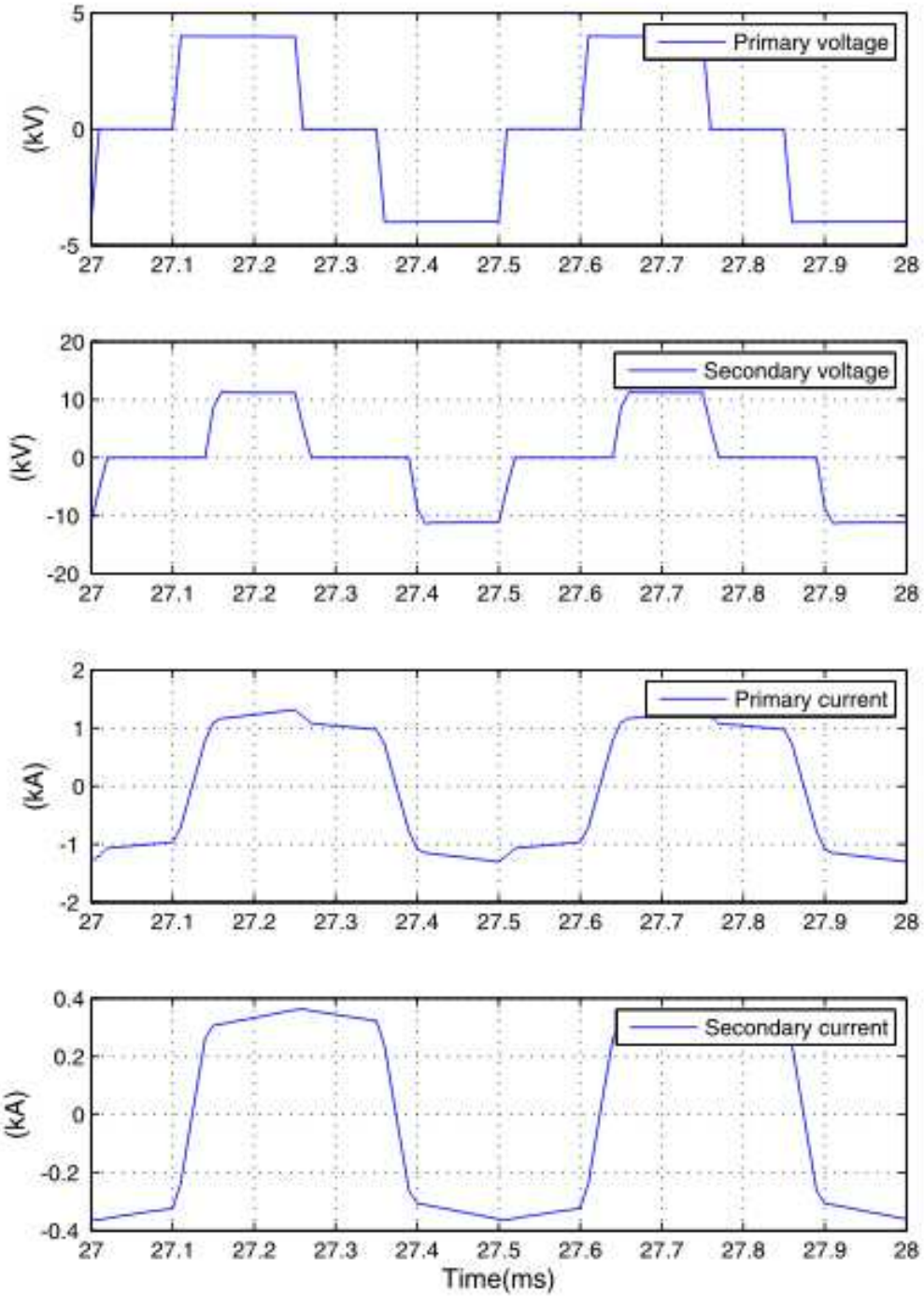

Fig. 5.8 The voltages and the currents of transformer-soft switching

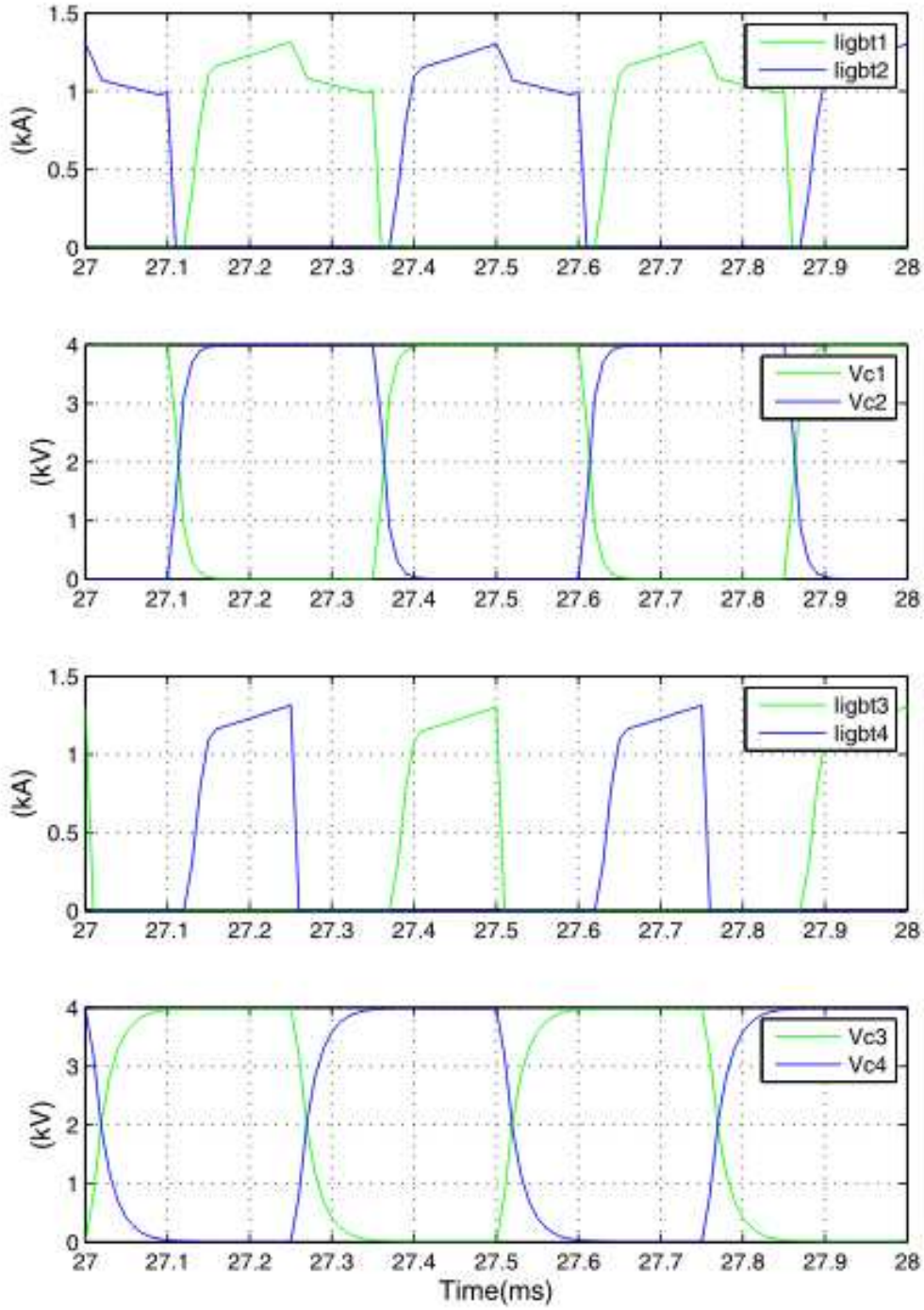

Fig. 5.9 The IGBTs current and the capacitors waveforms-Soft switching

Chapter 6

Conclusions and Future Work

In this chapter, results from the present work is summarized. Also, some suggestions for the future work is given.

6.1 Results from Present Work

In this thesis, different topologies for the DC-DC converter have been investigated and two of them is selected to design, simulate and evaluate. The selected topologies are the hard-switched fullbridge converter and the fullbridge converter with phase-shift control. These two topologies has been evaluated regarding their efficiencies at the different switching frequencies.

The mentioned hard switched and a zero-voltage switching full bridge converter are compared in terms of their losses. Loss evaluation is done for all the switches in the converter as well as for the magnetic components of the converter (transformer and the output filter inductor). Another key point in this thesis is to manage and utilize converter parasitics to achieve soft switching for different load conditions. So, the issue of the snubber design was another important issue during our work.

Based on the design and analysis of both hard and soft switching schemes of the high power density DC-DC full bridge converter, it has been concluded that since for the lower frequencies the efficiency is almost the same for the two topologies, hard switched is preferable due to the lower cost. However, for the higher frequencies where the total losses are dominated by the switching losses, the soft switched topology is superior. The core loss of the transformer which was exposed to high frequency square wave excitation has been calculated by using FEM simulation and it turns out that the transformer contribution of the total converter loss is about 30% for all three studied frequencies for the phase shift converter.

In the following the circuit diagram of the compared topologies are presented. Also, the type of the selected switches in the input bridge and the output bridge are shown. In addition, the total loss of the converter and the weight of the magnetic components of the converter are mentioned.

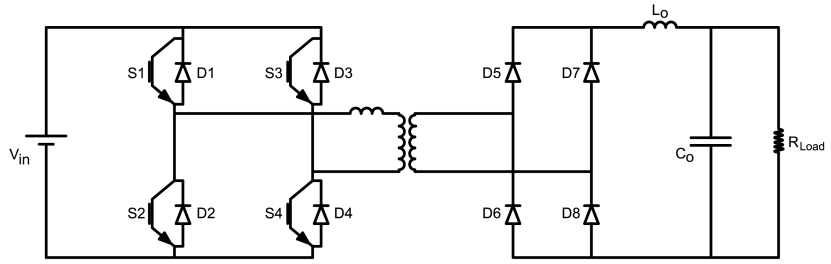

Fig. 6.1 First topology, hard-switched

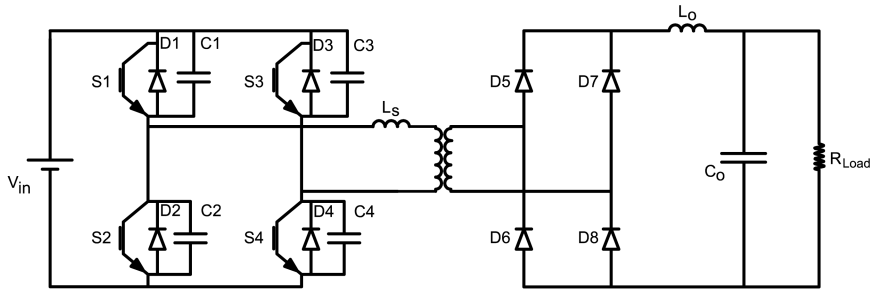

Fig. 6.2 Second topology, soft s-switched

Table 6.1: Total losses and efficiency of the converter, hard-switching mode

switching frequency	$500Hz$	$1KHz$	$2KHz$
IGBTs losses[W]	$28.48e3$	$33.83e3$	$44.56e3$
Freewheeling diodes[W]	$16.52e3$	$21.52e3$	$31.53e3$
Output diodes[W]	$7.37e3$	$12.6e3$	$23.05e3$
Transformer losses[W]	$14.8e3$	$20.6e3$	$30.8e3$
Inductor losses[W]	$11.08e3$	$13.01e3$	$13.67e3$
Total losses[W]	$75.25e3$	$101.56e3$	$143.61e3$
Efficiency[$\%$]	96.8	95.7	94.01

According to the voltage and current of the switches, different arrangement of the IGBTs can be defined . For this application, the IGBT module $5SNA0650J450300$ is selected. In this module when the current is $650A$ (half of this current value is allowed as maximum rms current) the collector emitter voltage can be $2800V$. For the output bridge the diode $5SLD0600J650100$ is selected from the ABB HiPak series. This diode module can

Table 6.2: Total losses and efficiency of the converter, soft-switching mode

switching frequency	$500Hz$	$1KHz$	$2KHz$
IGBTs losses[W]	$21.64e3$	$22.7e3$	$21.77e3$
Freewheeling diodes[W]	$6.42e3$	$11.42e3$	$21.44e3$
Output diodes[W]	$8.86e3$	$14.12e3$	$24.54e3$
Transformer losses[W]	$14.8e3$	$20.6e3$	$30.8e3$
Inductor losses[W]	$11.08e3$	$13.01e3$	$13.67e3$
Total losses[W]	$62.8e3$	$81.85e3$	$98.55e3$
Efficiency[$\%$]	97.3	96.58	95.32

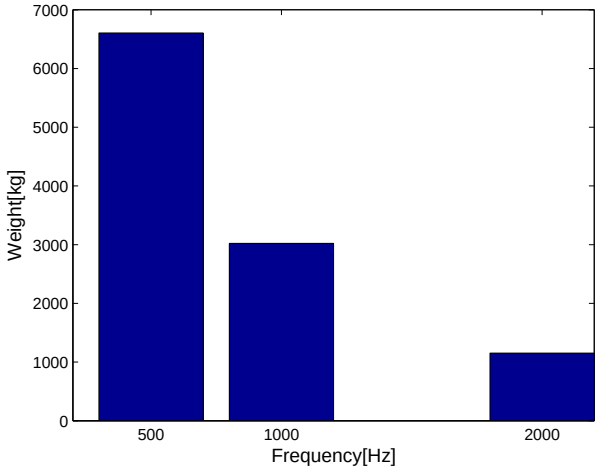

Fig. 6.3 Total weight of the converter magnetic components in 500Hz, 1kHz and 2kHz operating frequencies

handle $3600V$ reverse voltage and $600A$ forward current, but only half of this current is a suitable choice.

6.2 Future Work

As it was mentioned in the Chapter 2, there are different topologies for the DC-DC converters. In this thesis, two of them are selected and compared. It is a good idea to make a comparison of other topologies like the single active bridge converter, dual active bridge converter and etc.

There are two general methods to achieve zero-voltage and soft switching. One of them is by using resonant switch converters, which is the selected topology in this thesis. Another one is to achieve soft switching by using load resonant converter. A worthy further investigation is to compare these two resonant converters in terms of their losses, needed components, costs and complexity.

Since these converters need to be operated in different load conditions, a suitable topology to achieve soft switching in a wide range of the load conditions is a semi-soft fullbridge converter which is mentioned in chapter 4. A comparison between semi-soft and soft topology can be another interesting topic for research.

Since for these kind of investigations the switching transient is very important for the purpose of loss calculations and circuit operation, the software for doing the simulations should have precise and real model of switches (IGBTs, diodes and etc). Our suggestion is to use ANSOFT Simplorer for these kind of simulations.

Chapter 7

Appendix

7.1 Paper

Performance and Loss Evaluation of a Hard and Soft Switched 2.4 MW, 4 kV to 6 kV Isolated DC-DC Converter for a Wind Energy Application

M. Mobarrez, M. Fazlali, M. A. Bahmani and T. Thiringer
Division of Electric Power Engineering, Chalmers University of Technology, SE 41296, Gothenburg, Sweden
E-mail: mobarrez@student.chalmers.se

***Abstract* - In this paper, a hard switched and zero-voltage switching full bridge converter for high power applications are compared in terms of their losses. The important issue in designing these kinds of converters is to manage the converter parasitics. Moreover, evaluating the losses at the high frequency transformer with square wave input is another critical point in designing such a high power density converter. The proposed full bridge converters are designed to convert 4 kV input voltage to 6 kV with rated power of 2.4 MW. The comparison is done for three different frequencies: 500 Hz, 1 kHz and 2 kHz. Also, the simulation results and loss calculations are presented.**

Keywords - phase shift control, switching losses, DC-DC full bridge converter, zero-voltage switching, high power density transformer

I. INTRODUCTION

There is an increasing interest during recent decades for integrating renewable energies into power grids. Usually the distance between generation and consumption of the renewable energies is large, so transmission of the generated renewable energies with the AC system is not economic and DC system is used instead. Therefore, nowadays DC grid networks are becoming more popular and high power density DC-DC converters are one of the main components of these grids. One of the challenges for designing the high power density DC-DC converters is to reduce the weight and the volume of the magnetic components which are the bulkiest part of any conversion system. In order to make it more compact, one can increase the operating frequency, something already used in low power applications. But recently it is getting more popular to use higher frequency at high power applications due to the development of semiconductor devices such as IGBTs which can handle higher power densities with faster switching schemes. Increasing the operating frequency on one hand decreases the weight and size of the transformer and will lead to a compact design, and on the other hand the losses and especially the loss densities will be higher. Therefore a precise loss calculation is needed, particularly when the excitation is not sinusoidal [1-2].

Although there are several studies in comparison between different converter topologies, but most of them are for the half bridge topologies [3] and low powers in the range of some tens of kilowatts [4].

The aim of this paper is to compare a hard switched and a zero-voltage switching full bridge converter in terms of their losses. Loss evaluation is done for all the switches in the converter as well as the losses in the high frequency transformer with square wave input. Another key point in this paper is to manage and utilize converter parasitics to achieve soft switching. So, the issue of snubber design would be another scope of this paper.

There is no modification in the hard switch full bridge converter with duty cycle control to control the losses in the switches. Therefore there is a high switching loss in the input bridge switches, however low inductance in primary side of the transformer would prevent the high duty cycle losses. By replacing the duty cycle control with phase shift control, the switches on the lagging leg can be turned on with zero power dissipation. However, the conduction loss of the freewheeling diode will be added to the total losses.

In the full bridge converter with phase shift control, the switching losses reduce but still the conduction losses of the switches are high since the full current passes through the switches for relatively long time. By delaying the switching between the two legs of the converter the power through the converter can be controlled. The switching characteristics of these two legs are very different, so managing parasitic components of the converter is an important issue in converter design. Another important design criterion of the zero-voltage switching full bridge converter (ZVSFB) is the selection of the snubber capacitors for the leading and the lagging leg. In order to achieve soft switching in wide range of the load, these parameters should be calculated carefully.

The high frequency high power transformers at these converters are usually exposed to the non-sinusoidal waveforms and include harmonics [5]. Therefore, the influence of these non-sinusoidal waveforms on the total loss should be evaluated accurately. The difficulty of the core loss is due to the nonlinear nature of the magnetic materials. In this paper, the equivalent elliptical loop (EEL) method is utilized in order to compute the core loss in the three different transformers with square wave excitations and duty cycle of 0.5. EEL calculates the core loss by using the time domain magnetic induction obtained from the finite element simulation and it considers the effects of minor loops at core loss calculation [6].

II. DESIGN, SIMULATION AND EVALUATION OF THE TOPOLOGIES

Two topologies compared in this paper are designed and simulated under the following conditions: input voltage (V_{in}) $= 4000\,V$, output voltage $(V_o) = 6000\,V$ and rated power $(P_o) = 2.4MW$. The topologies are compared at three different frequencies $f_{sw} = 500, 1000, 2000\,Hz$.

Based on the voltage and the current ratings of the studied converter, the IGBT, 5SNA 1200G450300 HiPak module from ABB is used. Two IGBTs from this type should be used in series in each module of the converter circuit. The Diode, 5SLD 0600J650100 HiPak module from ABB was selected for the rectifier. Each freewheeling diode module consists of two parallel submodules that in each submodule four diodes are connected in series. Also, each output diode modules, consists of two parallel submodules that in each submodule two diodes are connected in series.

In order to a get smooth output voltage and current, it is necessary to design an appropriate output filter. The values of the inductor and capacitor of the output filter are calculated according the allowed ripples. In this design the current ripple limits to 10% and the voltage ripple limits to 1%.

A. Hard Switched DC-DC full bridge converter

The schematic of the hard switched DC-DC full bridge converter with phase shift control is shown in Fig. 1.

In this controlling method, the output voltage is controlled via phase shift control. It means, both halves of the bridge switch network operate with a 50% duty cycle, and the phase difference between the half bridge switch networks is controlled. [7]

By changing the transformer ratio and the phase shift angle the ratio between the input voltage and the output voltage can be changed. In the designed converter, the turn ratio of the transformer is 3 and its leakage inductance is found to be 8.9µH. The inductor and the capacitor of the output filter are 11mH and 83µF respectively.

The simulation results of the hard switched DC-DC full bridge converter are shown in Fig. 2.

The conduction and switching losses of the IGBT and

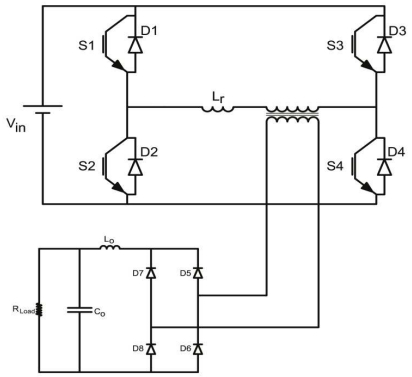

Fig. 1. Topology of the hard switched DC-DC full bridge converter

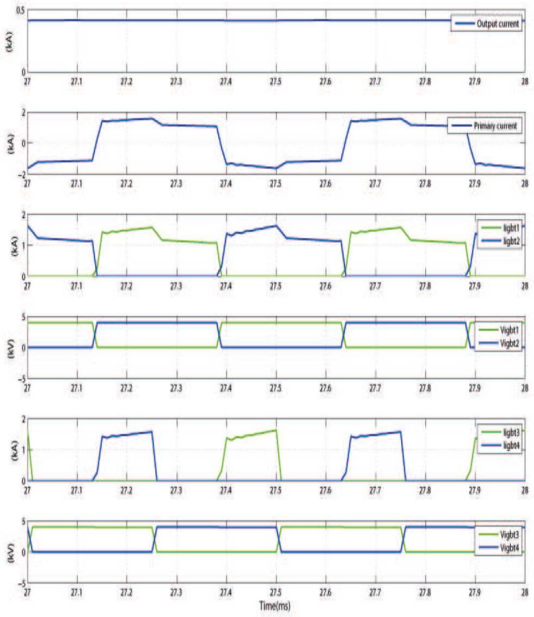

Fig. 2. Simulation results for the hard switched DC-DC full bridge converter

diodes are calculated using as

$$P_{c-igbt} = V_{igbt} I_{igbt-av} + R_{igbt-on} I^2_{igbt-rms} \quad (1)$$

$$P_{sw-igbt} = f_{sw} E_{sw} \left(\frac{1}{\pi} \frac{I_{igbt-max}}{I_{ref}}\right)^{K_i} \left(\frac{V_{igbt-max}}{V_{ref}}\right)^{K_v} \quad (2)$$

$$P_{c-diode} = V_f . I_{diode-av} + R_f I^2_{diode-rms} \quad (3)$$

$$P_{sw-diode} = f_{sw} E_{rec} \left(\frac{1}{\pi} \frac{I_{diode-max}}{I_{ref}}\right)^{K_i D} \left(\frac{V_{diode-max}}{V_{ref}}\right)^{K_v D} \quad (4)$$

Where P_{c-igbt} is the conduction loss of an IGBT, $P_{sw-igbt}$ is switching loss of an IGBT, E_{sw} is switching energy of the IGBT, V_{igbt} and $R_{igbt-on}$ are on-state voltage drop and on-state resistance of an IGBT, f_{sw} is switching frequency, $P_{c-diode}$ is the conduction loss of a diode, $P_{sw-diode}$ is the switching loss of a diode, V_f is the forward voltage of a diode, R_f is the on-state resistance of the diode, E_{rec} is the reverse recover energy of the diode, I_{ref} and V_{ref} are the reference current and the reference voltage of the diode or the IGBT.

Table I shows the power losses in the semiconductor devices for the hard switched DC-DC full bridge converter.

TABLE I
POWER LOSSES FOR THE HARD SWITCHED DC-DC CONVERTER

Switching frequency [Hz]		500	1000	2000
IGBTs	Conduction loss (W)	23136	23052	23012
	Switching Loss(W)	5388	10778	21556
Freewheeling Diodes	Conduction loss(W)	11520	11520	11520
	Switching loss(W)	5003	10007	20014
Output diodes	Conduction loss(W)	2154	2149	2147
	Switching loss(W)	5226	10453	20906
	Total(W)	52427	67959	99155

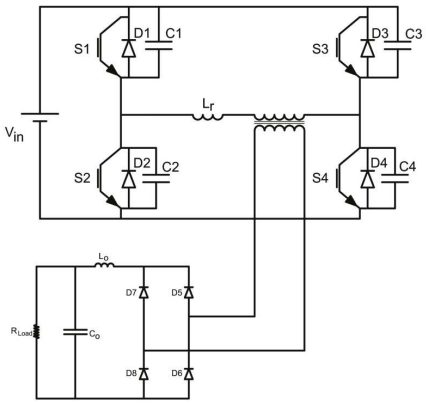

Fig. 3. Topology of the zero-voltage switching full bridge (ZVSFB) converter.

B. Zero-Voltage Switching Full Bridge (ZVSFB) converter

The topology of the ZVSFB converter with phase shift control is shown in Fig. 3. The Input voltage of the transformer can be achieved by turning two switches in different legs on. The difference between phase shift control and duty cycle control is the switching and off-state, one switch can be turned off and the load current flow through one switch and one diode. This method by having the snubber capacitors in parallel with the switches, leads to considerable decrease in switching losses. This converter uses parasitic components of the circuit to achieve soft switching. If these parasitic components are not large enough in the required load, additional inductance or capacitance should be used.

There are two states in this converter, passive and active state. During the passive state, S_1 conducts and the load current flows through D_3, therefore, the voltage over the transformer is zero. The active state initiates when S_1 is turned off, since D_3 is conducting, S_1 turns off at zero voltage. When S_1 has been turned off, the load current goes through the lagging leg snubber capacitors. The voltage across D_2 reaches zero and D_2 will be forward biased. So the current starts to flow through D_2 and D_3. Since the voltage over S_2 and S_3 is zero, they can be turned on at zero voltage. In active state when S_2 and S_3 are conducting, the voltage across the transformer is equal to the input voltage. The transition from active state to passive starts when S_3 is turned off and the load current flows through the leading leg snubber capacitors. When the voltage over D_4 reaches zero, the diode is forward biased, so one diode and one switch conduct. This state is called passive state. Operation principle is the same for the other half period. The energy stored in the leakage inductance of the transformer is used to charge the snubber capacitors of the lagging leg, however, the switching of the leading leg devices is done by using the energy stored in the output filter.

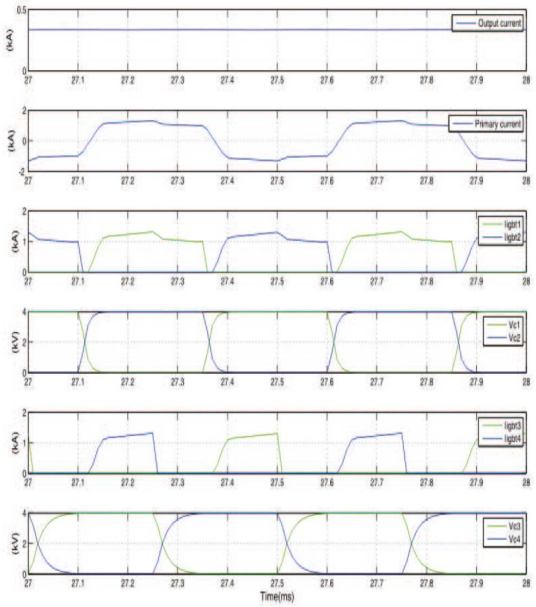

Fig. 4. Simulation results for the ZVSFB converter.

Fig. 4 shows the waveforms for the ZVSFB converter obtained from the simulation.

An important part in the design procedure of the ZVSFB is design and selection of the snubber capacitors for the leading leg and the lagging leg. Moreover, the additional inductance for the primary side of the transformer should be selected carefully. The procedure for selecting the snubber capacitors and primary inductance has the following steps:

1) The first issue that needs to be considered is the minimum value of the snubber capacitor that can be used. The time for charging snubber capacitor should be at least 5 times higher than the fall time of the IGBT current.
2) The second issue is to find a maximum value of the transformer leakage inductance. Very large inductances should be avoided due to high duty cycle losses.
3) The maximum value for the snubber capacitors of the lagging leg is calculated.
4) The minimum inductance required to charge the capacitors in the previous step is calculated.
5) The leading leg snubber capacitors are calculated based on the time required to charge them.

The turn-off snubber causes a decrease in the IGBT current and an increase in the IGBT voltage occurs simultaneously. Also the snubber capacitor increases the rise time of the voltage during turn-off. In this paper, the time for charging the snubber capacitors is considered to be 5 times higher than fall time of the current (t_{fi}). By this assumption, the

switching losses can be neglected. Based on this assumption, the minimum capacitor can be calculated as

$$C_{min} = \frac{5\, t_{fi}\, i_{in}}{V_{in}} \quad (5)$$

It is not reasonable to have a very large primary inductance to achieve soft switching. Since there are two current reversals in each period, large primary inductance results in high duty cycle losses. The maximum current reversal time in this paper is considered to be 10% of the whole period. Based on this assumption, L_{rmax} is calculated as

$$L_{rmax} = \frac{0.1\, V_{in}}{2 f_{sw} i_{in}} \quad (6)$$

Based on (6), the maximum value for the lagging leg snubber capacitors can be obtained by putting the energy stored in the maximum primary inductance equal to the energy stored in the capacitors.

$$C_{smax} = \frac{1}{2} \frac{L_{rmax}\, {i_{in}}^2}{{V_{in}}^2} \quad (7)$$

From (5) and (7), the snubber capacitor of the lagging leg can be selected between the two limits. The primary inductance of the transformer should be able to charge the snubber capacitors; therefore (8) should be fulfilled.

$$L_r > 2 \frac{C {V_{in}}^2}{{i_{in}}^2} \quad (8)$$

Another design consideration in designing the snubber capacitors is time for charging capacitors of the leading leg. In this paper, the maximum allowed time for charging the snubber capacitors of the leading leg is considered 2% of the whole period. Based on this assumption, the leading leg snubber capacitors are calculated as it is shown in (9).

$$C_{slead} = \frac{0.02\, i_{in}}{f_{sw} V_{in}} \quad (9)$$

The leakage inductance required to achieve soft switching of the lagging leg is shown in Fig. 5.

The result is that the switching losses of the IGBTs can be neglected in this topology. The conduction and switching losses for the other devices are calculated using (1), (3) and (4). Table II shows the power losses in the semiconductor devices for the zero-voltage switching full bridge converter.

TABLE II
POWER LOSSES FOR THE ZVSFB DC-DC CONVERTER

Switching frequency		500	1000	2000
IGBTs	Conduction loss (W)	22232	22226	21771
Freewheeling Diodes	Conduction loss(W)	1423	1417	1422
	Switching loss(W)	5003	10007	20014
Output diodes	Conduction loss(W)	3672	3672	3672
	Switching loss(W)	5226	10453	20906
	Total(W)	37556	47775	67785

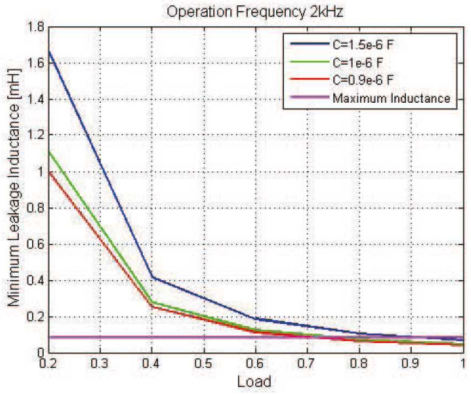

Fig. 5. Minimum leakage inductance required to achieve soft switching for different load conditions

III. HIGH POWER HIGH FREQUENCY TRANSFORMER

The high frequency high power transformer is the key element in the new generation of DC-DC converters. Decreasing the size of the transformer while keeping the power fixed as it was at 50 Hz, leads to high loss density of the transformer. Hence, the transformer would need a sophisticated thermal management which requires precise evaluations of the loss level of the transformer, particularly when it is exposed to the non-sinusoidal waveforms which makes the evaluation harder.

A. Core Material and Dimensions

One of the first and important issues in designing a transformer is selecting a suitable magnetic material. In high frequency high power applications, there are several parameters that should be taken into account when analyzing magnetic, electrical and mechanical properties. The parameters are core loss density, temperature characteristics, saturation flux density and relative permeability that is based on these parameters, different types of magnetic materials may fulfill high frequency requirements.

The soft magnetic material used at this paper is Metglas amorphous alloy 2605SA1 which has the saturation induction of 1.56 T and the coercivity of 1.7 A/m. The core loss for SA1 is extremely low at about 0.29 W/kg at 60 Hz, 1.35 T, however this value increases at higher frequencies but it is still lower than that for the conventional silicon steel.

The system specifications are the nominal operating values including secondary and primary voltages, Operating frequency and rated power of the transformer. Other parameters such as the maximum flux density and the number of primary turns can be selected and varied by the designers which are set to be 1.1 T and 6 turns respectively in this paper. The design parameters include the geometrical variables that should be obtained based on the two other categories such as the dimensions of the core and the windings [9].

Based on the characteristics of the magnetic material and the applied voltage, the proper effective cross section of the core can be obtained as

$$A_{core} = \frac{V_m.D}{4.N.f.B_m} \quad (10)$$

where A_{core} is the core sectional area of the core, V_m is the peak value of the primary voltage, D is the duty cycle of the applied voltage, N is the number of turns at primary widings, f is the operating frequency and B_m is the maximum magnetic flux density in the core which is usually set to be at 80% of the saturation level of the magnetic material [10].

B. Loss Evaluation

There are different methods of core loss calculations and each of them has some advantages and disadvantages. Designers usually use the well-known Steinmetz equations for core loss calculations that are valid only for sinusoidal equations. The method used in this paper for the core loss calculation is called equivalent elliptical loop (EEL). The advantages of this method are:

- It allows for considering the effects of minor loops in calculations of hysteresis loss.
- Arbitrary waveform can be used as excitation in time domain.

ANSYS Maxwell 3D [11] is used as the finite element software for all of the simulations in this paper. In three dimensional finite element transient analysis, three loss components will be obtained by (11), (12) and (13) [6]

$$P_h(t) = \left| H_x \frac{dB_x}{dt} \right| + \left| H_y \frac{dB_y}{dt} \right| + \left| H_z \frac{dB_z}{dt} \right| \quad (11)$$

$$P_c(t) = \frac{1}{2\pi^2} k_c \{ (\frac{dB_x}{dt})^2 + (\frac{dB_y}{dt})^2 + (\frac{dB_z}{dt})^2 \} \quad (12)$$

$$P_e(t) = \frac{1}{C_e} k_e \{ (\frac{dB_x}{dt})^2 + (\frac{dB_y}{dt})^2 + (\frac{dB_z}{dt})^2 \}^{0.75} \quad (13)$$

Where P_h, P_c and P_e are the static hysteresis loss, the classical eddy current loss and the excess eddy current loss respectively, H is the magnetic field intensity, B is the magnetic flux density, k are the loss coefficient which are extracted from the manufacturer's datasheet and C_e is equal to 8.763.

Fig. 6 shows an example of the core loss distribution in every single point of the core at a specific moment.

Table III shows the designed transformer core dimensions and the calculated core loss for three different transformers at three different operating frequencies. The interesting point is that by increasing the frequency from 500 Hz to 2 kHz, on one hand, the core loss would increase almost two times, but on the other hand, the weight of the transformer core would decrease 5 times and this is the main reason which justify to increase the frequency particularly at highly restricted applications such as traction or offshore wind farms.

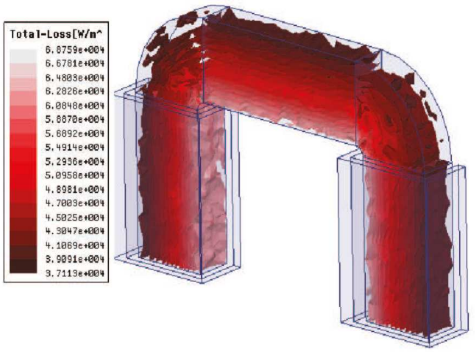

Fig. 6. Spatial core loss density distribution

It should be mentioned that in order to have the highest efficiency, the winding loss is assumed to be at the same level as the core loss.

TABLE III
Transformer Characteristics

	2.4 MW - 4/12 kV		
Frequency [Hz]	500	1000	2000
Duty Cycle	0.5	0.5	0.5
Acore [m2]	0.15	0.07	0.03
Window Height [mm]	98.99	148.49	197.98
Window Width [mm]	386.88	311.52	301.48
Core Loss [kW]	7.42	10.31	15.42
Core Weight [kg]	2429.02	991.5	452.13

IV. COMPARISON OF THE TOPOLOGIES

Table IV shows the loss results for the two converter topologies. It can be seen that both topologies have almost the same efficiency at lower frequencies, where the switching losses are not a large fraction of the total losses. However, the hard switched DC-DC full bridge converters suffer from high switching losses in high frequencies and to improve the efficiency at higher frequencies it is important to reduce this power loss. Zero voltage switching full bridge converters reduces this loss by managing the parasitic components of the converter to achieve zero voltage switching that results in a decrease of the total losses.

TABLE IV
POWER LOSSES FOR THE HARD SWITCHED DC-DC CONVERTER

Switching frequency	500	1000	2000
Hard switched DC-DC full bridge converter losses	67227	88559	129955
Zero-Voltage Switching Full Bridge (ZVSFB) converter losses	52356	68375	98585
Efficiency of the Hard switched	0.971	0.961	0.94
Efficiency of the Zero-Voltage	0.978	0.971	0.959

V. CONCLUSIONS

In this paper both hard and soft switching schemes of the high power density DC-DC full bridge converter has been proposed and analyzed. It has been concluded that since for the lower frequencies the efficiency is almost the same for the two topologies, hard switched is preferable due to the lower cost. However, for the higher frequencies where the total losses are dominated by the switching losses, the soft switched topology is superior.

The core loss of the transformer which was exposed to high frequency square wave excitation has been calculated by using FEM simulation and it shows that the transformer contribution at total loss of the converter is about 30% at all three studied frequencies for phase shift converter.

REFERENCES

[1] C. Meyer, “Key Components for Future Offshore DC Grids”, Ph.D. dissertation, RWTH Aachen, 2007.

[2] M. Carpita, M. Marchesoni, M. Pellerin, and D. Moser, “Multilevel converter for traction applications: Small-scale prototype tests results”, IEEE Trans. on Ind. Electron., vol. 55, no. 5, pp. 2203–2212, May 2008.

[3] R. L. Steigerwald, “A comparison of half-bridge resonant converter topologies ”, IEEE transactions on power electronics, vol. 3, no. 2, April 1988.

[4] R. L. Steigerwald, “A comparison of high-power DC-DC soft-switched converter topologies”, IEEE transactions on industry applications, vol. 3, no. 2, Sept/Oct 1996.

[5] Y. Nie, Q. Hu and Y. Huang, “The measurement and prediction of iron loss under nonsinusoidal voltage waveform with arbitrary frequency”, International Conference on Electrical Machines and Systems, pp. 232-236, 2008.

[6] D. Lin, P. Zhou, W. N. Fu, Z. Badics, and Z. J. Cendes, “A Dynamic Core Loss Model for Soft Ferromagnetic and Power Ferrite Materials in Transient Finite Element Analysis”, IEEE Trans. on Magnetics, vol. 40, No. 2, pp. 1318-1321, March 2004.

[7] R. W. Erickson and D. Maksimovic, Fundamentals of Power Electronics. Springer Science + Business Media,LLC, second edition, 2001.

[8] N. Mohan, T. M. Undeland, and W. P. Robbins, Power Electronics: Converters, Applications and Design. John Wiley and Sons INC., third edition, 2003.

[9] M. A. Bahmani, E. Agheb, T. Thiringer, H. K. Høidalen and Y. Serdyuk, “Magnetic Core Loss Behavior for High Frequency High Power Transformers-Part I: optimum topology”, submitted to the Journal of Renewable and Sustainable Energy.

[10] E. Agheb, M. A. Bahmani, H. K. Høidalen and T. Thiringer, “Magnetic Core Loss Behavior for High Frequency High Power Transformers-Part II: arbitrary excitation”, submitted to the Journal of Renewable and Sustainable Energy.

[11] ANSYS website

References

[1] B. Normark and E. K. Nielsen, "Advanced power electronics for cable connection of offshore wind," *Proc. Copenhagen Offshore Wind*, 2005.

[2] L. Max, *Energy Evaluation for DC/DC Converters in DC-Based Wind Farms, Thesis for the degree of licentiate of engineering*. PhD thesis, Department of Energy and Environment Chalmers university of technology, 2007.

[3] L. Max, *Design and Control of a DC Collection Grid for a Wind Farm, Thesis for the degree of doctor of philosophy*. PhD thesis, Department of Energy and Environment Chalmers university of technology, 2009.

[4] N. Mohan, T. Undeland, and W. Robbins, *Power electronics converters, applications, and design*. Wiley, 2 edition, 1995.

[5] D. M. Robert W. Erickson, *Fundamentals of Power Electronics*. Springer Science, 1999.

[6] L. Max, "An investigation of diffeerent dc-dc-converters for wind farm applications," *Technical Report*, 2005.

[7] R. F. J.A.Sabate, V.Vlatkovic and B.H.Cho, "Design considerations for high-voltage high-power full-bridge zero-voltage-switched pwm converter," *IEEE Paper*, 1990.

[8] A. B. Mehmet Timur Aydemir, "A critical evaluation of high power hard and soft switched isolated dc-dc converters," *IEEE Paper*, 2002.

[9] R. S. Bjorn Backlund, "Applying igbts," tech. rep., ABB Switzerland Ltd, 2009.

[10] A. Wintrich, "Theory of loss and temprature calculatio," *SEMIKRON, inovation+service*, 2008.

[11] P. C. Sen, *Power Electronics*. Tata McGraw Hill Publishing Company Limited, New Delhi, 1987.

[12] W. Shen, *Design of High-density Transformers for High-frequency High-power Converters*. PhD thesis, Blacksburg, Virginia, 2006.

[13] C. W. T. McLymon, *Transformer and Inductor Design Handbook*. CRC Press Taylor and Francis Group, 2011.

[14] *www.metglas.com*.

[15] T. H. M.A.Bahmani, E.Agheb, “Core loss behaviour in high frequency high power transformers-part i: effect of core topology,” *Journal of Renewable and Sustainable Energy, AIP*, 2012.

[16] *http://metglas.com/downloads/powerlite.pdf*.